Bipolar Electrochemistry: Chemical Analysis Based on Electrochemiluminescence and Surface Enhanced Raman Spectroscopy

by

Sanjun Fan

A thesis submitted to the Graduate Faculty of
Auburn University
in partial fulfillment of the
requirements for Degree of
Master of Science

Auburn, Alabama
August 1, 2015

Keywords: Bipolar Electrochemistry, Electrochemiluminescence, Quenching Effect, Surface Enhanced Raman Scattering

Approved by

Curtis G. Shannon, Chair, Professor of Chemistry and Biochemistry
Vincenzo Cammarata, Associate Professor of Chemistry and Biochemistry
Christopher J. Easley, Associate Professor of Chemistry and Biochemistry
Wei Zhan Associate Professor of Chemistry and Biochemistry

Abstract

Bipolar electrochemistry has a variety of applications ranging from chemical analysis, material modification and synthesis, to generate motions, etc, and it is also a very simple, cheap, useful technology. The main goal of this thesis is to analyze chemicals based on electrochemiluminescence (ECL) and surface enhanced Raman spectroscopy. Since bipolar electrochemistry does not have a direct readout in current, electrochemiluminescence is becoming a more and more useful technique for electroanalysis on bipolar electrochemistry. Small molecules like O_2 capable of quenching ECL can be detected according to Stern−Volmer equation. A linear potential gradient was created going through the solution along the bipolar electrode when the external voltage is sufficient on the bipolar cell. As the redox reactions were relative to the potential applied, the extent of reaction on bipolar electrode was different due to the potential gradient, which can be observed by surface enhance Raman scattering. Consequently, the potential distribution was obtained.

Chapter 1 presents a detailed literature review on the principle and application of bipolar electrochemistry including chemical analysis based on electrochemiluminescence and electrodissolution, material modification, synthesis and generating motions, concentration enrichment and separation. Additionally, a short introduction of electrochemiluminescence and Raman spectroscopy was given at the end of chapter 1.

Chapter 2 describes the detection of small molecules like 1-ferrocenylmethanol (1-hydroxymethyl ferrocene) and oxygen capable of quenching the electrochemiluminescence via

energy or electron transfer in terms of Stern−Volmer equation in a bipolar electrochemical cell. It opens a new area of research using ECL quenching to detect small molecules based on bipolar electrochemistry.

Chapter 3 illustrates different quenching effect of halide ions (Cl^-, Br^-, and I^-), indicating the quenching ability of the halides follows the order $I^- > Br^- > Cl^-$, and the quenching rate constants are also related to their formal oxidation potential.

Chapter 4 deals with the potential distribution on bipolar electrode by observing the Raman intensity change of a surface enhanced Raman scattering probe at the cathodic pole when the external voltage is sufficient to drive redox reactions. The Raman intensities of 2-AQS and 2-H_2AQS corresponded to the amount of them on bipolar electrode, respectively, and the relative population of 2-AQS to 2-H_2AQS will vary at different positions according to the potential gradient going through the solution along bipolar electrode.

Chapter 5 gives a summary of my research work and the future work.

Acknowledgments

I would like to express my sincere gratitude to my advisor Dr. Curtis Shannon for his wonderful guidance, continuous motivation and great support for my life and study in Auburn University. When I first met him, I already knew he was a very clever, thoughtful, and kind professor and decided to make big progress in his group, and the fact that he teaches me a lot without any hesitation also proves it. Without him, I cannot make big progress in research especially in bipolar electrochemistry. I appreciate his great encouragement when I was sick. I appreciate his generous heart even though I am wrong. I appreciate his huge support for my study and research.

I would like to give lots of thanks to my committee members, Dr. Christopher Easley, Dr. Wei Zhan, Dr. Vince Cammarata for their great suggest for my research and the preparation of the thesis. I would like to give special thanks to Dr. Christopher Easley is a very easy going and kind professor, and ready to provide wonderful suggestions and immense courage whenever I need. Dr. Zhan is also a wonderful professor, he is happy to provide biggest help in my research. I appreciate a lot to the introduction of Dr. Vince Cammarata in his class for his careful and patient teaching. I also appreciate his kindness whenever I have questions. I would like to give my sincere thanks to Dr. Rik Blumenthal for his great guidance and support in study. I would like to give my sincere thanks to Dr. David Stanbury for his great advice and courage in my study. I would like to give my sincere thanks to Dr. J. V. Ortiz for his support in my study. I

would like to give my sincere thanks to Dr. Jimmy Mills for his support in my study. I would like to give my sincere thanks to Dr. Anne Gorden and Dr. John Gorden for their great suggestions in research and kind advice in my study. I would like to give my sincere thanks to the courage of Dr. Bradley Merner and Dr. Stewart Schneller in my study. I would like to give my sincere thanks to the great collaboration with Dr. Chris Goldsmith and Mr. Mengyu. I would like to give my sincere thanks to Dr. Joonyul Kim and Mr. Subramaniam Somasundaram for his good advice in research.

I would like to give my sincere thanks to the people in Dr. Curtis Shannon's group. Dr. Yajiao Yu, Dr. Tangyu Wang, Dr. Axline Sangapi, Ms. Li Zhang, Ms. Apu Mazumder, Mr. Buhua Wang, Mr. Songyan Yu. I am very glad to have so many great labmates. I would like to give my sincere thanks to the great help from Ms. Jessica Brooks, Mr. Walter Casper, and Mr. Nicholas Klann.

I would like to give my sincere thanks to my parents and my sister for their great support of my study.

† These authors contributed equally.

* Corresponding author

Table of Contents

List of Tables

List of Figures

List of Schemes

Chapter 1

Introduction

1.1 Bipolar electrochemistry

Bipolar electrochemistry with a wide range of applications like sensors,[1-14] electrodeposition,[15-18] microobject and Janus particles,[19-24] lighting swimmers,[25-27] motions,[28-31] electrocatalyst,[32, 33] fluorescence,[34-36] materials enrichment and separation[37, 38] polymer synthesis,[39-41] corrosion,[42, 43] and Metal-Organic Framework (MOF) synthesis[44] has received considerable attention throughout the world in the past twenty years, because it is a powerful, simple and low-cost analytical technique.[45] Electrochemical reactions can be generate at the extremes of bipolar electrode (BPE) when applied sufficient voltage without direct connection with the power supply, which results in a voltage gradient along the bipolar electrode.[46] The bipolar electrode can be made from any conductive object such as gold, platinum, stainless steel, carbon bead, glassy carbon particles, carbon nanotubes, paper, etc.[14, 47-50] Bipolar electrochemistry has been applied in a variety of fields from materials to analysis.[51, 52] For instance, interestingly, Shinsuke Inagi's group deposited poly(3,4-ethylenedioxythiophene) film on the bipolar electrode obtaining a multicolored gradient along the film, confirmed by UV-Vis and energy dispersive X-ray analyses,[41] and they later modified conducting polymer surface on bipolar electrode with electro-click chemistry reaction in a gradient manner,[40] most recently, they firstly used

electrochemically mediated atom transfer radical polymerization (eATRP) to form a gradient and patterned polymer brushes by the use of bipolar electrochemistry.[53] Since Dr. Andreas Manz first introduced electrochemiluminescence (ECL) into bipolar electrochemistry and Dr. R.M. Crooks further developed the electrochemical generated chemiluminescence with the marriage of bipolar electrochemistry as a report in the pursuit of the detection of benzyl viologen and DNA,[2, 54] more and more analytical chemists adopted this technique to analyze materials quantitatively with great interest. Jing-Juan Xu's group has done lots of work in this area,[9, 10, 49, 55-57] and recently, they described a new platform to detect cancer biomarker based on a closed bipolar electrode array.[58] Erkang Wang's group developed a novel sensing platform based single or multichannel close bipolar system obtaining 100% efficiency in theory.[11, 12] More interestingly, Alexander Kuhn's group developed the "swimmer" in which ECL reaction was generated at one side and the hydrogen gas was generated in the other side to propel the "swimmer" move.[59] They also prepared different kinds and applications of "Janus particles" by bipolar electrochemistry.[21, 23, 60, 61] Our group previously synthesized gradients of CdS and Ag-Au alloys using bipolar electrodeposition characterized by Raman spectroscpy.[15, 16] Recently, Shinsuke Inagi's group achieved bifunctional modified conductive particles with gold or platinum deposited on the both sides by employing alternating current power supply. However, it seems hard to modify because of the size and difficult to control deposition area of Au on glassy carbon particles since the oxygen generated can influence the potential drop during experiment.[50] Bipolar electrochemistry has been a useful, simple and low-cost analytical technique in a wide range of applications for chemists, both now

and future.

1.1.1 Principle of bipolar electrochemistry

Bipolar electrochemical cell consists of two driving electrodes connected with an external voltage and one bipolar electrode fixed on the bottom of the bipolar electrochemical cell. When sufficient voltage "E_{appl}" was applied on the bipolar electrochemical cell, reactions would be triggered at the ends of bipolar electrode. Reduction reaction occurred at the cathode of bipolar electrode directly opposite the positive driving electrode, on the contrary, oxidation reaction occurred at the anode of bipolar electrode directly opposite negative driving electrode in Figure 1.1.1.[54, 62]

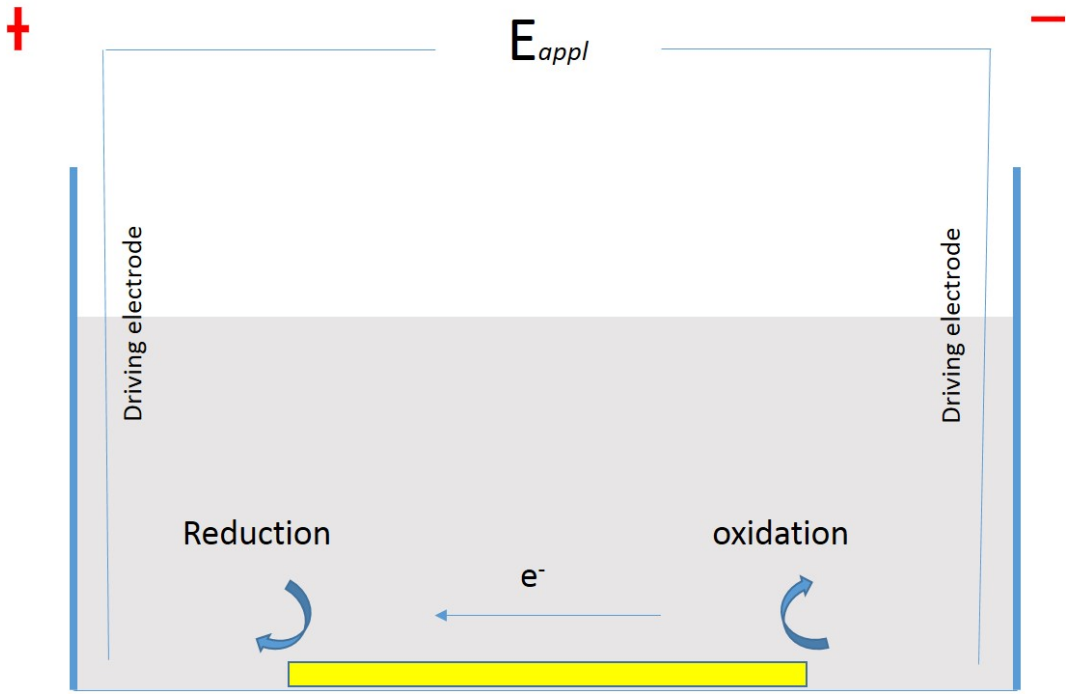

Figure 1.1.1 Bipolar electrochemical cell consists of two driving electrodes which connected with an external voltage "E_{appl}". Reactions (Reduction and Oxidation) occur at the two extremes of the

bipolar electrode fixed in the middle of the cell fulfilled with solution.

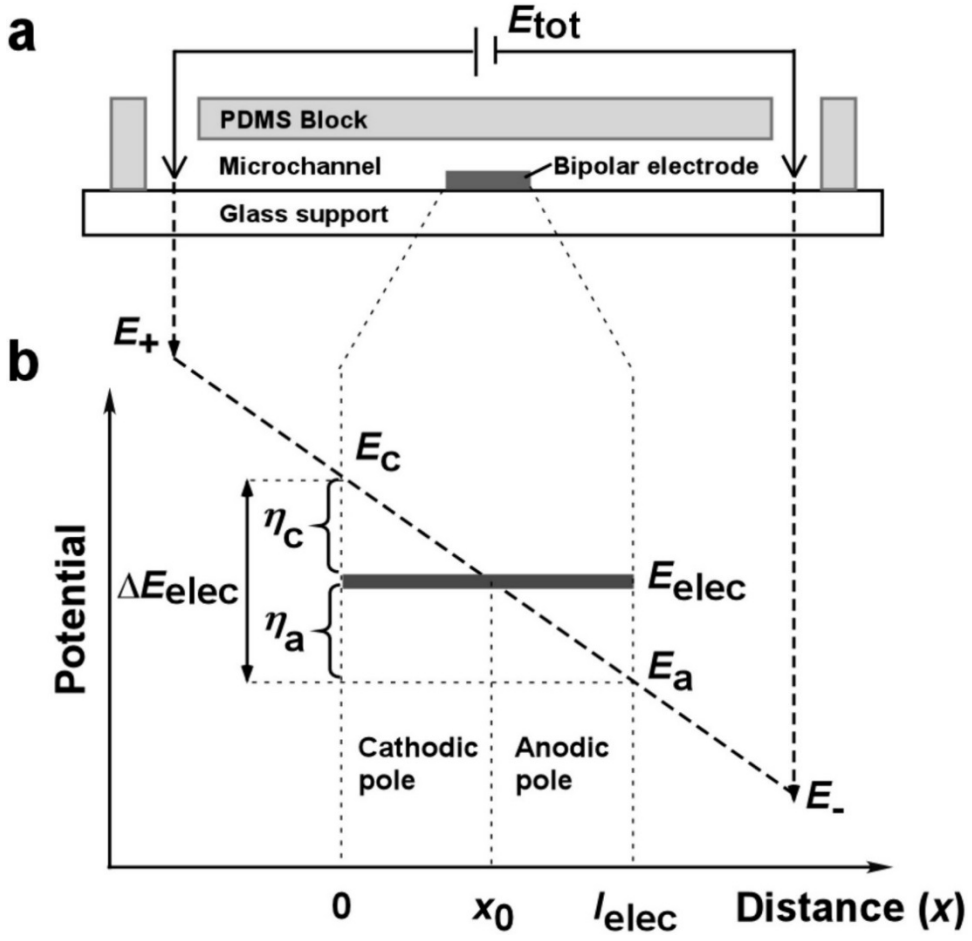

Figure 1.1.2 a) Bipolar electrochemical cell consists of a simple PDMS microfluidic channel, one bipolar electrode fixed in the middle of the cell, and two driving electrodes connected to a voltage "E_{tot}" b) An interfacial potential difference decreased linearly along the bipolar electrode fixed on the bottom of bipolar electrochemical cell. (Reprinted with permission from Anal. Chem. 2009, 81, 6218–6225. Copyright 2009 American Chemical Society)

The potential in solution dropped exponentially near the driving electrodes when applied

voltage (E_{tot}) on the bipolar electrochemical cell. There also exit a potential drop between the two ends of the bipolar electrode fixed in the bipolar electrochemical cell because of solution resistance, and it approximately linearly dropped along the interface between bipolar electrode and solution.[63]

$$\Delta E_{elec} = E_c - E_a = V_0 \times l_{elec} = \frac{E_{tot}}{l_{\text{channel}}} l_{elec} \quad (1)^{63}$$

Here, ΔE_{elec} is the potential difference between two poles (cathode and anode) of BPE (E_c and E_a), E_{tot} represents the driving voltage applied on the feeding electrodes, l_{channel} is the length of the bipolar cell, l_{elec} is the length of BPE, and electric field $V_0 = \frac{E_{tot}}{l_{\text{channel}}}$ if the potential drop around the feeding electrodes is negligible.

According to the equation (1), the potential difference between the BPE is related to the voltage applied on the electrochemical cell, the length of BPE, and the length of the channel in the cell. So a higher E_{tot} and longer BPE can lead to a bigger potential difference between the bipolar electrode, in contrast, it will decrease with the longer length of the bipolar cell. In addition, the potential difference is also determined by the concentration of solution.

X_0 in Figure 1.1.2 b is a particular position on bipolar electrode at which solution potential is equal to an equilibrium value (E_{elec}), which also divided the bipolar electrode into two parts: one is cathode and another is anode.[63] At the cathode part ($x < x_0$), $E_x > E_{elec}$, (E_x is the potential at bipolar electrode at the location x in solution) oxidants obtain electrons and gets reduced, on the other hand, at the anode part, ($x > x_0$), $E_x < E_{elec}$, reductant losses electrons and gets oxidized.[63] The redox reactions at both sides of bipolar electrode must maintain electroneutrality on the electrode surface. $\eta_{(x)}$ represents the difference in potential between the

electrode and the solution at one position x and it is calculated by the equation (2) as followed:

$$\eta_{(x)} = E_{elec} - E_x = V_0 \times (x_0 - x) = \frac{\Delta E_{elec}}{l_{elec}} (x_0 - x) \quad (2)^{63}$$

Here, E_x is the potential at bipolar electrode at the location x.

According to the equation (2), $\eta_{(x)}$ is the driven force which triggers the electrochemical oxidation at anode of BPE and reduction at the cathode of BPE and it linearly changes with the positon x along the bipolar electrode when the electric field is considered constant.[63]

1.1.2 Application of bipolar electrochemistry

1.1.2.1 Electrochemical analysis based on electrogenerated chemiluminescence

Electrogenerated chemiluminescence (ECL) is an electrochemical process at electrode surface which can generate excited states materials that emit light by electro-transfer reactions.[64] It has been used widely in science and application because its high sensitivity and selectivity.[65-67] $Ru(bpy)_3^{2+}$/TPrA or $Ru(bpy)_3^{2+}/C_2O_4^{2-}$ system is often used to detect chemicals based on bipolar electrochemistry.[1, 14, 49]

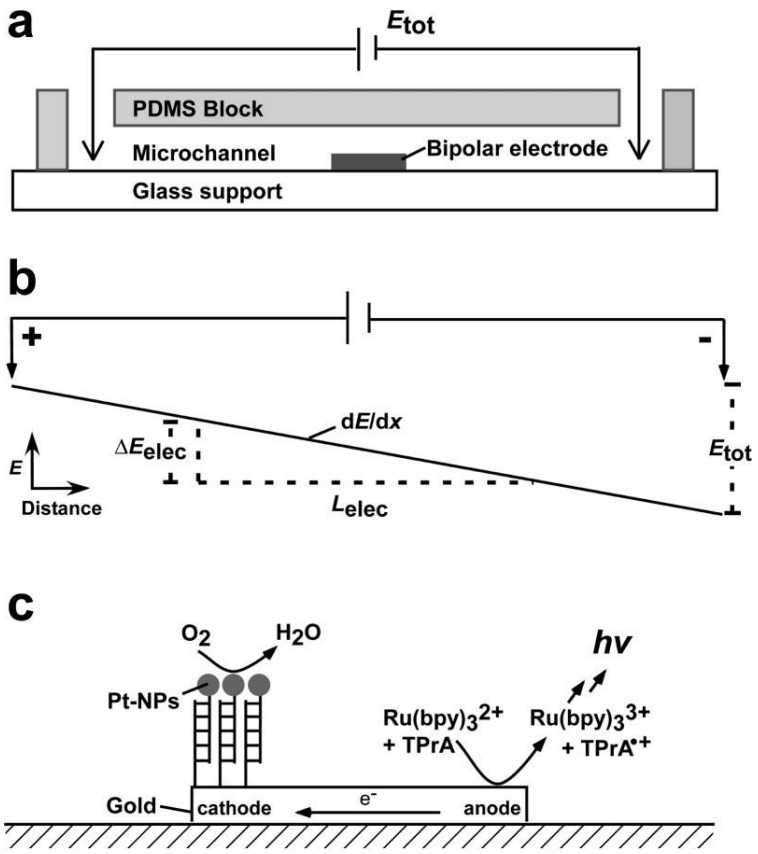

Figure 1.1.3 a) Bipolar electrodes were fixed in a microfluidic channel on the bottom of a bipolar cell b) An external potential E_{tot} is applied on the bipolar cell, and it leads to a linear potential gradient (dE/dx) across the bipolar electrode because of the resistance of electrolyte c) faradaic electrochemical process at the ends of bipolar electrode, oxygen reduction at the cathode, and ECL reaction at the anode (Reprinted with permission from J. Am. Chem. Soc. 2008, 130, 7544–7545. Copyright 2008 American Chemical Society)

Figure 1.1.3 shows how Crook's group detected DNA with electrochemiluminescence based on bipolar electrode.[3] Modified electrodes as bipolar electrodes were fixed in a microfluidic channel on the bottom of a bipolar cell connected to an external voltage E_{tot} in Figure 1.1.3 a.[3] As

discussed in 1.1.1, the potential difference between two ends of bipolar electrode can be adjusted by changing E_{tot} in Figure 1.1.3 b. Faradaic electrochemical processes (oxygen reduction and ECL oxidation) will generate at two ends of bipolar cell if the E_{tot} is sufficient enough in Figure 1.1.3 c.[3] The intensity of ECL at anode of bipolar cell corresponds to the amount of oxygen reduced at the cathode, because charge balance should be kept on the bipolar electrode, which means this system has the same rate of electron transfer at both ends.[3] It can indirectly measure the amount of DNA labeled with Pt on the cathode of bipolar electrode, overcoming the deficiency in bipolar electrochemistry that there is no method to gauge the current flow going through the bipolar electrode.[1-3]

Figure 1.1.4 a is the top-view schematic illustration of the microdevice, in which three Au electrodes microfabricated on a glass slide in the middle of the electrochemical bipolar cell and paralleled to each other.[3] (See in Figure 1.1.4 b) Prior to begin the experiment, these three Au electrodes were immobilized with thiol-functionalized DNA and then exposed to target DNA labeled with Pt-NPs.[3] Red emission can be seen in Figure 1.1.4 c at these three gold electrode after applied 16.0 V in phosphate buffer (pH = 6.9) solution containing 5.0 mM $Ru(bpy)_3^{2+}$ and 25.0 mM TPrA, which means oxygen was reduced catalyzed by Pt-NPs at the cathode.[3] To order to prove the emission is related to the Pt-NPs catalyst, two control experiments were done. There is no signal on the electrodes without exposure to the DNA labeled with Pt-NPs at 16.0 V in Figure 1.1.4 d. However, in Figure 1.1.4 e, signals can be detected on the top two electrodes exposed to targets, and no light was observe on the bottom one without hybridization with targets at 16.0 V.[3]

So the light emitted at the anode of bipolar electrode is related to the catalytic reaction on the cathode part of bipolar electrode. When the voltage was improved to 22.0 V from 16.0 V, light can be observed on the gold electrode without any treatment. This is because of uncatalyzed faradaic process, for instance, hydrogen ions were reduced at the cathode part of bipolar electrode.[3]

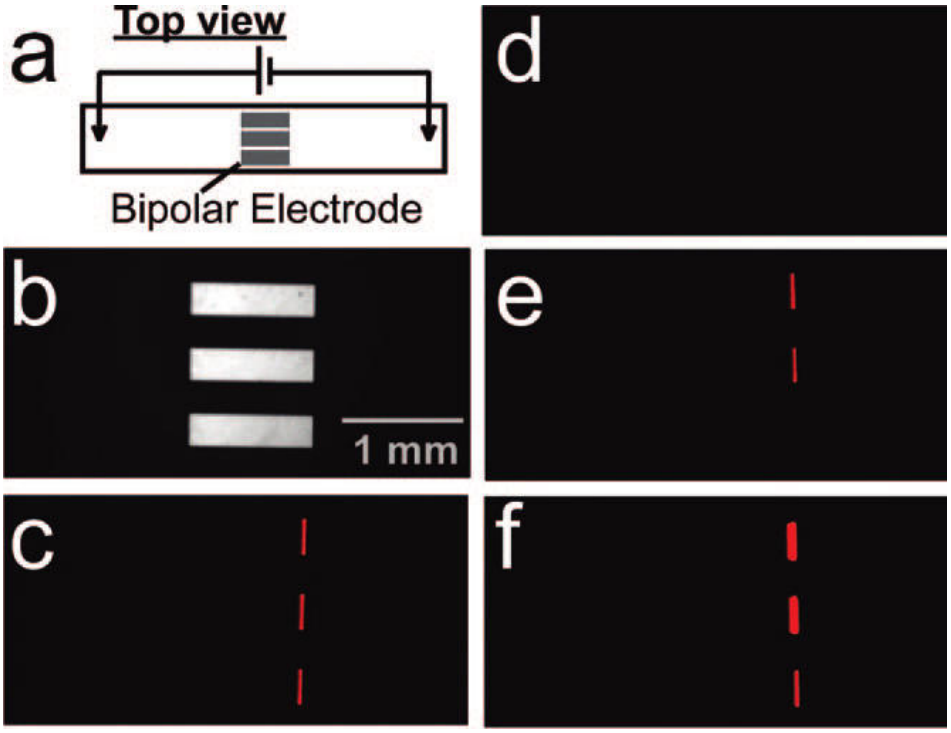

Figure 1.1.4 (a) Top-view schematic illustration of the microdevice. (b) Optical micrograph of the bipolar electrode configuration used to obtain the data in the other panels of this Figure. False-color luminescence micrographs showing (c) the ECL emitted at E_{tot} = 16.0 V when complementary target DNA functionalized with Pt-NPs is hybridized to probe DNA present on the electrode surface; (d) no ECL emitted at 16.0 V prior to hybridization; (e) the ECL emitted at 16.0 V when only the top two electrodes of the device are exposed to the labeled target; and (f) the ECL emission at E_{tot} = 22.0 V for the device in (e). (Reprinted with permission from J. Am. Chem. Soc.

2008, 130, 7544–7545. Copyright 2008 American Chemical Society)

Crooks group then scaled this system without microfluidic channel and increased the number of BPEs.[68] Figure 1.1.5 is the scheme illustrating how the principle of bipolar electrochemistry was employed in this system, specifically, Figure 1.1.5 a described how to assemble a bipolar electrochemical cell with BPEs, two driving electrodes, and an external voltage E_{tot}. As explained before, the potential drop between BPEs related to the length of themselves inherently and external environment like the length of bipolar cell and voltage. As such, ΔE_{elec} of each BPE is identical because of same length and situation in Figure 1.1.5 b.[68] Due to keep charge neutral, oxidation reaction at the anode of BPE and reduction reaction at the cathode of BPE will occur simultaneously, as a result, the rate of electron involved in the reduction reaction can be indirectly detected at the anode by oxidation reaction in Figure 1.1.5 b.[2, 68] When 85 V was applied, faradaic reactions were triggered on the BPEs, of which the ΔE_{elec} is about 2 V.

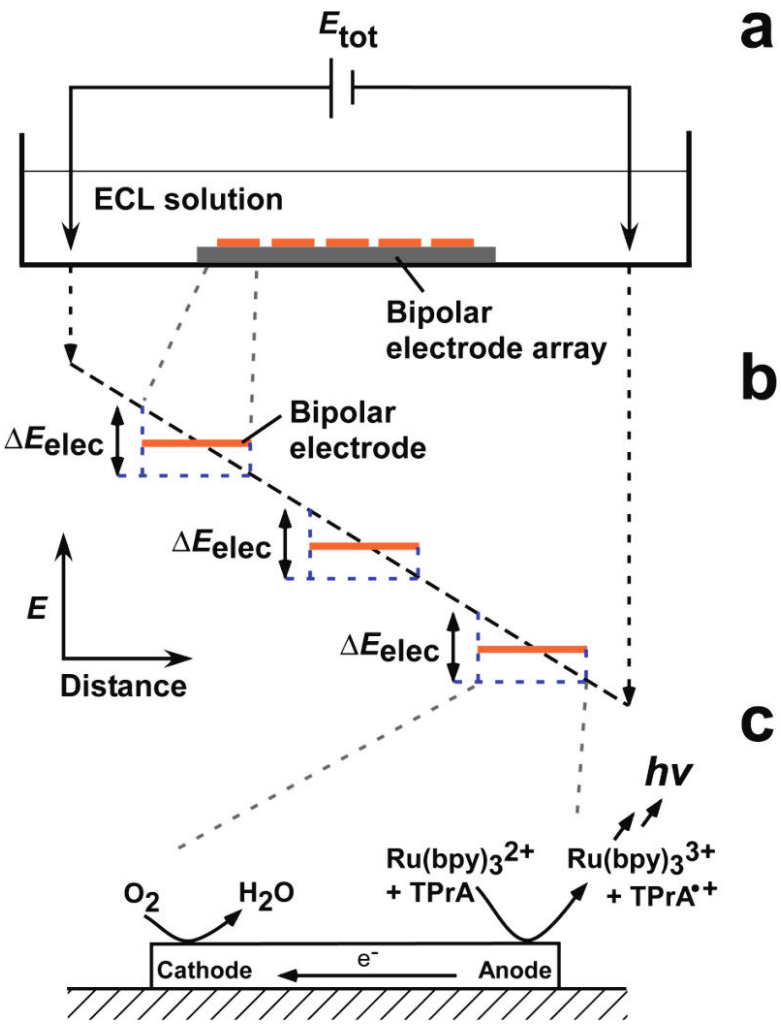

Figure 1.1.5 a) Bipolar electrochemical cell configuration, in which there are 1000 small BPE fixed in the middle. An external voltage E_{tot} between the two driving electrode was connected to the cell. b) E_{tot} creates a linear potential gradient going through the solution in bipolar electrochemical cell, and the ΔE_{elec} of each BPE is the same of the length and situation. c) Faradaic reactions occur at two sides of each BPE, O_2 was reduced on the cathode of BPE and $Ru(bpy)_3^{2+}$/TPrA were oxidized at the anode of BPE. (Reprinted with permission from J. Am. Chem. Soc. 2009, 131, 8364–8365. Copyright 2009 American Chemical Society)

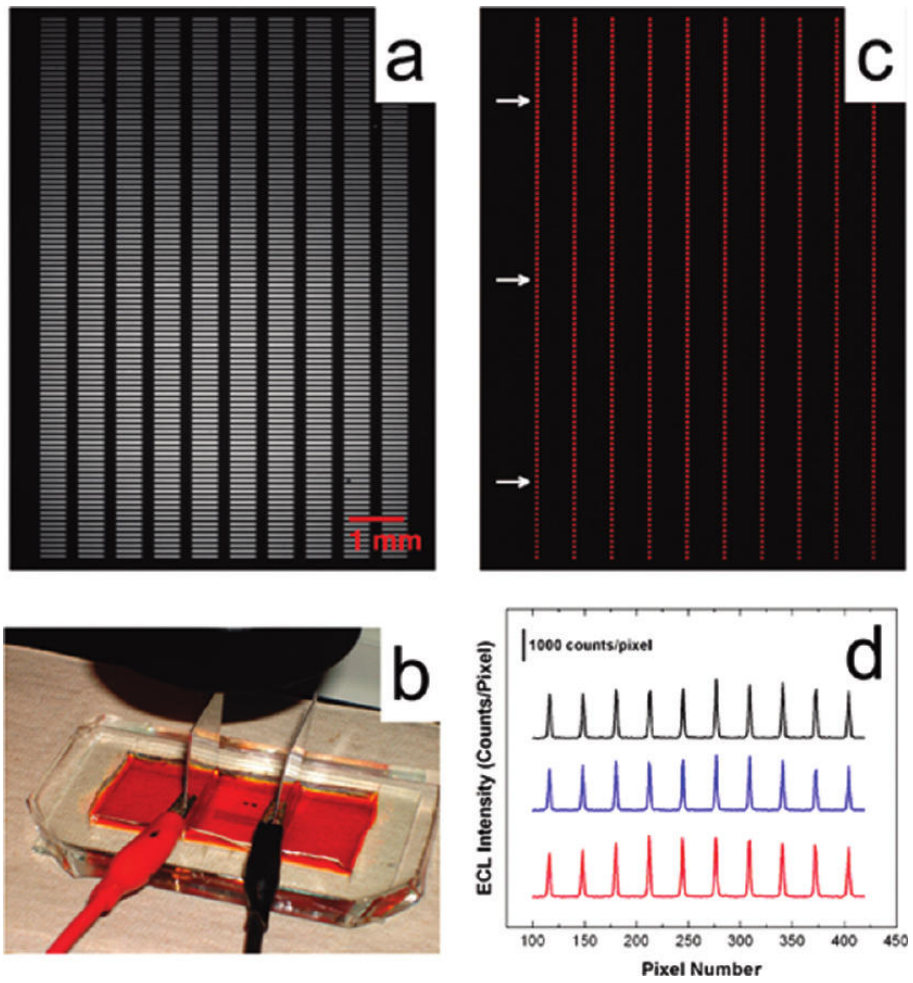

Figure 1.1.6 a) Optical micrograph of an array comprising 1000 individual BPEs having dimensions of 500 × 50 μm. b) Photograph of the cell configuration used to activate this array. c) Luminescence micrograph showing the ECL response of the array when E_{tot} = 85.0 V. d) ECL intensity profile obtained along the rows of BPEs indicated by arrows in (c). (Reprinted with permission from Anal. Chem, 2010, 82, 8766-8774. Copyright 2010 American Chemical Society)

The microelectrochemical array in Figure 1.1.6 a) included 1000 Au BPEs, each of them is 500 μm long and 50 μm wide.[54] Figure 1.1.6 b) is the actual structure of the electrochemical bipolar

cell, which consisted of a glass slide microfabricated with 1000 Au BPE in the middle of the cell filled with ECL solution and two driving electrode connected with two clamp. When sufficient voltage (E_{tot} = 85 V) was applied, faradaic reactions were triggered at two sides of electrodes, and the light from the anode of BPEs can be observed in Figure 1.1.6 c).[54] The uniform ECL intensity from three different rows demonstrate the viability and feasibility of this sensing platform for future test and application.[54] One drawback of this device is that it would be contaminated by the products from driving electrodes, which may dissolve in the electrolyte solution and affect the reactions on the BPEs.[68]

One of the disadvantages of this setup (also called open configuration system) is the interference between reporting materials and targeting materials. In order to prevent it, Wang's team developed a novel sensing platform based single or multichannel closed bipolar system obtaining 100% efficiency in theory.[11, 12] Based on this design, a higher current efficiency and ECL efficiency were reported, another advantage is eliminating the noisy signal from the driving electrode shown in Figure 1.1.7.[11] The good result with detection of TPrA, dopamine, H_2O_2, and $K_3Fe(CN)_6$ based on this device indicated that it is a promising and powerful bipolar electrochemical system in the field of electrochemical analysis.[11]

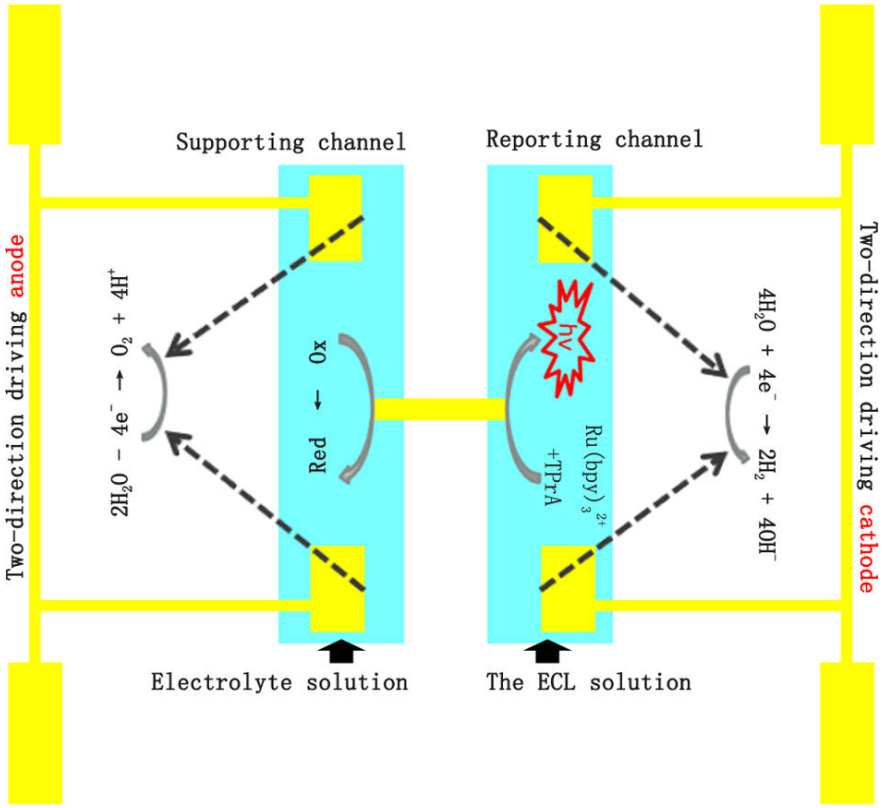

Figure 1.1.7 Fundamental Principle of the Dual-Channel Bipolar ECL Sensor (Reprinted with permission from Anal. Chem. 2013, 85, 5335−5339. Copyright 2013 American Chemical Society)

Figure 1.1.8 is the fundamental structure of BP-LED-E, which integrated one light emitting diode (LED) into a split bipolar electrode.[69] Because very high current efficiency can be obtained in this device, lower voltage is required to trigger the reactions and the light is easier to be observed.[69] In addition, one advantage of the device is that it is simple, reusable and cheap by replacing expensive luminescent agent.[69]

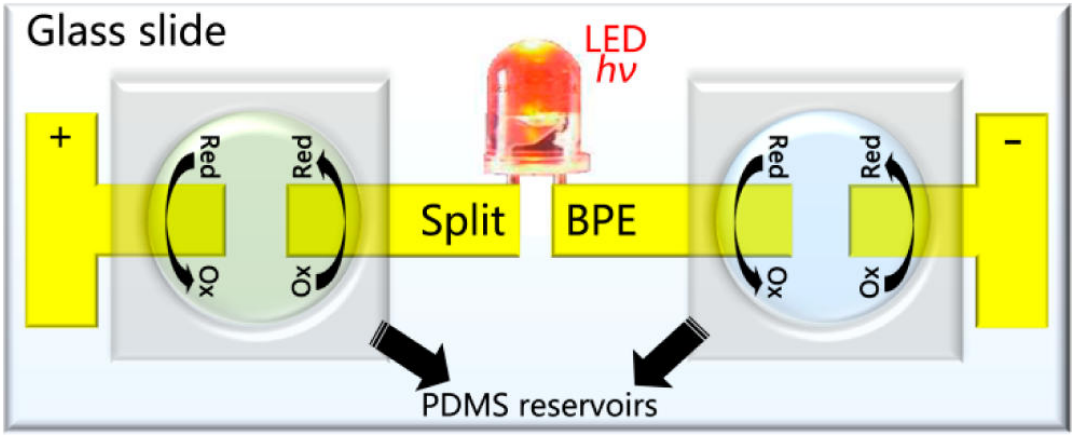

Figure 1.1.8 Fundamental structure of bipolar LED electrode (BP-LED-E) (Reprinted with permission from Anal. Chem. 2015, 87, 4612–4616. Copyright 2015 American Chemical Society)

Different concentration of H_2O_2 and AA were added into four anodic cell of BP-LED-E array and the other sides were filled with phosphorous buffer (0.1 M, pH 7.4).[69] It was found that the LED light intensity processed by PhotoShop histogram was related linearly with the logarithm values of them in Figure 1.1.9 a, b.[69] Another example is different concentration of glucose pretreated with 1 mg/mL glucose oxidase (GOD) in a pH = 6.0 solution incubated in a 37 ℃ water bath for 30 mins.[69] The light intensity obtained in the same way with the detection of H_2O_2 in Figure 1.1.9 c.[69] In order to know the selectivity of the method, four different materials (lactose, maltose, fructose and glucose) were detected simultaneously and the result in Figure 1.1.9 d demonstrated an excellent selectivity of glucose under the same conditions.[69] PB (0.1 M, pH = 6.0) was placed in the anodic section of the first and third cell, and diluted serum was put in the other two cells in Figure 1.1.9 e, the result showed that no extra noise was produced in the cell including diluted serum.[69] So the sugar level of two blood samples can be rapidly achieved based on the

result.[69] 0.1 mM and 0.6 mM incubated glucose solutions were added in the first and fourth anodic cells, respectively.[69] Blood sample from diabetes and another one from normal person were added in the second and third anodic sample.[69] As expected, the light intensity of the second cell is higher than that of the first cell due to a higher value of glucose in this sample Figure 1.1.9 f.[69] Likewise, the intensity of the third cell was a little weaker than that of the first cell, just because of the absence of glucose in this sample in Figure 1.1.9 f.[69]

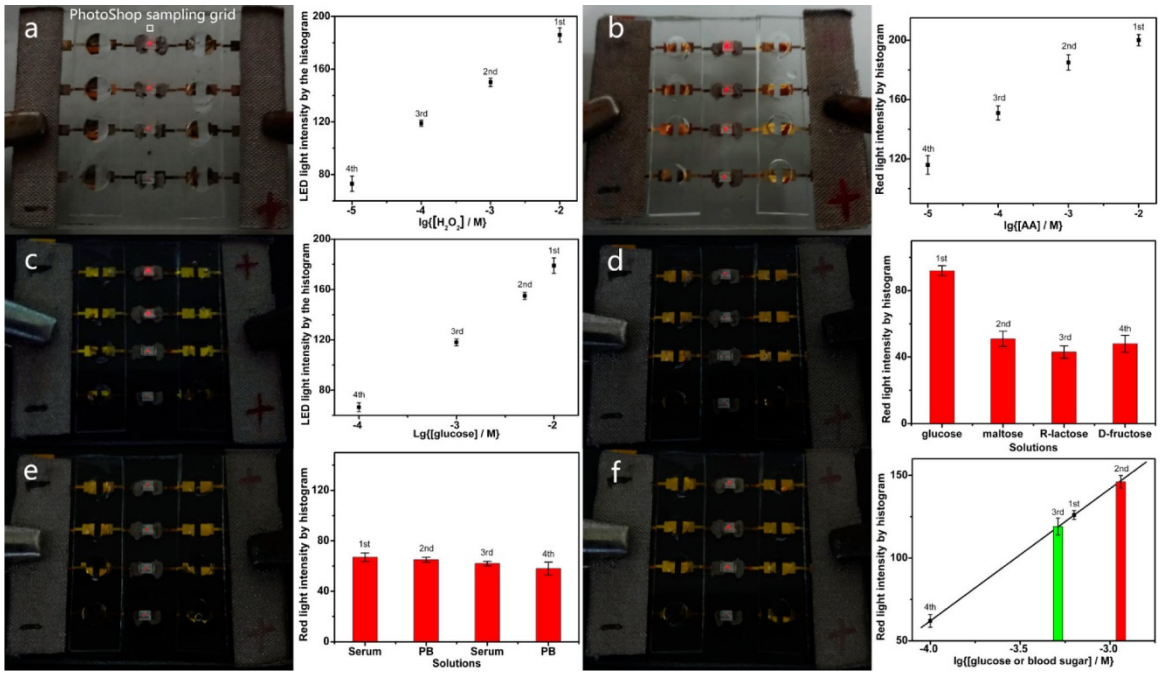

Figure 1.1.9 Determination of different analytes: naked-eye sensing images and the red light intensity data obtained from the PhotoShop histogram. (a) H_2O_2; (b) AA; (c) glucose; (d) selectivity toward the glucose; (e) background of the diluted serum; (f) blood sugar test. (Reprinted with permission from Anal. Chem. 2015, 87, 4612–4616. Copyright 2015 American Chemical Society)

This design for detection is very promising and desirable in environmental monitor and daily diagnosis because of low-cost, simplicity, good selectivity, very high electrochemical efficiency and reducibility.[69]

1.1.2.2 Electrochemical analysis based on electrodissolution of bipolar electrode

A new sensing platform was developed by Crooks group, in which metal stripped at the anode part of BPE, corresponding to the charge transferred at the cathode due to charge neutrality.[4, 32, 70]

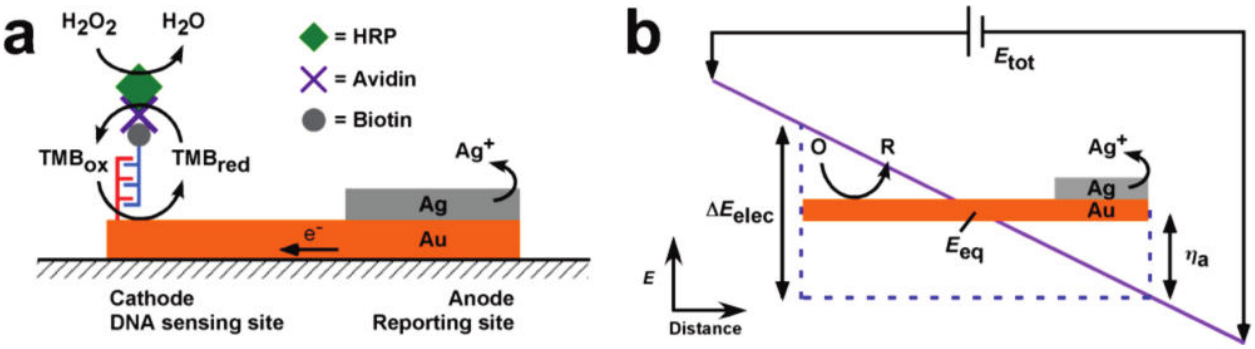

Figure 1.1.10 a) Faradaic reactions occur at both sides of bipolar electrode, one is the sensing part at the cathode of BPE, and the other is the reporting part at the anode of BPE. b) Operation Principle of bipolar electrochemistry was exploited in this study. (Reprinted with permission from J. Am. Chem. Soc. 2010, 132, 9228–9229. Copyright 2010 American Chemical Society)

At the cathode part of bipolar electrode in Figure 1.1.10 a, the oxidation of tetramethylbenzidine (TMB) was activated by hybridization of DNA labeled with horseradish peroxidase (HRP) in the solution containing H_2O_2.[4] If the electrochemical cell was applied enough voltage (E_{tot}), faradaic reactions were triggered at both sides of BPE. Specifically, oxidized TMB was reduced at the cathode of BPE, at the same time, silver present on the anode part of BPE was

oxidized and dissolved in Figure 1.1.10 a.[4] E_{tot} applied on the cell can create a linear potential gradient going through the solution on the bipolar electrode, which keep the bipolar electrode inside float to an equilibrium value relative to the solution.[4] In this sensing platform, the dissolution of Ag is directly correlated to DNA hybridization, which means the rate of oxidation reaction at the anode part of bipolar electrode should be identical to the reduction reaction at the cathode part of bipolar electrode.[4]

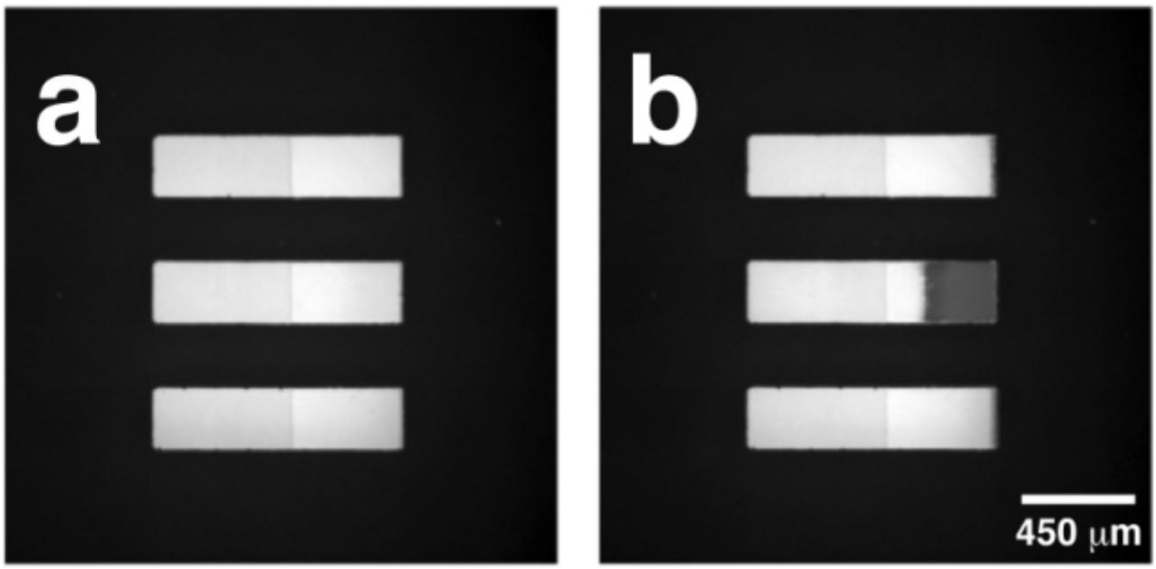

Figure 1.1.11 a) Optical micrographs of the DNA-sensing device showing (middle) DNA-modified and (top and bottom) thiol-modified electrodes (a) before and (b) after E_{tot} = 12.0 V was applied for 90 s. (Reprinted with permission from J. Am. Chem. Soc. 2010, 132, 9228–9229. Copyright 2010 American Chemical Society)

The middle BPE in Figure 1.1.11 modified with 20 nucleotide long, thiol-modified capture DNA was parallelly placed with the other two BPEs modified with 6-mercaptohexanol in the

bipolar electrochemical cell, after that, they were exposed to one solution containing biotin-modified complementary target DNA and then another solution including avidin-functionalized HRP.[4] Acetate buffer (0.1 M), 0.42 mM TMB and 1.3 mM H_2O_2 were added into this cell to carry out the experiment, in which the reduction of H_2O_2 catalyzed by HRP was accompanied with the oxidation of the reduced form of TMB.[4] When the electrochemical bipolar cell was applied sufficient E_{tot}, the produced oxidizing state of TMB was reduced back to reducing state of TMB at the cathode part of bipolar electrode, which triggered the oxidation of Ag at the anode part of bipolar electrode that can be seen by naked eyes.[4]

The advantage of this method by dissolving metal at the anode part of bipolar electrode to quantitatively measure the amount of hybridization DNA is that it not only retains the desirable attributes of BPEs like simpleness, easy manipulation and low-cost, but also possesses new features, for example, the sensitivity and limitation of the detection of this method depends on the thickness and length of Ag coated on the anode part of bipolar electrode.[4]

In this paper, Crooks group evaluated various catalysts by observing the dissolution of Ag coated on the anode part of bipolar electrode.[32] Operation principle of bipolar electrochemistry was exploited in this sensing platform shown in Figure 1.1.12 b, if it was applied sufficient value of E_{tot}, faradaic reactions were trigger on both sides of the bipolar electrode. At the cathode part of BPE, O_2 was reduced along with the dissolution of Ag at the anode part of BPE.[32] As described before, the amount of dissolved Ag was exactly correlated to the O_2 reduced. So the catalytic ability of catalysts can be determined by counting the number of Ag left on the bipolar electrodes

in Figure 1.1.12 a. As the Ag dissolved gradually from the distal end of bipolar electrode, the effective length of bipolar electrode dropped with the result of the decrease in the overpotential between the bipolar electrode to a threshold at which the oxidation reaction of Ag began to stop,[32] that is, how many bonds of Ag dissolved at the anode part of bipolar electrode depends on which kind of electrocatalyst with overpotential to trigger ORR (oxygen reduction reaction) on the cathode part of bipolar electrodes,[32] because Ag dissolution will stop when the overpotential drop over the threshold and not capable to drive electrically faradaic processes.[32]

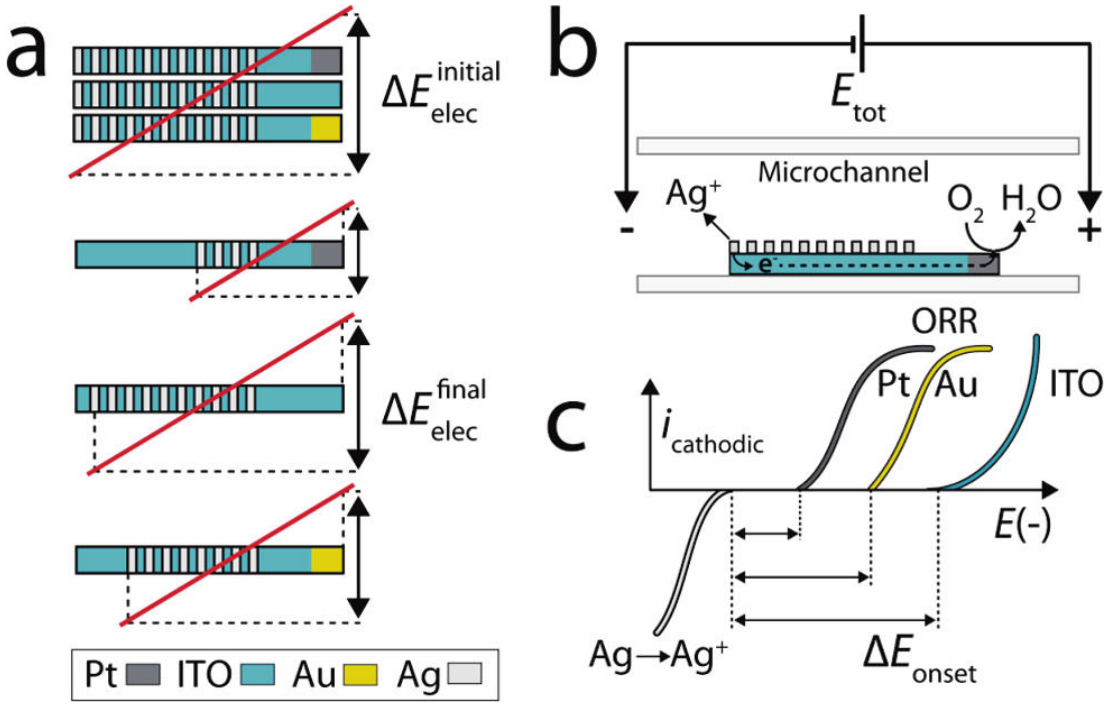

Figure 1.1.12 a) the difference of initial ΔE_{elec} and final ΔE_{elec} b) Electrochemical bipolar cell with a bipolar electrode coated Ag, microfluidic channel, and two driving electrodes connected with Etot c) ΔEonset of different substrate at the same conditions. (Reprinted with permission from J. Am. Chem. Soc. 2012, 134, 863−866.Copyright 2012 American Chemical Society)

There are 26 Ag microband electrodes on the anode part of bipolar electrodes was deposited with a length of 15 μm and a space of 10 μm with each other in Figure 1.1.13 a.[32] Three BPEs were modified in different methods with G_6-OH (Pt_{225}) on the top, G_6-OH (Au_{225}) on the bottom and ITO in the middle, respectively.[32] (225 means 225atoms in the individual catalytic nanoparticles; G_6-OH [sixth-generation poly(amidoamine) (PAMAM) dendrimers terminated with hydroxyl functional groups] was used to encapsulate this catalyst)[32] As expect according to the principle of bipolar electrochemistry, the more bands of Ag on the anode of bipolar electrode will dissolve with the higher catalyst on the cathode part of bipolar electrode. Figure 1.1.13 a is the beginning of the experiment at time 0 s without voltage applied on the electrochemical cell. Upon a sufficient voltage E_{tot} = 10 V was applied, Ag microbands dissolved obviously and can be observed by naked eyes at time 60 s in Figure 1.1.13 b. In Figure 1.1.13 c-f, Ag microbands dissolved continuous at E_{tot} = 4 V until the time 730 s.[32] Due the number of dissolved Ag microbands at the anode part of bipolar electrode is directly correlated to the activity of electrocatalysts present on the cathode part of bipolar electrode, it is easy to tell that the catalytic ability of ORR decreases in this sequence: Pt > Au > ITO.[32] The advantage of this method compared with the literature[4] is that the number of the microbands is very convenient and simple to measure than the length.[4]

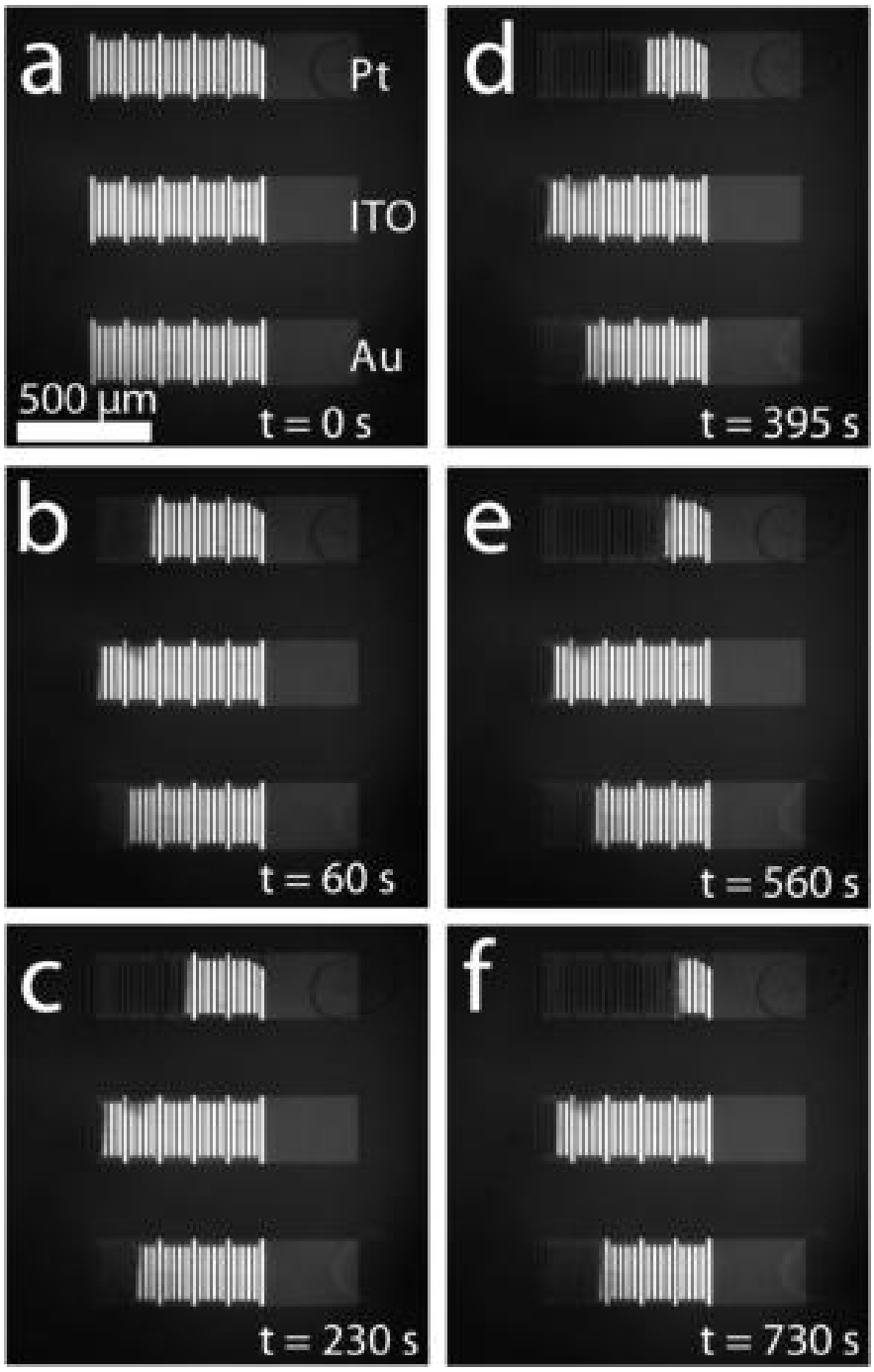

Figure 1.1.13 (a) Optical micrograph of three BPEs. The top BPE was spotted with G6-OH(Pt_{225}), the middle BPE was naked ITO, and the bottom BPE was modified with G6-OH(Au_{225}). The BPEs were placed in a microfluidic channel consisting of a silicone gasket and a poly(dimethylsiloxane)

block. The channel was 12.5 mm long, 3 mm wide, and 0.5 mm tall and filled with air-saturated 0.10 M acetate buffer (pH 4.0). Two Ag/AgCl electrodes were used to apply E_{tot}. (b−f) Micrographs of the three BPEs after application of E_{tot} for the indicated times. E_{tot} was 10.0 V for the first 60 s of the experiment and 4.0 V thereafter. No further Ag electrodissolution was observed after 730 s (f). (Reprinted with permission from J. Am. Chem.Soc. 2012, 134, 863-866.Copyright 2012 American Chemical Society)

1.1.2.3 Material modification, synthesis, and motions

Bradley's group has demonstrated metal or polymer deposition with contactless method on micrometer size particles or carbon nanopipes.[71-78] After that, several groups made a deep research in the deposition using bipolar electrochemistry.

Figure 1.1.14 described the formation of Cu wire between two particles. At the beginning, in Figure 1.1.14 a, H^+ was reduced at the left particle, and copper ions were released from the right particle if there existed electrical field in the aqueous environment.[72] The concentration of copper ions around the right side of left particle increased as time goes on, and the reduction of copper ions occurred and the wire began to grow with the side facing the other particle when there was sufficient copper ions at the right side of left particle.[72] Finally the electrochemical processes stopped and potential differences disappeared between particles as a result of direct connection with each other through the wire produced in Figure 1.1.14 d.[72]

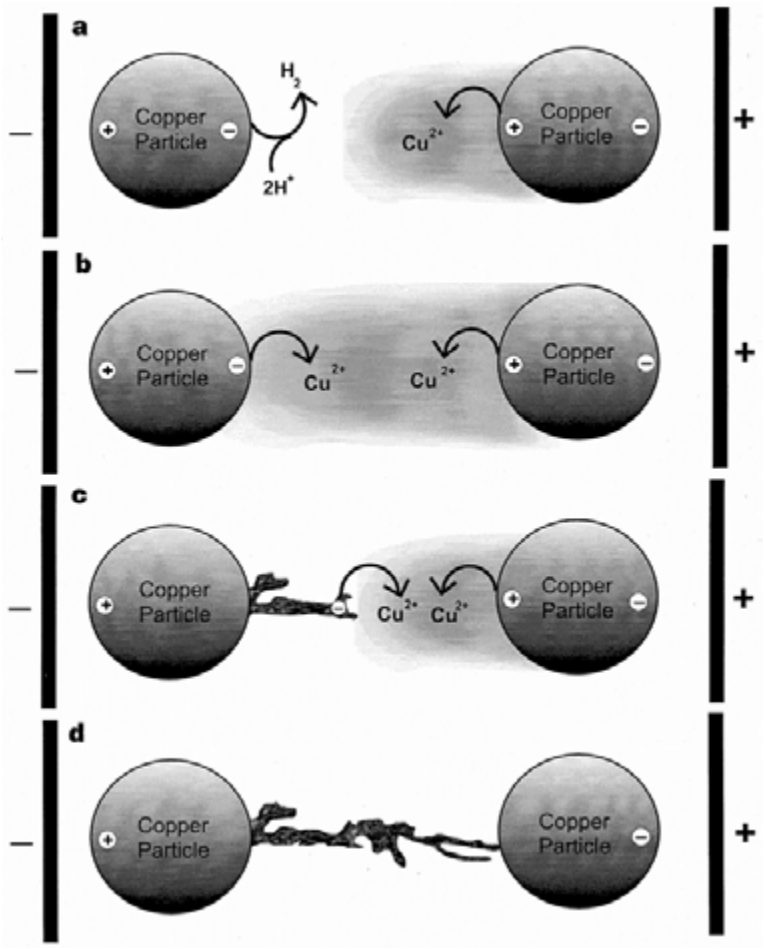

Figure 1.1.14 Diagram of wire formation between two particles under bipolar conditions. a) Two copper particles are placed in an aqueous environment and an electric field is applied. The polarization of each particle is shown. Initially the particle on the right liberates copper ions while the particle on the left reduces water. The shaded area represents a hypothetical distribution of the ionic cloud. (For clarity only the phenomena in the interparticle region are shown). b) When the copper-ion concentration near the particle on the left is high enough electrodeposition occurs and the wire begins to grow on the side facing the other particle. c) Electrodeposition occurs preferentially at the wire tip where cathodic polarization is expected to be highest. d) When the wire reaches the particle on the right, electrical contact is made. At this point there is no potential

difference between the particles and electrochemical processes in the interparticle region cease. (Reprinted with permission from NATURE, 1997, 389, 268-271. Copyright 1997 Nature, Macmillan Publishers Ltd)

Two competing wire branches formed while the solution was applied an electrical field (E = 30.3 Vcm^{-1}), in Figure 1.1.15 a-d, and one interesting phenomenon is that the velocity of growth increased as the wire branch was approaching the other particle.[72] Figure 1.1.15 e-h) illustrated the growth of wire depended on the external electrical field applied in the solution, that is, a higher electrical field can lead to a greater velocity in growth of wire.[72] A thick bushes formed after adding 2.5 mM $Cu(NO_3)_2$, which were located between the particles and at the side close to feeding electrode of the right particle.[72] The shortest route of growing wire was taken by observing two particles slightly slanted relative to the external electrical field.[72]

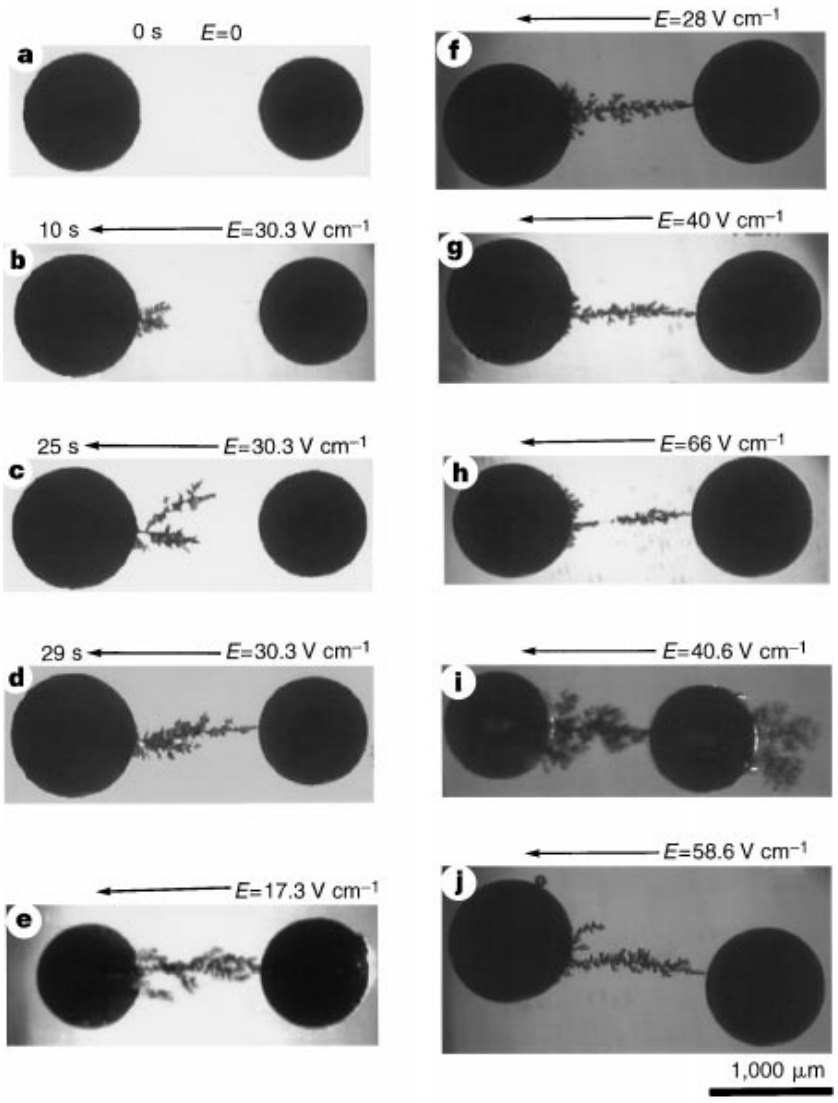

Figure 1.1.15 Wire formation between two copper particles. a) Before application of a 30.3 Vcm^{-1} field in the direction indicated by the black arrow. b) Several wires begin to grow on the left particle after a 10 s induction period. c) Two competing wire branches survive to the interparticle midpoint 25 s after the application of the field. d) Only one branch survives and spans the interparticle gap 29 s after the application of the field and establishes electrical contact between the two particles. We note the great acceleration in growth velocity as the wire approaches the second particle. e–h) Wires grown at increasing field strengths. Notice the reduction in branching

and wire width with increasing fields. i) A wire grown between two particles with externally added 2.5 mM $Cu(NO_3)_2$. Instead of a thin wire forming exclusively between the particles, a thick bush forms both between the particles and on the particle closest to the feeder anode. j) A wire grown between two particles slightly slanted with respect to the external field showing that the shortest possible route was taken. Except for i, the aqueous medium contained 0.1mM H_2SO_4 and 0.01% Nonidet-P40 (Sigma). The feeder electrodes were made of two parallel 1-mm-diameter Pt wires separated by 1.5 cm. (Reprinted with permission from NATURE, 1997, 389, 268-271. Copyright 1997 Nature, Macmillan Publishers Ltd)

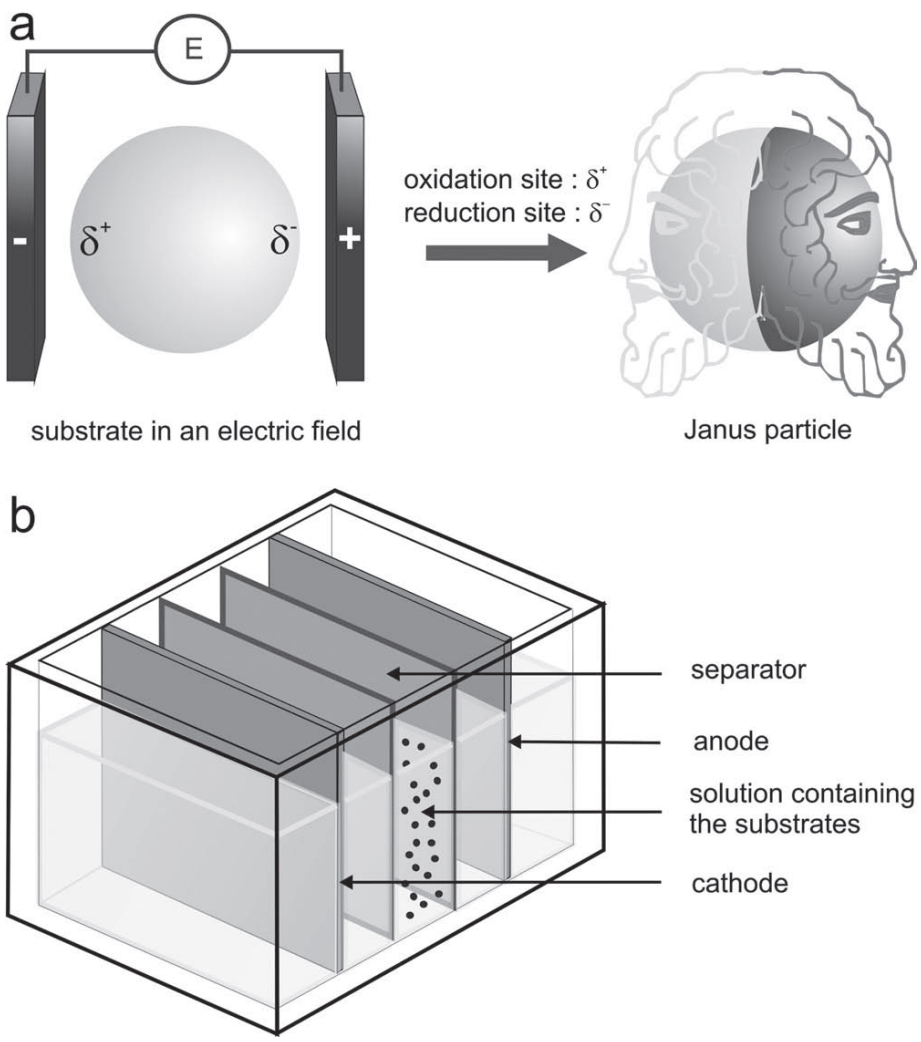

Figure 1.1.16 Bipolar electrodeposition for the synthesis of Janus particles. a) Principle of bipolar electrochemistry: a sufficient polarization of a conducting substrate allows the symmetry to be broken. b) Scheme of the cell used for bipolar electrodeposition. (Reprinted with permission from Adv. Mater. 2012, 24, 5111–5116. Copyright 2012 Wiley-VCH)

Alexander Kuhn's group developed a new device to synthesize Janus particles on which different chemistry or polarity was exhibited on two sides.[61, 79-81] Figure 1.1.16 a is the bipolar electrochemical cell, in which one global substrate was immersed in solution without direct

connection with driving electrode applied external voltage.[61] Two different reactions occur on two opposite sites as long as the electrical field is high enough, as a result, two sides of it can be modified and Janus particle was synthesized.[61] In order to separate the substrates and reagents from the two feeding electrode (gold or platinum plates), two membranes made from sintered glass or polymer as separator were inserted in the middle of the electrochemical cell in Figure 1.1.16 b.[61] As a result, it will last about 2 mins when the cell was applied high voltage before the first bubbles appeared.[61] The materials chosen to be the separator depended on mechanical stability, permeability, and conductivity, which may delay the time of bubble production, reduce the evaporation of solvent, or affect ohmic heating in solution.[61]

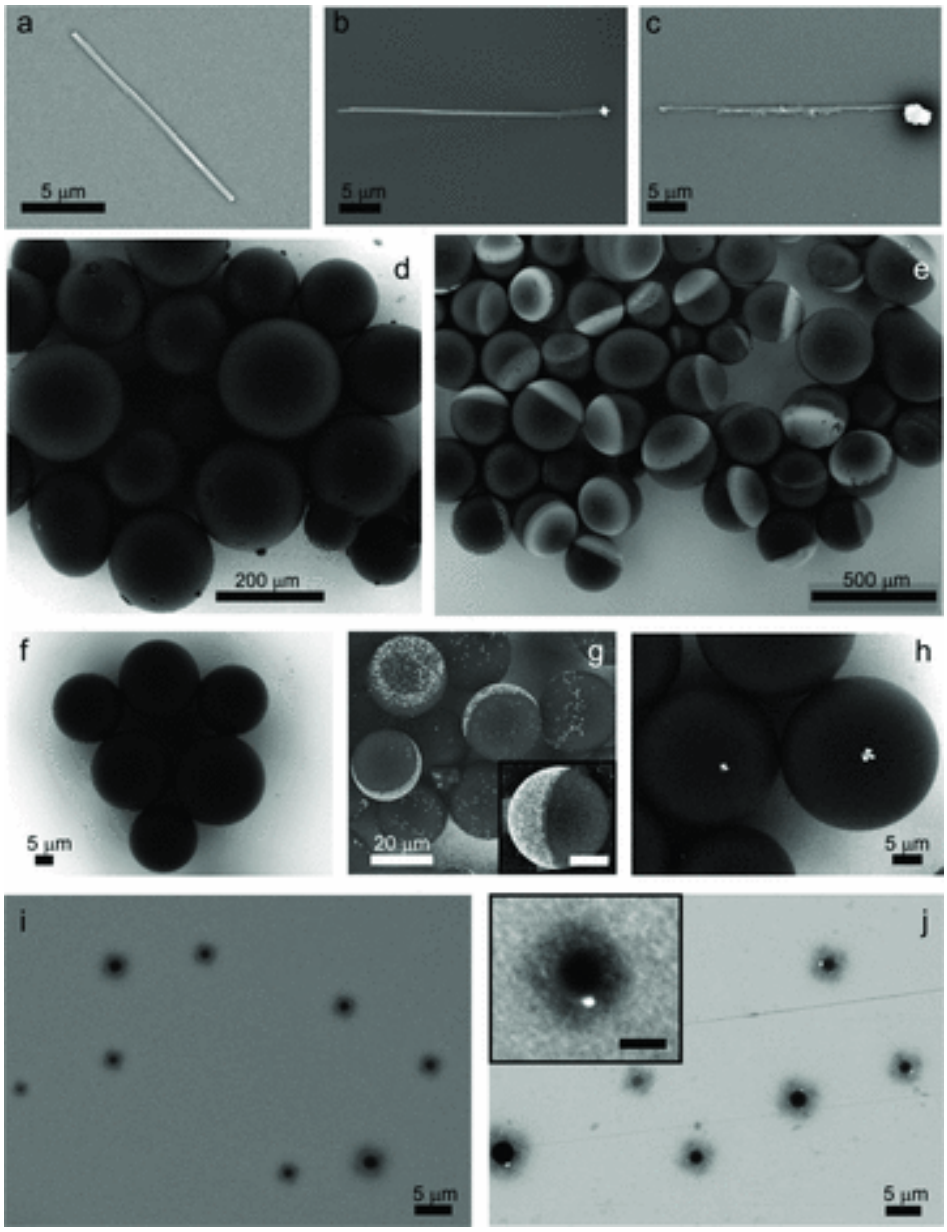

Figure 1.1.17 Anisotropic and isotropic carbon/metal Janus objects. SEM images of the particles before and after bipolar electrodeposition. a) Unmodified carbon tube. b) Carbon tube modified with gold. c) Carbon tube modified with platinum. d) Unmodified glassy carbon beads with diameters ranging from 200 to 400 µm. e) Glassy carbon beads with diameters ranging from 200 to 400 µm modified with gold. f) Unmodified glassy carbon beads with diameters ranging from 20

to 50 μm. g) Glassy carbon beads with diameters ranging from 20 to 50 μ m modified with gold. Inset: Detail of a Janus bead (scale bar represents 10 μm). h) Glassy carbon beads modified with silver. i) Unmodified micrometer-sized glassy carbon beads. j) Micrometer-sized glassy carbon beads modified with gold. Inset: Detail of a micrometer-sized bead modified with gold (scale bar represents 1 μm). (Reprinted with permission from Adv. Mater. 2012, 24, 5111–5116. Copyright 2012 Wiley-VCH)

Carbon tube/gold or platinum Janus objects were synthesized according to the above method in 1 mM $AuCl_4^-$ and 10 mM $PtCl_6^{2-}$, respectively, in Figure 1.1.17 a-c.[61] Different sizes of carbon beads were used as substrates to synthesize Janus particles with gold or platinum deposition. As mentioned above, the amount of deposition is related to electrical field, the concentration of solution, the length of bipolar electrochemical cell, geometrical configuration of substrates and intrinsic kinetics of redox reactions occurring on both sides of substrates.[61] As a consequent, the solution with a lower conductivity can lead to the increase of polarization and the fraction of current,[61] because the conductivity of bipolar electrode higher than the surrounding medium will favor the redox reactions on the bipolar electrode.[54, 82] Another issue which should be concerned is that adding gelling agents can slow down the rotational movement by increasing the viscosity of the solution involved.[61] There are two kinds of gelling agent, agarose and ethyl-cellulose. Agarose was normally added in water to do the modification in Figure 1.1.17 g-i, however, it may cause a problem that a spontaneous reduction of tetrachloroaurate which is not desired occurred in

the case of the washing process requiring a heating step.[61] In Figure 1.1.17 e, the rate of output (80%) was achieved after counting the number of Janus beads and the total number of beads on SEM images.[61] It should be noted that gold is easier to deposit on beads than silver because gold is a noble metal, and smaller size of carbon beads need higher electrical field than bigger size of carbon beads to perform the same ratio of deposition because bigger size particles can obtain higher fraction of external voltage .[61]

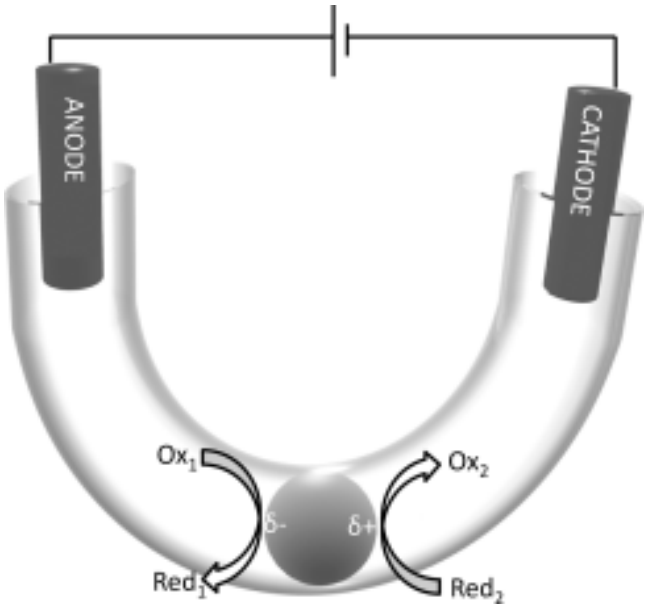

Figure 1.1.18 Representation of the polarization of a conducting spherical particle in an electric field between two feeder electrodes. Oxidation and reduction reactions occur at the anodic and cathodic parts of the object, respectively. (Reprinted with permission from Chem. Eur. J. 2013, 19, 1577–1580. Copyright 2013 Wiley-VCH)

It is the first time to synthesize Janus-type beads by Alexander Kuhn's group, on which diazonium salts were reduced to form an organic layer in a bipolar electrochemical cell.[21] Figure

1.1.18 is the bipolar electrochemical cell, in which one bead was introduced into a capillary and physically block the capillary with advantage in the stability of bead in electrical field due to approximate same diameter of them.[21] Redox reactions were triggered on the polarized bead (BPE) in bipolar electrochemical cell upon it was applied sufficient external voltage.[21] The potential drop generated by electrical field between two ends of bead is in proportion with the effective length of particle.[83]

As explained before, diazonium electrografting is possible to the bead as BPE in bipolar electrochemical cell when the applied potential on it is bigger than a threshold value which is at least 1313 V m^{-1} in this experiment.[21] The first step of modification is that 4-nitrobenzenediazonium tetrafluoroborate in aqueous hydrochloric acid (HCl, 1 mM) was reduced by one electron transfer at the cathode pole of the bead as the BPE when sufficient potential drop goes across it.[21] The resulting nitrobenzene radical attached to the cathodic part of glassy carbon by a hydrogen abstraction mechanism, and then the remaining functional nitro group was converted to amino group at E = −0.60 V vs Ag/AgCl in Figure 1.1.19 a.[21, 84] The second step of it is that the functional amino groups (NH_3^+) interacted with the citrate anions in terms of electrostatic effects, which can stabilize the colloidal gold nanoparticles capped by citrate in Figure 1.1.19 b.[21, 85, 86] Finally, this group prepared glassy carbon bead with 4-aminobenzene layer labeled by gold nanoparticles revealed by SEM.[21]

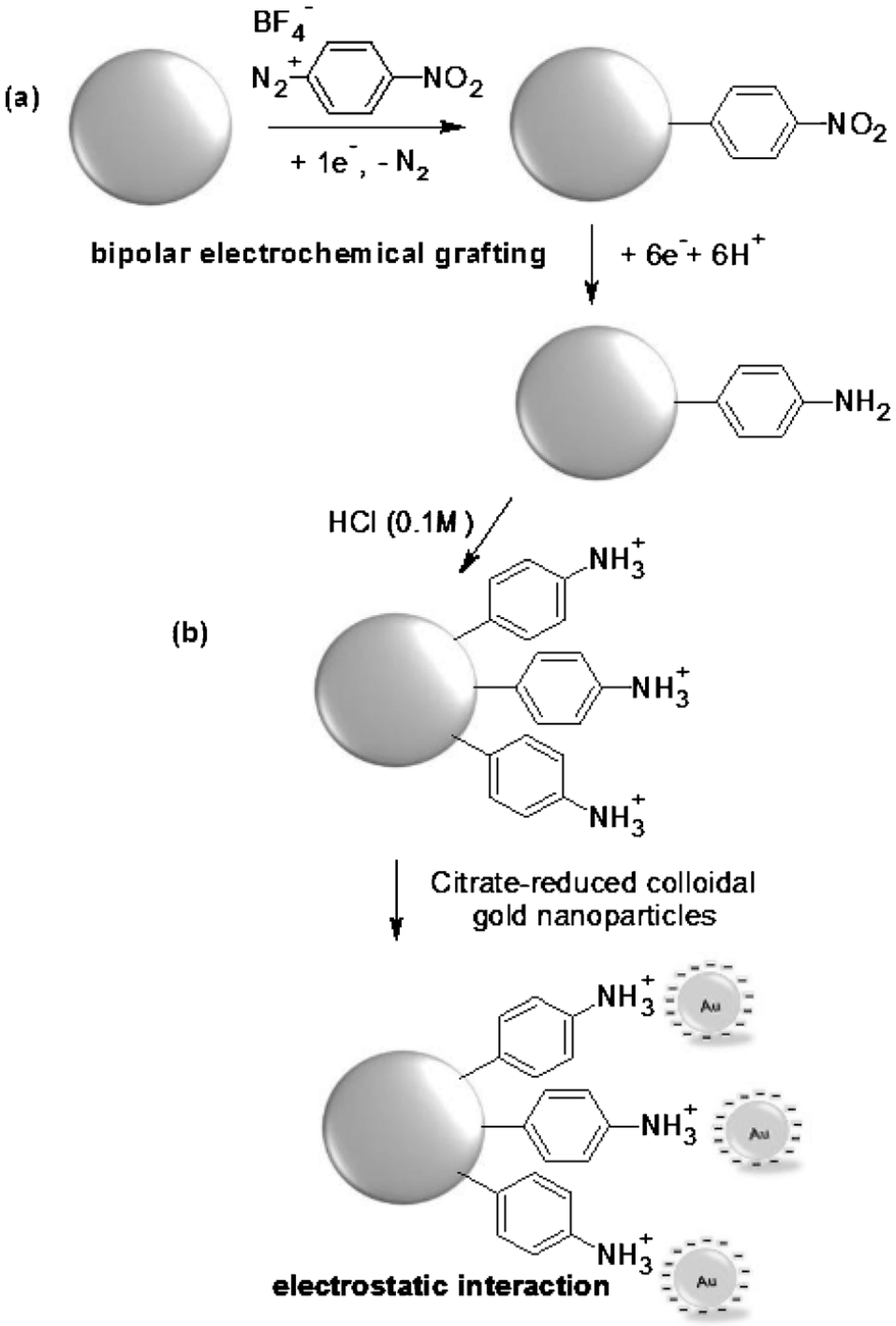

Figure 1.1.19 The modification of a glassy carbon bead by a) asymmetric electrografting of 4-aminobenzene in aqueous HCl solution, followed by b) electrostatic interaction with citrate-capped colloidal gold nanoparticles. (Reprinted with permission from Chem. Eur. J. 2013, 19, 1577–1580.

Copyright 2013 Wiley-VCH)

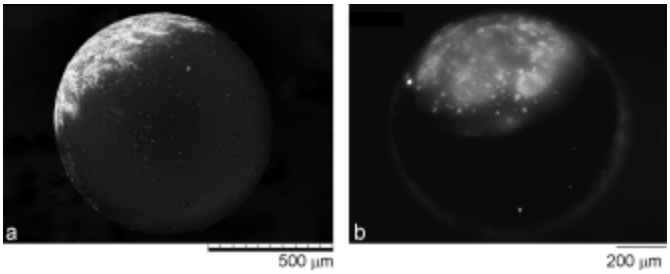

Figure 1.1.20 a) Scanning electron micrograph of asymmetrically modified 630 mm glassy carbon beads by applying an electric field of 4 kVm^{-1} for 90 seconds in an aqueous solution of 5 mM 4-nitrobenzenediazonium tetrafluoroborate/1 mM HCl and subsequent interaction with a citrate-reduced colloidal gold solution. b) Fluorescent micrograph of asymmetrically modified 630 mm glassy carbon beads by applying an electric field of 4 kVm^{-1} for 120 seconds in an aqueous solution of 5 mM 4-aminobenzoic acid/10 mM $NaNO_2$/10 mM HCl and subsequent reaction with EDC and fluoresceinamine. (Reprinted with permission from Chem. Eur. J. 2013, 19, 1577–1580. Copyright 2013 Wiley-VCH)

Figure 1.1.20 indicated 4- nitrobenzenediazonium salts were successfully reduced on the cathode portion of glassy carbon bead by observing the gold particles on the SEM images.[21] The formation of a 4-aminobenzene layer on glassy carbon bead can also be verified by the presence of fluorescence at one side of glassy carbon shown in Figure 1.1.20 b.[21]

Alexander Kuhn's group also study the motions of bipolar electrodes based on bipolar electrochemistry,[22, 24, 59, 87-91] after other group's work in motions of micro particles.[92-98]

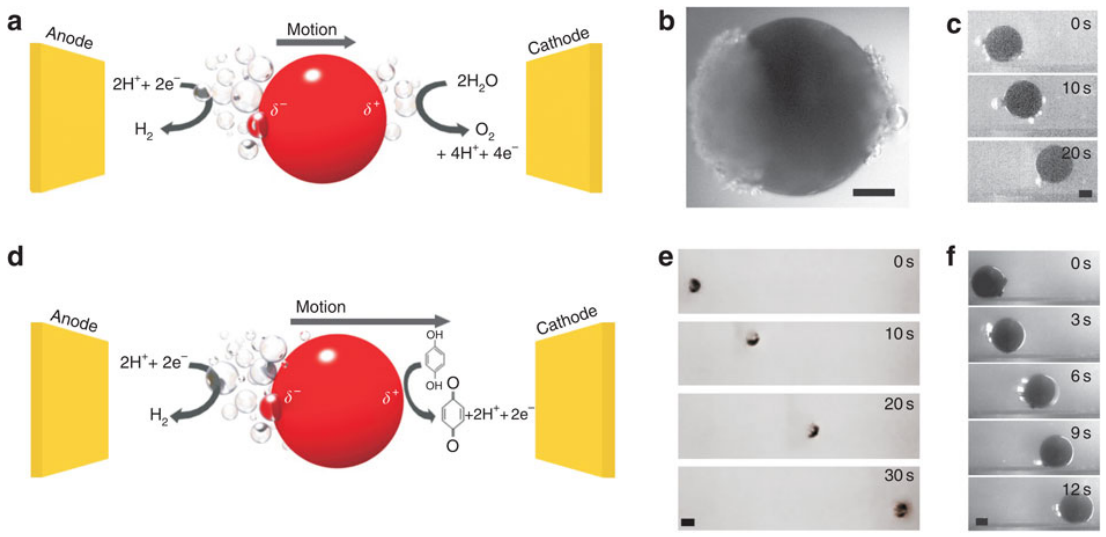

Figure 1.1.21 Linear motion of spherical objects. (a–c) Competing bubble production. (a) Scheme of the water splitting by bipolar electrochemistry. (b) Optical micrograph of a stainless steel 1 mm spherical metal particle exposed to a 1.6 kV m^{-1} electric field in aqueous 24 mM H_2SO_4. The left part of the bead is the cathodic pole where H_2 bubbles are produced and the right part is the anodic pole where O_2 bubbles are produced. Scale bar, 250 μm. (c) Translational motion generated with a 285-μm glassy carbon sphere in a PDMS microchannel exposed to a 5.3 kV m^{-1}electric field in aqueous 7 mM H_2SO_4. Scale bar, 100 μm. (d–f) Quenching of O_2 bubble production. (d) Scheme of proton reduction and HQ oxidation. (e) Translational motion generated on a 1-mm stainless steel bead exposed to a 1.3 kV m^{-1} electric field in 24 mM HCl and 48 mM HQ. Scale bar, 1 mm. (f) Translational motion generated with a 275-μm glassy carbon sphere in a PDMS microchannel with a 4.3 kV m^{-1} electric field in an aqueous solution of 7 mM HCl and 14 mM HQ. Scale bar, 100 μm. (Reprinted with permission from Nature communication, 2011, 2, 535. Copyright 2011 Nature communication, Macmillan Publishers Ltd)

Gas bubbles were produced at both sides of 1-mm metal particle that is a bipolar electrode located in a 1.6 kVm^{-1} electric field in Figure 1.1.21 a.[22] Specifically, protons in solution were reduced to hydrogen gas at the cathode part of BPE, and the water split to oxygen gas was triggered at the anode part of BPE, however, the electron production or consumption of these two reactions due to maintain electroneutrality at the bipolar electrode.[22] In this experiment, the amount of hydrogen gas produced at the cathode part of BPE is twice than it of oxygen generated at the anode part of BPE,[22] as a consequence, the bipolar electrode in the bipolar electrochemical cell was propelled towards to the cathode with the speed of 20 μms^{-1} because of this asymmetric gas production in Figure 1.1.21 a-c.[22] In order to know how reactions on bipolar electrode affect the speed of it, a low redox potential of the hydroquinone/benzoquinone (HQ/BQ) was used to take place of water spilt reaction at the anode part of BPE.[22] As shown in Figure 1.1.21 d, at the left side of the bipolar electrode, hydrogen ions were reduced, on the contrary, HQ was oxidized to BQ at the right side of it. Based on the same reason as above, the bipolar electrode located in a polydimethysiloxane (PDMS) microchannel was pushed towards the cathode at the speed of 62 μms^{-1}, which is expected to be higher than the speed ($20\mu ms^{-1}$) of bipolar electrode without adding HQ in Figure 1.1.21 d-f.[22] There are three main parameters that can influence the measured velocity by a change of reaction kinetic or thermodynamic reactions, 1) The potential difference of the bipolar electrode, 2) pH value, 3) The concentration of HQ added.[22] Another issue should be concerned is that the friction on bipolar electrode will increase because of the surface to volume ratio when the size of bipolar electrode is becoming very small, and also Brownian motion may

play an important role in the motion of BPE, which is needed to be overcome by driving force.[22]

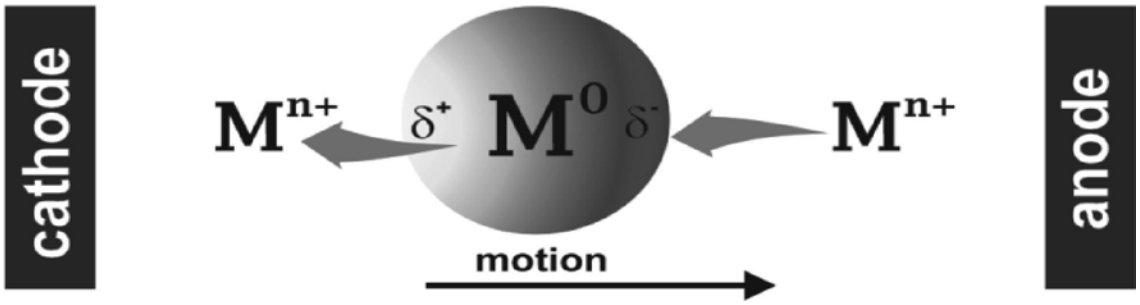

Figure 1.1.22 Dynamic Bipolar Self-Regeneration Principle (Reprinted with permission from J. AM. CHEM. SOC. 2010, 132, 15918–15919. Copyright 2010 American Chemical Society)

An ingenious work in self-regeneration movement was also done by Alexander Kuhn's group in bipolar electrochemistry.[89] The principle of dynamic bipolar self-regeneration is illustrated in Figure 1.1.22, in which the particle of interest was located without direct connection with driving electrodes which were connected to an external voltage in a bipolar electrochemical cell. When sufficient voltage was applied, metal dissolved at the anode of BPE, and metal deposited at the cathode of BPE to maintain the electroneutrality, which can propel the motion of a metallic object.[89]

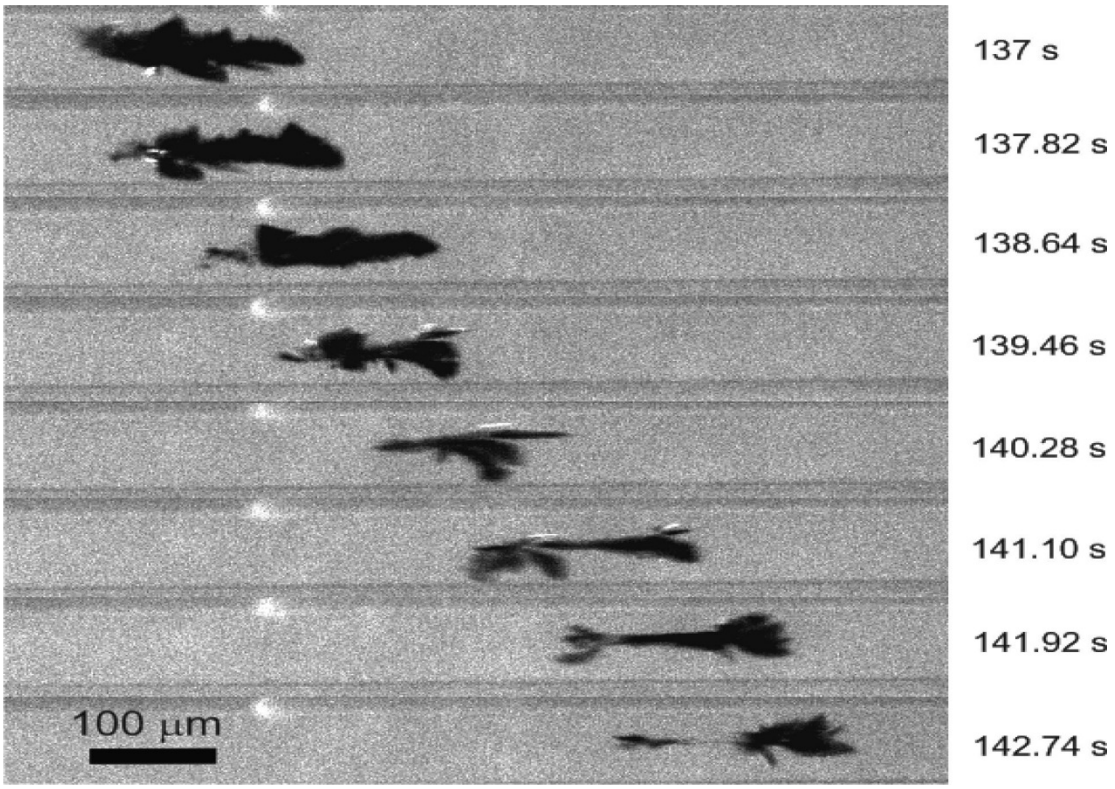

Figure 1.1.23 Optical micrographs of a zinc dendrite in a glass capillary filled with a zinc sulfate solution at pH ≈ 5 under the influence of an external electric field (Reprinted with permission from J. AM. CHEM. SOC. 2010, 132, 15918–15919. Copyright 2010 American Chemical Society)

One zinc dendrite was used as a bipolar electrode isolate in a 100 μm inner diameter capillary, which was filled with a zinc sulfate solution with an adjustable pH value by adding small amount of acid, preventing zinc oxide from happening in the experiment.[89] Located in an external electric field (7 kVm^{-1}), zinc dendrite was propelled with a speed of 80 μms^{-1}, that is because redox reactions were triggered on this zinc dendrite in Figure 1.1.23.[89]

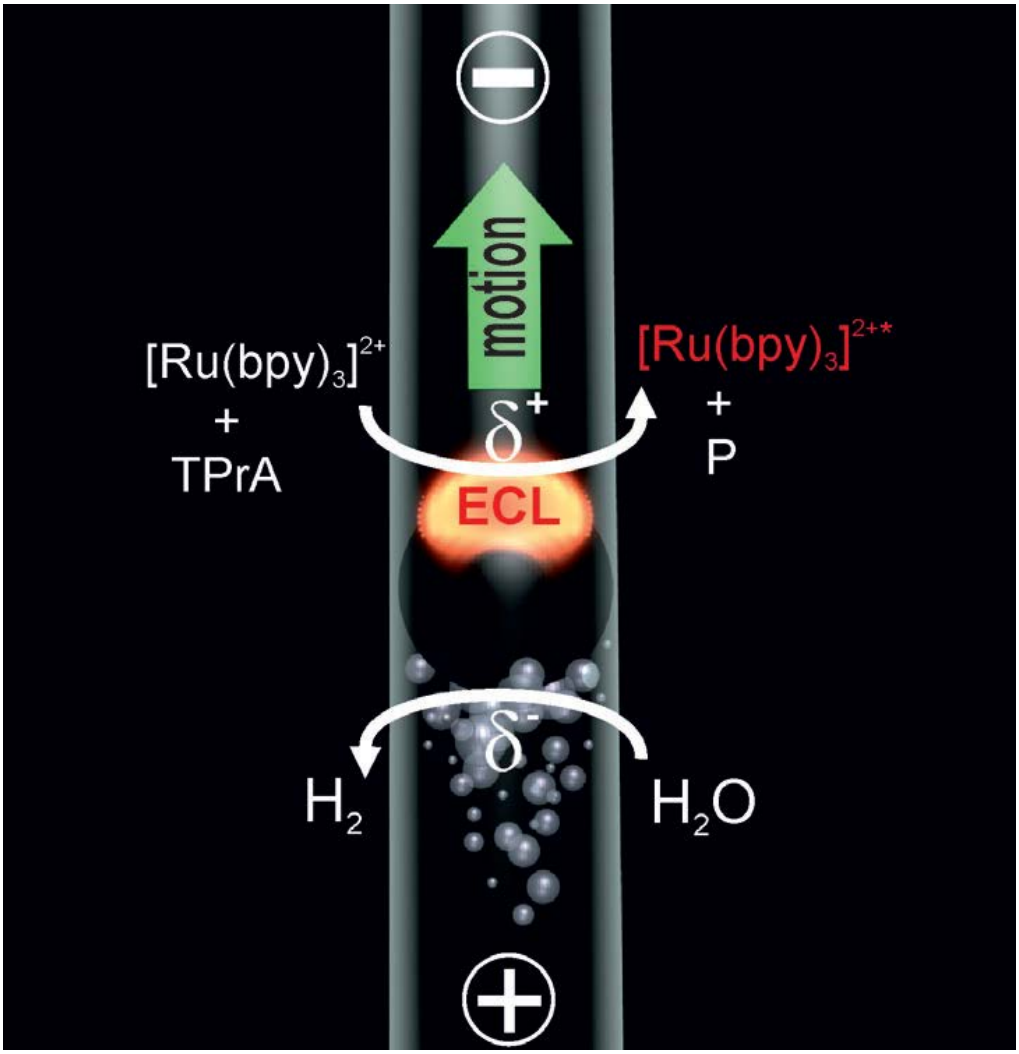

Figure 1.1.24 Asymmetric light-emitting electrochemical swimmer. Simultaneous reduction of H_2O at the cathodic pole (bottom of the bead) and oxidation of ECL reagents at the anodic pole (top of the bead) induces both motion and light emission from the bead in a glass capillary. P corresponds to a side product of the TPrA radicals formed during the ECL process. (Reprinted with permission from Angew. Chem. 2012, 124, 11446 –11450. Copyright 2012 Wiley-VCH)

One interesting experiment has been also done by them in motions combined with ECL by

the use of bipolar electrochemistry.[59] Figure 1.1.24 demonstrated a glassy carbon (GC) was chosen as the "swimmer" which can move up when the glass cell was applied sufficient external voltage.[59] Specifically, as shown in Figure 1.1.24, water split was occuring at the negative charged pole of GC and on the other side light emission reaction was generated simultaneous in order to maintain electroneutrality.[59] The hydrogen generated in this process was the fuel which can propel the GC move up, and at the same time the movement was accompanying with light emission.[59] The speed or the levitation height should be related to external electrical field, the diameter of bead, ambient environment, and intrinsic properties like density.[59]

1.1.2.4 Concentration enrichment and separation

Concentration enrichment has been done a lot with vairous methods like electric field gradient focusing (EFGF), electrophoresis, and electrokinetic supercharging.[99-112] Crook's group spent a lot interest inelectric field gradients for enrichment (EFGF), in which the migration of charged analytes is related to the electrical field gradient generated by a driving voltage across a channel.[37, 113] And they have done a lot of work in material erichment of separation using bipolar chemistry.[37, 100, 114-118]

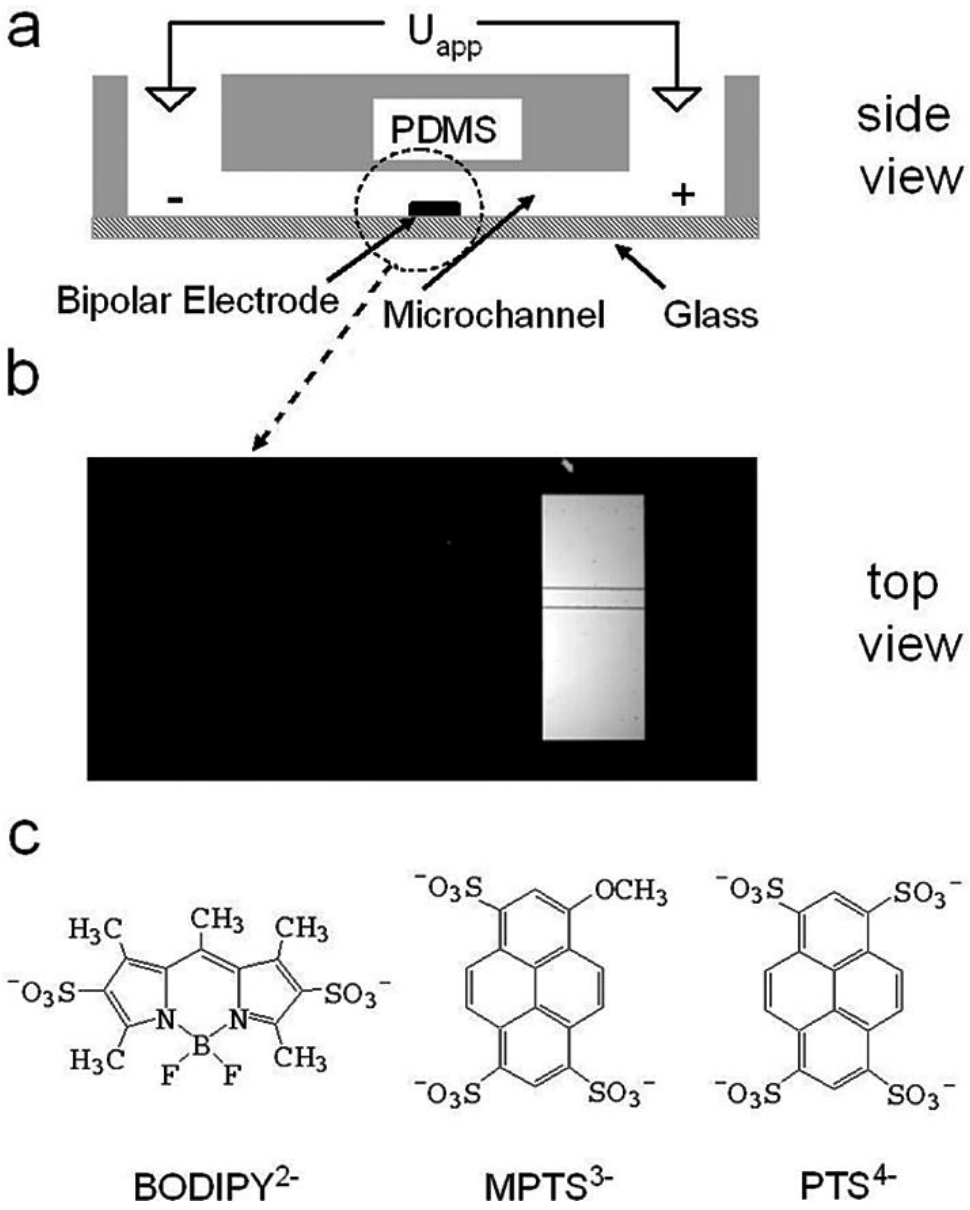

Figure 1.1.25 a) Schematic illustration of the fluidic system used in these experiments, b) optical micrograph of the BPE region of a typical device, and c) structures of the anionic dyes (tracers). (Reprinted with permission from Anal. Chem. 2009, 81, 8923-8929. Copyright 2009 American Chemical Society)

Figure 1.1.25 a-b is the configuration of bipolar electrochemical cell, in which BPE was

situated in the middle of a channel in a bipolar electrochemical cell, and Figure 1.1.25 c illustrated the structures of the three fluorescent dyes that was used as tracers in this paper.[37]

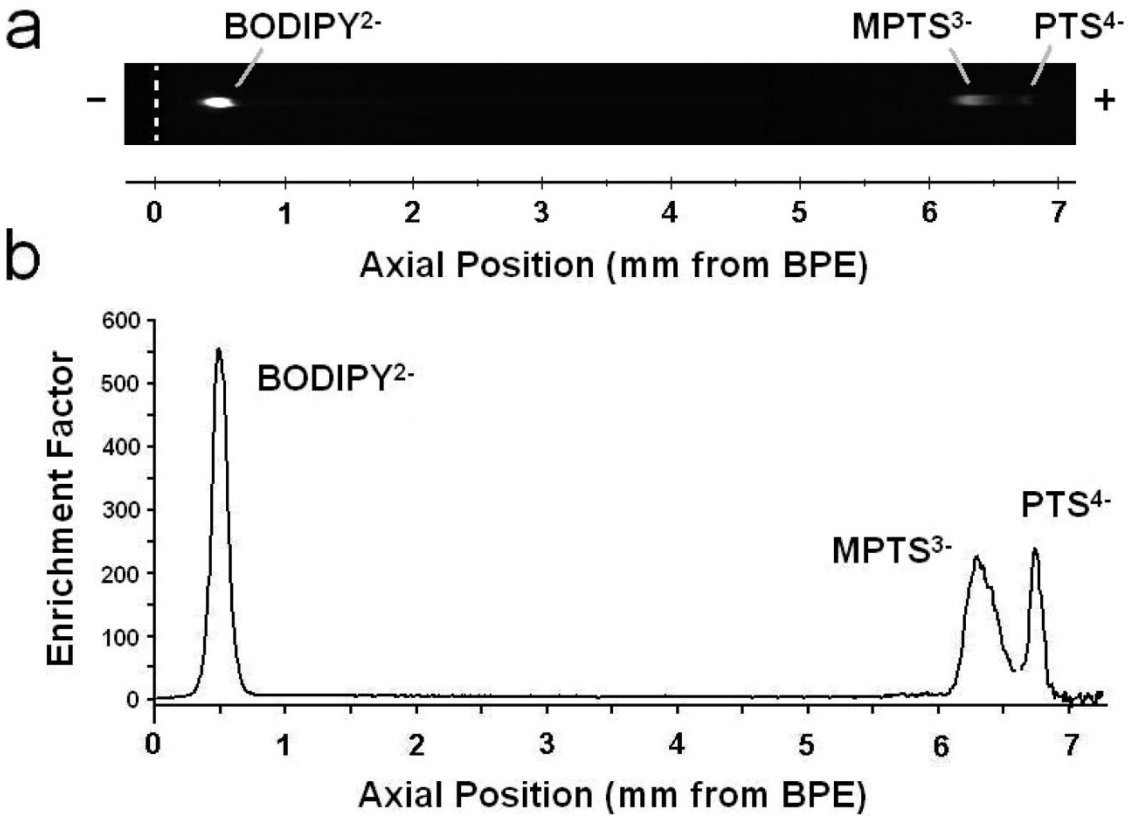

Figure 1.1.26 (a) Fluorescence micrograph (top view) showing separation of $BODIPY^{2-}$, $MPTS^{3-}$, and PTS^{4-} in 5.0 mM TRIS 200 s after application of Uapp) 40 V (XF115-2 and XF02-2 filter sets overlaid, see Supporting Information) in a 12 mm-long, Pluronic-modified channel. (b) Plot of enrichment factor vs axial location corresponding to part a. (Reprinted with permission from Anal. Chem. 2009, 81, 8923-8929. Copyright 2009 American Chemical Society)

Negative charged fluorescent dyes moved to left because of electroosmotic flow (EOF), but they began to accumulate at the time when electrophoretic force equals to the EOF due to the

electric field gradient generated by the cathodic part of BPE in figure 1.1.26.[100] The three enriched zones can be observed after 100 s if the driving voltage went up to 90 V in the solution containing 5.0 mM TRIS, 0.1 μM $BODIPY^{2-}$, 0.4 μM $MPTS^{3-}$, and 0.8 μM PTS^{4-}.[37] After 200 s, three resolved analyte zones can be seen and their enrichment factors are 560, 225, and 245 for $BODIPY^{2-}$, $MPTS^{3-}$, and PTS^{4-}, respectively.[37] The experiment provided a promising, simple and low-cost method to separate different materials using bipolar electrochemistry.

1.2 Electrochemiluminescence

Electrochemiluminescence which is also called electrogenerated chemiluminescence is a process that excited states generated on the surface of the electrode under a certain voltage from another electro-active species can emit light to relax to ground state.[64] It was the first time to observe electrochemical luminescence on Rubrene, DPA (9,10-diphenylanthracene) and related compounds in the 1960's.[119, 120] Bard's group found the electrochemical behaviour of tris-2,2-bipyridylruthenium (II) ($Ru(bpy)_3^{2+}$) that is widely used nowdays not only in the industry but also in analytical research in 1973.[121] Since then, electrochemiluminescence has been extensively used in the area of capillary electrophoresis, nanostructured materials, organic or inorganic materials, DNA probe, immunoassay, small molecules detection and functional nucleic acid sensors, because it has the advantages of simplicity, high selectivity and sensitivity, and low background, in addition, the mechanism and application of ECL has been compresively studied in recent review papers.[64, 122-135]

A intermediate capable of emitting light on the surface of an electrode is produced by electron

transfer from one material in ground state in the process of electrochemiluminescence.[64]

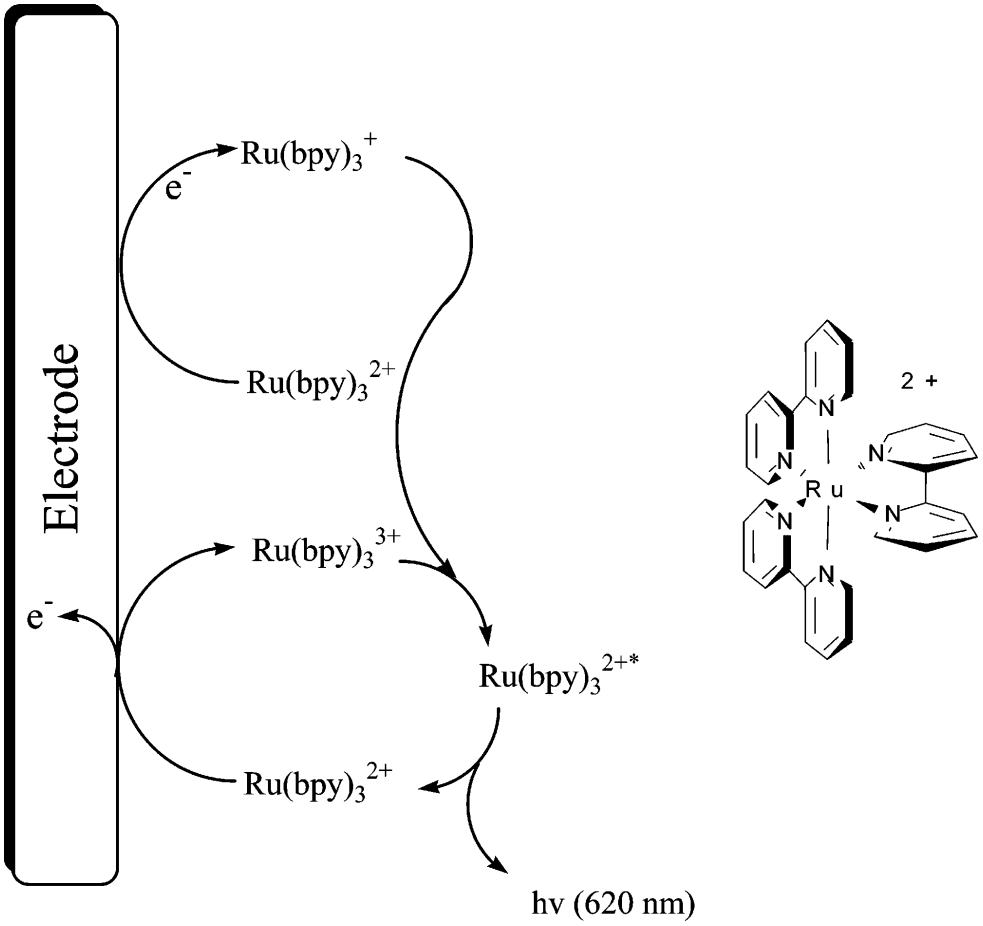

Figure 1.2.1 Structure of $Ru(bpy)_3^{2+}$ and proposed mechanism for $Ru(bpy)_3^{3+}/Ru(bpy)^{+}$ ECL system. (Reprinted with permission from Chem. Rev. 2004, 104, 3003-3036. Copyright 2004 American Chemical Society)

Figure 1.2.1 illustrated the production of light by generating oxidized $Ru(bpy)_3^{3+}$ and reduced $Ru(bpy)_3^{+}$ on an electrode in tetrabutylammonium tetrafluoroborate/acetonitrile solution.[64, 136] $Ru(bpy)_3^{2+*}$ was produced in the reaction of $Ru(bpy)_3^{3+}$ and $Ru(bpy)_3^{+}$, which represented an intermediate that can emit light.[64]

The mechanism of ECL normally involved annihilation ECL, coreactant ECL, and cathodic luminescence.[64] Annihilation ECL was illustrated in Figure 1.2.1, in which two species (oxidized and reduced) generated by alternate pulsing of the electrode potential would react with each other and create an intermediate that can emit light.[64, 135] Coreactant ECL involved electrochemical reactions between intermediate from coreactant and oxidized or reduced ECL luminophore and then emitted light.[64, 137] The process of it normally included four procedures, 1) redox reactions of coreactants and ECL luminophore at one electrode, 2) homogeneous chemical reactions, 3) the formation of excited species, 4) relaxation and emit light.[136] $C_2O_4^{2-}$/$Ru(bpy)_3^{2+}$, $S_2O_8^{2-}$/$Ru(bpy)_3^{2+}$, and TprA/$Ru(bpy)_3^{2+}$ systems are the commonly used in ECL experiment, and luminol is also an option to produce ECL.[136]

1.3 Raman spectroscopy

Inelastic light scattering was proposed by Adolf Smekal in 1923 and then the Raman scattering phenomenon was first found by C. V. Raman in 1928. The shift in wavelength of emitted photon away from the incoming light can be observed when a photon interacted with a molecule.[138] Raman scattering is an inelastic scattering resulting in two kinds of photons, one is called stokes Raman scattering with lower energy than the incident light, and another one is called anti-stokes Raman scttering with higher energy than the incident light. The proprietary characteristics of every moleclue in Raman spectrum is owing to the characteristic vibrational energies from different functional groups in the molecle.[138] The intensity of raman scattering depends on the change of dipole-electric dipole polarization, for which aromatic molecules has a greater Raman scattering

than aliphatic molecules.[138] Van Duyne's group discovered a magnified Raman scattering of pyridine which was adsorbed on a roughened silver substrate which can produce very strong electromagnetic fields when visible light excited the localized surface plasmon resonance of nanoscale location on silver,[139] which provided a new technique for scientists study and analyze unknown materials in chemistry, biochemistry, physics, and materials.[140-150] Confocal Raman spectroscopy, as one of Raman techniques, offers us the possibility to analyze a sample in the Z-axis and also improve the spatial resolution in it.

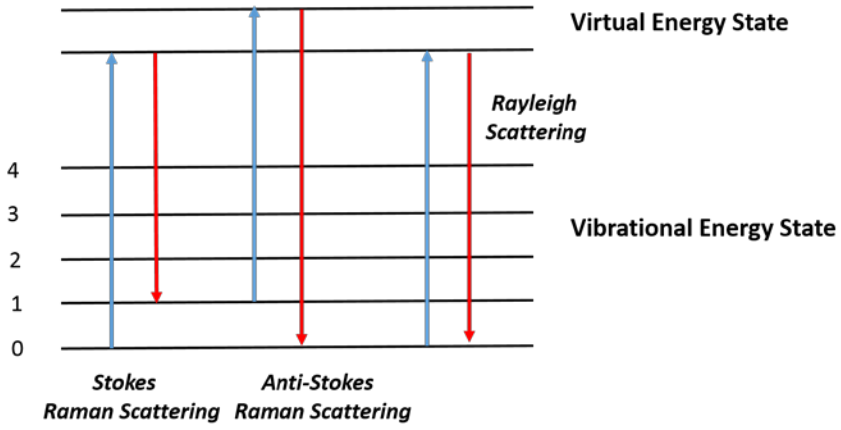

Figure 1.3.1 Energy-level diagram of Raman signal.

Figure 1.3.1 illustrated the principle of Raman spectroscopy involving inelastic scattering after the interaction between an incident laser and molecule of interest. In Figure 1.3.1, there are three kinds of scattering, Rayleigh scattering, stoke Raman scttering, anti-stoke Raman scattering. The Rayleigh scattering has the same wavelenghth with the layer beam and would be filtered out, while Raman scattering can be detected by a detector after going through a notch filter or a band pass filter. Note that anti-stoke Raman scattering has higher energy than stoke Raman scttering.

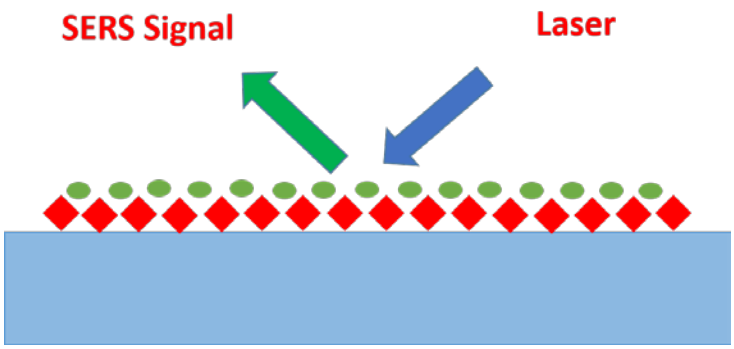

Figure 1.3.2 Conceptual illustration of SERS.

Surface enhanced Raman spectroscopy (also called surface enhance Raman scattering) has a much higher sensitive technique than Raman spectrocopy with 10^{10} to 10^{14} signal enhancement. The main reason in the enhancement is the localized surface plasmons was excited by a incident laser on a roughened metal surface (Au or Ag), on which molecule was aborbed. The signal of Raman scattering was then enhanced due to the electromagnetic enhancement mechanism. Figure 1.3.2 clearly illustrate the principle of surface enhanced Raman scattering.

Reference

1. Arora, A.; Eijkel, J. C. T.; Morf, W. E.; Manz, A. *Anal. Chem* **2001,** 73, (22), 5633-5633.

2. Zhan, W.; Alvarez, J.; Crooks, R. M. *J. Am. Chem. Soc* **2002,** 124, (44), 13265-13270.

3. Chow, K. F.; Mavre, F.; Crooks, R. M. *J. Am. Chem. Soc* **2008,** 130, (24), 7544-7545.

4. Chow, K. F.; Chang, B. Y.; Zaccheo, B. A.; Mavre, F.; Crooks, R. M. *J. Am. Chem. Soc* **2010,** 132, (27), 9228-9229.

5. Wu, S.; Zhou, Z.; Xu, L.; Su, B.; Fang, Q. *Biosens. Bioelectron* **2014,** 53, 148-153.

6. Feng, Q. M.; Pan, J. B.; Zhang, H. R.; Xu, J. J.; Chen, H. Y. *Chem. Commun* **2014,** 50, (75), 10949-10951.

7. Wu, M. S.; Xu, B. Y.; Shi, H. W.; Xu, J. J.; Chen, H. Y. *Lab. Chip* **2011,** 11, (16), 2720-2724.

8. Wu, M. S.; Yuan, D. J.; Xu, J. J.; Chen, H. Y. *Anal. Chem* **2013,** 85, (24), 11960-11965.

9. Wu, M. S.; Yuan, D. J.; Xu, J. J.; Chen, H. Y. *Chem. Sci* **2013,** 4, (3), 1182-1188.

10. Wu, M. S.; Qian, G. S.; Xu, J. J.; Chen, H. Y. *Ana.l Chem* **2012,** 84, (12), 5407-5414.

11. Zhang, X. W.; Chen, C. G.; Li, J.; Zhang, L. B.; Wang, E. K. *Anal. Chem* **2013,** 85, (11), 5335-5339.

12. Zhang, X. W.; Li, J.; Jia, X. F.; Li, D. Y.; Wang, E. K. *Anal. Chem* **2014,** 86, (11), 5595-5599.

13. Chang, B. Y.; Chow, K. F.; Crooks, J. A.; Mavre, F.; Crooks, R. M. *Analyst* **2012,** 137, (12), 2827-2833.

14. Wang, T. Y.; Fan, S. J.; Erdmann, R.; Shannon, C. *Langmuir* **2013,** 29, (51), 16040-16044.

15. Ramakrishnan, S.; Shannon, C. *Langmuir* **2010,** 26, (7), 4602-4606.

16. Ramaswamy, R.; Shannon, C. *Langmuir* **2011,** 27, (3), 878-881.

17. Loget, G.; Roche, J.; Gianessi, E.; Bouffier, L.; Kuhn, A. *J. Am. Chem. Soc* **2012,** 134, (49), 20033-20036.

18. Ongaro, M.; Roche, J.; Kuhn, A.; Ugo, P. *Chemelectrochem* **2014,** 1, (12), 2048-2051.

19. Fattah, Z.; Garrigue, P.; Lapeyre, V.; Kuhn, A.; Bouffier, L. *J. Phys. Chem. C* **2012,** 116, (41), 22021-22027.

20. Loget, G.; Roche, J.; Kuhn, A. *Adv Mater* **2012,** 24, (37), 5111-5116.

21. Kumsapaya, C.; Bakai, M. F.; Loget, G.; Goudeau, B.; Warakulwit, C.; Limtrakul, J.; Kuhn, A.; Zigah, D. *Chem. Eur. J.* **2013,** 19, (5), 1577-1580.

22. Loget, G.; Kuhn, A. *Nat. Commun* **2011,** 2, 535.

23. Sopha, H.; Roche, J.; Svancara, I.; Kuhn, A. *Anal. Chem* **2014,** 86, (21), 10515-10519.

24. Roche, J.; Carrara, S.; Sanchez, J.; Lannelongue, J.; Loget, G.; Bouffier, L.; Fischer, P.; Kuhn, A. *Sci. Rep* **2014,** 4, 6705.

25. Sentic, M.; Loget, G.; Manojlovic, D.; Kuhn, A.; Sojic, N. *Angew. Chem. Int. Ed* **2012,** 51, (45), 11284-11288.

26. Bouffier, L.; Zigah, D.; Adam, C.; Sentic, M.; Fattah, Z.; Manojlovic, D.; Kuhn, A.; Sojic, N. *Chemelectrochem* **2014,** 1, (1), 95-98.

27. Sentic, M.; Arbault, S.; Goudeau, B.; Manojlovic, D.; Kuhn, A.; Bouffier, L.; Sojic, N. *Chem. Commun* **2014,** 50, (71), 10202-10205.

28. Loget, G.; Kuhn, A. *Lab. Chip* **2012,** 12, (11), 1967-1971.

29. Paxton, W. F.; Sundararajan, S.; Mallouk, T. E.; Sen, A. *Angew. Chem. Int. Ed* **2006,** 45, (33), 5420-5429.

30. Loget, G.; Kuhn, A. *Nat. Commun* **2011,** 2.

31. Loget, G.; Kuhn, A. *J. Am. Chem. Soc* **2010,** 132, (45), 15918-15919.

32. Fosdick, S. E.; Crooks, R. M. *J. Am. Chem. Soc* **2012,** 134, (2), 863-866.

33. Fosdick, S. E.; Berglund, S. P.; Mullins, C. B.; Crooks, R. M. *Acs. Catal* **2014,** 4, (5), 1332-1339.

34. Oja, S. M.; Guerrette, J. P.; David, M. R.; Zhang, B. *Anal. Chem* **2014,** 86, (12), 6040-6048.

35. Guerrette, J. P.; Percival, S. J.; Zhang, B. *J. Am. Chem. Soc* **2013,** 135, (2), 855-861.

36. Bouffier, L.; Doneux, T.; Goudeau, B.; Kuhn, A. *Anal. Chem* **2014,** 86, (8), 3708-3711.

37. Laws, D. R.; Hlushkou, D.; Perdue, R. K.; Tallarek, U.; Crooks, R. M. *Anal. Chem* **2009,** 81, (21), 8923-8929.

38. Perdue, R. K.; Laws, D. R.; Hlushkou, D.; Tallarek, U.; Crooks, R. M. *Anal. Chem* **2009,** 81, (24), 10149-10155.

39. Inagi, S.; Ishiguro, Y.; Atobe, M.; Fuchigami, T. *Angew. Chem. Int. Ed* **2010,** 49, (52), 10136-10139.

40. Shida, N.; Ishiguro, Y.; Atobe, M.; Fuchigami, T.; Inagi, S. *Acs Macro Lett* **2012,** 1, (6), 656-659.

41. Ishiguro, Y.; Inagi, S.; Fuchigami, T. *Langmuir* **2011,** 27, (11), 7158-7162.

42. Munktell, S.; Tyden, M.; Hogstrom, J.; Nyholm, L.; Bjorefors, F. *Electrochem. Commun* **2013,** 34, 274-277.

43. Munktell, S.; Nyholm, L.; Björefors, F. *J. Electroanal. Chem* **2015,** 747, (0), 77-82.

44. Yadnum, S.; Roche, J.; Lebraud, E.; Negrier, P.; Garrigue, P.; Bradshaw, D.; Warakulwit, C.; Limtrakul, J.; Kuhn, A. *Angew. Chem. Int. Ed* **2014,** 53, (15), 4001-4005.

45. Mavre, F.; Anand, R. K.; Laws, D. R.; Chow, K. F.; Chang, B. Y.; Crooks, J. A.; Crooks, R. M. *Anal. Chem* **2010,** 82, (21), 8766-8774.

46. Fosdick, S. E.; Knust, K. N.; Scida, K.; Crooks, R. M. *Angew. Chem. Int. Ed* **2013,** 52, (40), 10438-10456.

47. Warakulwit, C.; Nguyen, T.; Majimel, J.; Delville, M. H.; Lapeyre, V.; Garrigue, P.; Ravaine, V.; Limtrakul, J.; Kuhn, A. *Nano lett.* **2008,** 8, (2), 500-504.

48. Renault, C.; Scida, K.; Knust, K. N.; Fosdick, S. E.; Crooks, R. M. *J. Electrochem. Sci. Technol.* **2013,** 4, (4), 146-152.

49. Feng, Q. M.; Pan, J. B.; Zhang, H. R.; Xu, J. J.; Chen, H. Y. *Chem. commun* **2014,** 50, (75), 10949-10951.

50. Koizumi, Y.; Shida, N.; Tomita, I.; Inagi, S. *Chem. Lett* **2014,** 43, (8), 1245-1247.

51. Loget, G.; Zigah, D.; Bouffier, L.; Sojic, N.; Kuhn, A. *Acc. Chem. Res* **2013,** 46, (11), 2513-2523.

52. Fosdick, S. E.; Knust, K. N.; Scida, K.; Crooks, R. M. *Angew. Chem. Int. Ed* **2013,** 52, (40), 10438-56.

53. Shida, N.; Koizumi, Y.; Nishiyama, H.; Tomita, I.; Inagi, S. *Angew. Chem. Int. Ed* **2015,** 54, 1-6.

54. Mavre, F.; Anand, R. K.; Laws, D. R.; Chow, K. F.; Chang, B. Y.; Crooks, J. A.; Crooks, R. M. *Anal. Chem* **2010,** 82, (21), 8766-8774.

55. Wu, M. S.; Xu, B. Y.; Shi, H. W.; Xu, J. J.; Chen, H. Y. *Lab. chip* **2011,** 11, (16), 2720-2724.

56. Zhang, H. R.; Wang, Y. Z.; Wu, M. S.; Feng, Q. M.; Shi, H. W.; Chen, H. Y.; Xu, J. J. *Chem. commun* **2014,** 50, (83), 12575-12577.

57. Shi, H. W.; Wu, M. S.; Du, Y.; Xu, J. J.; Chen, H. Y. *Biosens. Bioelectron* **2014,** 55, 459-463.

58. Wu, M. S.; Liu, Z.; Shi, H. W.; Chen, H. Y.; Xu, J. J. *Anal. Chem* **2015,** 87, (1), 530-537.

59. Sentic, M.; Loget, G.; Manojlovic, D.; Kuhn, A.; Sojic, N. *Angew. Chem. Int. Ed* **2012,** 51, (45), 11284-11288.

60. Loget, G.; Roche, J.; Gianessi, E.; Bouffier, L.; Kuhn, A. *J. Am. Chem. Soc* **2012,** 134, (49), 20033-20036.

61. Loget, G.; Roche, J.; Kuhn, A. *Adv. Mater* **2012,** 24, (37), 5111-5116.

62. Fleischmann, M.; Ghoroghchian, J.; Rolison, D.; Pons, S. *J. Phys. Chem* **1986,** 90, (23), 6392-6400.

63. Mavre, F.; Chow, K. F.; Sheridan, E.; Chang, B. Y.; Crooks, J. A.; Crooks, R. M. *Anal. Chem* **2009,** 81, (15), 6218-6225.

64. Richter, M. M. *Chem. Rev* **2004,** 104, (6), 3003-3036.

65. Mccord, P.; Bard, A. J. *J. Electroanal. Chem* **1991,** 318, (1-2), 91-99.

66. Blackburn, G. F.; Shah, H. P.; Kenten, J. H.; Leland, J.; Kamin, R. A.; Link, J.; Peterman, J.; Powell, M. J.; Shah, A.; Talley, D. B.; Tyagi, S. K.; Wilkins, E.; Wu, T. G.; Massey, R. J. *Clin. chem* **1991,** 37, (9), 1534-1539.

67. Kenten, J. H.; Casadei, J.; Link, J.; Lupold, S.; Willey, J.; Powell, M.; Rees, A.; Massey, R. *Clin. chem* **1991,** 37, (9), 1626-1632.

68. Chow, K. F.; Mavre, F.; Crooks, J. A.; Chang, B. Y.; Crooks, R. M. *J. Am. Chem. Soc* **2009,** 131, (24), 8364-8365.

69. Zhang, X. W.; Chen, C. G.; Yin, J. Y.; Han, Y. C.; Li, J.; Wang, E. K. *Anal. Chem* **2015,** 87, (9), 4612-4616.

70. Fosdick, S. E.; Berglund, S. P.; Mullins, C. B.; Crooks, R. M. *Anal. Chem* **2013,** 85, (4), 2493-2499.

71. Bradley, J. C.; Ma, Z. M. *Angew. Chem. Int. Ed* **1999,** 38, (11), 1663-1666.

72. Bradley, J. C.; Chen, H. M.; Crawford, J.; Eckert, J.; Ernazarova, K.; Kurzeja, T.; Lin, M. D.; McGee, M.; Nadler, W.; Stephens, S. G. *Nature* **1997,** 389, 268-271.

73. Bradley, J. C.; Crawford, J.; McGee, M.; Stephens, S. G. *J. Electrochem. Soc* **1998,** 145, (3), L45-L47.

74. Bradley, J. C.; Ma, Z. M.; Stephens, S. G. *Adv. Mater* **1999,** 11, (5), 374-378.

75. Babu, S.; Ndungu, P.; Bradley, J. C.; Rossi, M. P.; Gogotsi, Y. *Microfluid Nanofluid* **2005,** 1, (3), 284-288.

76. Bradley, J. C.; Ma, Z. M.; Clark, E.; Crawford, J.; Stephens, S. G. *J. Electrochem. Soc* **1999,**

146, (1), 194-198.

77. Bradley, J. C.; Babu, S.; Mittal, A.; Ndungu, P.; Carroll, B.; Samuel, B. *J. Electrochem. Soc* **2001,** 148, (9), C647-C651.

78. Bradley, J. C.; Crawford, J.; Ernazarova, K.; McGee, M.; Stephens, S. G. *Adv. Mater* **1997,** 9, (15), 1168-1171.

79. de Gennes, P. G. *Science* **1992,** 256, (5056), 495-497.

80. Jiang, S.; Chen, Q.; Tripathy, M.; Luijten, E.; Schweizer, K. S.; Granick, S. *Adv. Mater* **2010,** 22, (10), 1060-1071.

81. Du, J.; O'Reilly, R. K. *Chem. Soc. Rev* **2011,** 40, (5), 2402-2416.

82. Loget, G.; Kuhn, A. *Anal. Bioanal. Chem* **2011,** 400, (6), 1691-704.

83. Bradley, J. C.; Babu, S.; Ndungu, P. *Fuller. Nanotub. Car. N* **2005,** 13, (3), 227-237.

84. Brooksby, P. A.; Downard, A. J. *Langmuir* **2004,** 20, (12), 5038-5045.

85. Bradley, M.; Garcia-Risueno, B. S. *J. Colloid. Interf. Sci* **2011,** 355, (2), 321-327.

86. Noel, J. M.; Zigah, D.; Simonet, J.; Hapiot, P. *Langmuir* **2010,** 26, (10), 7638-7643.

87. Fattah, Z.; Loget, G.; Lapeyre, V.; Garrigue, P.; Warakulwit, C.; Limtrakul, J.; Bouffier, L.; Kuhn, A. *Electrochim. Acta* **2011,** 56, (28), 10562-10566.

88. Loget, G.; Larcade, G.; Lapeyre, V.; Garrigue, P.; Warakulwit, C.; Limtrakul, J.; Delville, M. H.; Ravaine, V.; Kuhn, A. *Electrochim. Acta* **2010,** 55, (27), 8116-8120.

89. Loget, G.; Kuhn, A. *J. Am. Chem. Soc* **2010,** 132, (45), 15918-15919.

90. Loget, G.; Kuhn, A. *Lab. chip* **2012,** 12, (11), 1967-1971.

91. Sentic, M.; Arbault, S.; Goudeau, B.; Manojlovic, D.; Kuhn, A.; Bouffier, L.; Sojic, N. *Chem. commun* **2014,** 50, (71), 10202-10205.

92. Wang, Y.; Hernandez, R. M.; Bartlett, D. J., Jr.; Bingham, J. M.; Kline, T. R.; Sen, A.; Mallouk, T. E. *Langmuir* **2006,** 22, (25), 10451-10456.

93. Wang, J.; Manesh, K. M. *Small* **2010,** 6, (3), 338-345.

94. Campuzano, S.; Kagan, D.; Orozco, J.; Wang, J. *Analyst* **2011,** 136, (22), 4621-4630.

95. Wang, J. *Acs. Nano* **2009,** 3, (1), 4-9.

96. Kagan, D.; Calvo-Marzal, P.; Balasubramanian, S.; Sattayasamitsathit, S.; Manesh, K. M.; Flechsig, G. U.; Wang, J. *J. Am. Chem. Soc* **2009,** 131, (34), 12082-12083.

97. Balasubramanian, S.; Kagan, D.; Hu, C. M. J.; Campuzano, S.; Lobo-Castanon, M. J.; Lim, N.; Kang, D. Y.; Zimmerman, M.; Zhang, L. F.; Wang, J. *Angew. Chem. Int. Ed* **2011,** 50, (18), 4161-4164.

98. Demirok, U. K.; Laocharoensuk, R.; Manesh, K. M.; Wang, J. *Angew. Chem. Int. Ed* **2008,** 47, (48), 9349-9351.

99. Dolnik, V.; Liu, S.; Jovanovich, S. *Electrophoresis* **2000,** 21, (1), 41-54.

100. Hlushkou, D.; Perdue, R. K.; Dhopeshwarkar, R.; Crooks, R. M.; Tallarek, U. *Lab. chip* **2009,** 9, (13), 1903-1913.

101. Kelly, R. T.; Woolley, A. T. *J. Sep. Sci* **2005,** 28, (15), 1985-1993.

102. Meighan, M. M.; Staton, S. J.; Hayes, M. A. *Electrophoresis* **2009,** 30, (5), 852-65.

103. Myers, P.; Bartle, K. D. *J. chromatogr. A* **2004,** 1044, (1-2), 253-258.

104. Shimura, K. *Electrophoresis* **2009,** 30, (1), 11-28.

105. Hofmann, O.; Che, D.; Cruickshank, K. A.; Muller, U. R. *Anal. Chem* **1999,** 71, (3), 678-86.

106. Gebauer, P.; Mala, Z.; Bocek, P. *Electrophoresis* **2009,** 30, (1), 29-35.

107. Ross, D.; Locascio, L. E. *Anal. Chem* **2002,** 74, (11), 2556-64.

108. Kim, S. M.; Sommer, G. J.; Burns, M. A.; Hasselbrink, E. F. *Anal. Chem* **2006,** 78, (23), 8028-35.

109. Kim, S. M.; Burns, M. A.; Hasselbrink, E. F. *Anal. Chem* **2006,** 78, (14), 4779-85.

110. Xu, Z.; Timerbaev, A. R.; Hirokawa, T. *J. chromatogr. A* **2009,** 1216, (4), 660-670.

111. Long, Z.; Liu, D.; Ye, N.; Qin, J.; Lin, B. *Electrophoresis* **2006,** 27, (24), 4927-4934.

112. Hlushkou, D.; Dhopeshwarkar, R.; Crooks, R. M.; Tallarek, U. *Lab. chip* **2008,** 8, (7), 1153-1162.

113. Koegler, W. S.; Ivory, C. F. *J J. chromatogr. A* **1996,** 726, (1-2), 229-236.

114. Anand, R. K.; Sheridan, E.; Knust, K. N.; Crooks, R. M. *Anal. Chem* **2011,** 83, (6), 2351-8.

115. Perdue, R. K.; Laws, D. R.; Hlushkou, D.; Tallarek, U.; Crooks, R. M. *Anal. Chem* **2009,** 81, (24), 10149-10155.

116. Dhopeshwarkar, R.; Hlushkou, D.; Nguyen, M.; Tallarek, U.; Crooks, R. M. *J. Am. Chem. Soc* **2008,** 130, (32), 10480-10481.

117. Sheridan, E.; Hlushkou, D.; Knust, K. N.; Tallarek, U.; Crooks, R. M. *Anal. Chem* **2012,** 84, (17), 7393-7399.

118. Sheridan, E.; Hlushkou, D.; Anand, R. K.; Laws, D. R.; Tallarek, U.; Crooks, R. M. *Anal.*

Chem **2011,** 83, (17), 6746-6753.

119. Visco, R. E.; Chandross, E. A. *J. Am. Chem. Soc* **1964,** 86, (23), 5350-5351.

120. Santhana.Ks; Bard, A. J. *J. Am. Chem. Soc* **1965,** 87, (1), 139-140.

121. Tokeltak.Ne; Hemingwa.Re; Bard, A. J. *J. Am. Chem. Soc* **1973,** 95, (20), 6582-6589.

122. Dini, D. *Chem Mater* **2005,** 17, (8), 1933-1945.

123. Yin, X. B.; Wang, E. *Anal. Chim. Acta* **2005,** 533, (2), 113-120.

124. Pyati, R.; Richter, M. M. *Annual Reports Section "C" (Physical Chemistry)* **2007,** 103, (0), 12-78.

125. Du, Y.; Wang, E. K. *J. Sep. Sci* **2007,** 30, (6), 875-890.

126. Miao, W. J. *Chem. Rev* **2008,** 108, (7), 2506-2553.

127. Bertoncello, P.; Forster, R. J. *Biosens. Bioelectron* **2009,** 24, (11), 3191-3200.

128. Hu, L. Z.; Xu, G. B. *Chem. Soc. Rev* **2010,** 39, (8), 3275-3304.

129. Ludvik, J. *J. Solid. State. Electr* **2011,** 15, (10), 2065-2081.

130. Su, M.; Wei, W.; Liu, S. Q. *Anal. Chim. Acta* **2011,** 704, (1-2), 16-32.

131. Guo, L.; Fu, F.; Chen, G. *Anal. Bioanal. Chem* **2011,** 399, (10), 3323-43.

132. Chen, X. M.; Su, B. Y.; Song, X. H.; Chen, Q. A.; Chen, X.; Wang, X. R. *Trac-Trend Anal. Chem* **2011,** 30, (5), 665-676.

133. Wei, H.; Wang, E. *Luminescence* **2011,** 26, (2), 77-85.

134. Huang, H. P.; Li, J. J.; Zhu, J. J. *Anal. Methods-Uk* **2011,** 3, (1), 33-42.

135. Huang, B. M.; Zhou, X. B.; Xue, Z. H.; Lu, X. Q. *Trac-Trend. Anal. Chem* **2013,** 51, 107-116.

136. Tokel, N. E.; Bard, A. J. *J. Am. Chem. Soc* **1972,** 94, (8), 2862-2863.

137. Miao, W. *Chem. Rev* **2008,** 108, (7), 2506-2553.

138. Haynes, C. L.; McFarland, A. D.; Van Duyne, R. P. *Anal. Chem* **2005,** 77, (17), 338a-346a.

139. Jeanmaire, D. L.; Vanduyne, R. P. *J. Electroanal. Chem* **1977,** 84, (1), 1-20.

140. Fan, M. K.; Andrade, G. F. S.; Brolo, A. G. *Anal. Chim. Acta* **2011,** 693, (1-2), 7-25.

141. Schlucker, S. *Angew. Chem. Int. Ed* **2014,** 53, (19), 4756-4795.

142. Leopold, N.; Lendl, B. *J. Phys. Chem. B* **2003,** 107, (24), 5723-5727.

143. Doering, W. E.; Nie, S. M. *J. Phys. Chem. B* **2002,** 106, (2), 311-317.

144. Xie, J. P.; Zhang, Q. B.; Lee, J. Y.; Wang, D. I. C. *Acs. Nano* **2008,** 2, (12), 2473-2480.

145. Bell, S. E. J.; Sirimuthu, N. M. S. *J. Am. Chem. Soc* **2006,** 128, (49), 15580-15581.

146. Le Ru, E. C.; Meyer, M.; Etchegoin, P. G. *J. Phys. Chem. B* **2006,** 110, (4), 1944-1948.

147. Dick, L. A.; McFarland, A. D.; Haynes, C. L.; Van Duyne, R. P. *J. Phys. Chem. B* **2002,** 106, (4), 853-860.

148. He, D.; Hu, B.; Yao, Q. F.; Wang, K.; Yu, S. H. *Acs. Nano* **2009,** 3, (12), 3993-4002.

149. Yan, B.; Reinhard, B. *Abstr. Pap. Am. Chem. S* **2010,** 240.

150. Braun, G.; Pavel, I.; Morrill, A. R.; Seferos, D. S.; Bazan, G. C.; Reich, N. O.; Moskovits, M. *J. Am. Chem. Soc* **2007,** 129, (25), 7760-7761.

Chapter 2

Detection of Ferrocenemethanol and Molecular Oxygen Based on Electrogenerated Chemiluminescence Quenching at a Bipolar Electrode

This project is the collaboration with TanYu Wang and I who contributed equally in this work

2.1 Abstract

Small molecules, such as ferrocenemethanol (FcMeOH) and O_2, that are capable of quenching the $Ru(bpy)_3^{2+}$ excited state via energy or electron transfer, can be quantitatively detected in a bipolar electrochemical cell based on the attenuation of steady-state electrogenerated chemiluminescence (ECL). FcMeOH quenches ECL generated by the $Ru(bpy)_3^{2+}$ oxalate coreactant system, exhibiting a linear dependence on [FcMeOH] with a Stern−Volmer slope of 921 M^{-1}, corresponding to a quenching rate constant of 2×10^9 M^{-1} s^{-1}. We used the bipolar ECL quenching platform to measure dissolved O_2 and validated the results using a standard Clark electrode. The detection limit for local [O_2] measured using ECL quenching was found to be 300 ppb. This work opens up the possibility of utilizing ECL quenching at bipolar electrodes for a wide range of applications.

2.2 Introduction

Over the past decade, bipolar electrochemistry, which allows sensor read-out without a direct

electrical connection to the working electrode, has emerged as an alternative to conventional amperometry.[1, 2] The bipolar platform is much easier to miniaturize, multiplex, integrate with lab-on-a-chip systems, and use to carry out spatially resolved analytical measurements.[3] In sensor applications, reading out the state of a bipolar electrode presents unique challenges because of the lack of a direct physical connection. Manz and co-workers were the first to use electrogenerated chemiluminescence (ECL) to detect analytes separated by micellar electrokinetic chromatography (MEKC) using a "wireless" detector.[4] Since then, ECL, especially the $Ru(bpy)_3^{2+}$ coreactant system, has frequently been used as an indirect reporter of the bipolar current.[5,6] ECL does not require an excitation light source, and the reaction can be performed in a very small sample volume, making it ideal for integration with portable devices at low cost.[7] The marriage of ECL and bipolar electrochemisty has great potential for carrying out highly multiplexed detection using arrays of BPEs.[8] In this sensor format, the analyte of interest is reduced at the cathodic pole of the BPE, and this reaction triggers ECL at the anodic pole in direct proportion to the BPE current.[9, 10] More recently, Nyholm and co-workers[11] used BPEs to detect electrochemically active compounds by applying an electric field to induce bipolar behavior between two Au bands. The split design facilitates the direct measurement of current passing through the BPE, at the cost of complicating the detection system with an external electrical connection. Crooks et al.[12] utilized the stripping of Ag from the anodic pole of a BPE to signal a cathodic sensing event. The amount of Ag dissolved provided a record of the state of the BPE sensor. The combination of fluorescence-based assays with Forster resonance energy transfer (FRET) quenching has led to the development of powerful

new methods for sequence specific DNA detection[13] and techniques for single molecule detection.[14] Although the mechanism for ECL quenching can be more complex than fluorescence quenching, several well characterized systems do exist. Landers and co-workers developed an intramolecular ECL quenching assay for the detection of DNA hybridization based on using $Ru(bpy)_3^{2+}$-labeled capture ssDNA. ECL intensity was found to decrease in direct proportion to the concentration of complementary oligonucleotides tagged with a ferrocene methanol (FcMeOH) quencher.[15]

Here, we report a bipolar electrochemical detection scheme based on steady-state ECL quenching for the direct detection of small molecules such as FcMeOH and O_2.

2.3 Experimental Section

Materials and Reagents. Tris(2,2′-bipyridyl)dichlororuthenium-(II) hexahydrate (Sigma-Aldrich), sodium oxalate (99.5+%, Sigma-Aldrich), and ferrocenemethanol (FcMeOH) (99%, Sigma-Aldrich) were used as received. $HClO_4$ (70%, Fisher Scientific) was diluted with deionized (DI) water to prepare 1.0 mM stock solutions (pH 3.4). Ethanol, H_2O_2, and sulfuric acid (all HPLC grade) were obtained from commercial sources and used as received. Millipore-Q purified (DI) water (18.2 MΩ.cm) was used to prepare all solutions and to rinse electrodes.

Assembly of Bipolar Devices. BPEs were made from Pt wire (l_{elec} = 1.4 cm, diameter = 0.7 mm), and two Au foil electrodes were used to drive the bipolar cell using a separation distance of 4 cm. Au electrodes were polished using an aqueous slurry of 0.05 μm alumina and were then washed with water and ethanol in an ultrasonic cleaner. The Pt-BPE was immersed in fresh piranha

solution (H_2SO_4/H_2O_2, 3:1 (v/v)) for about 5 min, rinsed with DI water, and dried under nitrogen gas. Caution: piranha solution is dangerous to human health and should be used with extreme caution and handled only in small quantities. The Pt-BPE was then fixed in place near the center of a glass cell (diameter = 5 cm) using epoxy. The cell was constructed to allow us to maintain an oxygen-free environment as shown in Scheme 2.1.

Bipolar ECL Measurements. Test solutions consisted of 5 mM $Ru(bpy)_3^{2+}$ and 25 mM $Na_2C_2O_4$ in 0.001 M $HClO_4$. Solutions were purged with N_2 for 20−30 min to exclude O_2 and were then kept under a blanket of N_2. A potential of 15 V was imposed across the driver electrodes using a regulated dc power supply (Hewlett-Packard model 6010). ECL signals were recorded using a Nikon D3100 or an Olympus OMD-EM5 digital camera in a darkened room. Exposures of 1 s at f/1.8 were acquired at an ISO value of 1600. Images were processed and corrected for dark current using ImageJ. We measured the average ECL intensity over the active (ECL emitting) part of the BPE anode. A background measurement was obtained from a dark part of the image (using the same total area) and subtracted from the average ECL intensity.

Electrochemical Measurements. Chronoamperometry (CA) was performed using a conventional three-electrode setup in the cell shown in Scheme 2.1. Note: the reference and counter electrodes are not shown to avoid clutter in the diagram. The supporting electrolyte was 1.0 mM $HClO_4$. The reference electrode was Ag/AgCl/KCl(sat) (Bioanalytical Systems, Inc.), the counter electrode was Pt gauze, and the working electrode was a Pt disk (diameter = 1.6 mm, Bioanalytical Systems, Inc.). Before electrochemical measurements, the

solution was purged with N_2 for at least 20 min. The electrochemical circuit was controlled using an Epsilon electrochemistry workstation (Bioanalytical Systems, Inc.). Amperometric measurements were performed by stepping the potential from ca. +0.7 to 0.0 V to ensure diffusion limited reduction of O_2. A Clark sensor from Milwaukee Instruments (model MW600) was used to validate the CA and ECL measurements.

2.4 Results and discussion

The principle of operation of the sensor platform is illustrated in Scheme 2.1. An external potential difference, V, is applied between two Au driver electrodes immersed in an electrolyte, generating a linear potential gradient. The difference in potential between the two poles of the Pt BPE, ΔV, is the fraction of V dropped across the length of the BPE. When this potential difference is sufficiently large, electrochemical reactions will occur simultaneously at both poles of the BPE. Under the experimental conditions used here, ECL is the predominant Faradaic process occurring at the anodic pole, while hydrogen evolution occurs at its diffusion-limited rate at the cathodic pole. This results in a stable, steady-state ECL intensity which can be observed visually and recorded using a digital camera. When a molecule capable of quenching ECL (i.e., FcMeOH or O_2) is introduced into the system, the ECL intensity is expected to decrease in direct proportion to its concentration. To study the feasibility of detecting analytes using the ECL quenching mechanism in a bipolar cell, FcMeOH was employed as a model because its quenching mechanism has been thoroughly investigated.[15] We used the $Ru(bpy)_3^{2+}$/oxalate system to generate ECL according to the pathway shown in Scheme 2.1.[16-18]

Landers et al. proposed the following electron transfer mechanism for ECL quenching by FcMeOH, where $FcMeOH^+$ is generated at the electrode surface.[15]

$$FcMeOH \rightarrow FcMeOH^+ + e^-$$

$E_{1/2}$(vs Ag/AgCl) = 0.230 V (1)

$$FcMeOH^+ + Ru(bpy)_3^{2+*} \rightarrow FcMeOH + Ru(bpy)_3^{3+} \quad (2)$$

A test solution containing 5 mM $Ru(bpy)_3^{2+}$ and 25 mM sodium oxalate dissolved in 10 mL of 0.001 M $HClO_4$ (pH = 3.4) was degassed with nitrogen for 20 min to eliminate the possibility of quenching involving molecular oxygen.[19] Then, V = 15 V was applied to the driver electrodes, resulting in a ΔV of 1.97 V across the BPE. Under these conditions, a stable, intense ECL signal was recorded using a digital camera. To test whether significant amounts of oxygen are generated at the anodic pole of the BPE, we studied the dependence of ECL intensity on applied voltage. We observe a monotonic increase in the ECL intensity as the driving voltage is increased, up to about 14 V, at which point the ECL intensity reaches a limiting value. A small decrease in ECL intensity is observed at 16 V. Thus, under our experimental conditions, generation of O_2 at the BPE anode appears to be negligible. Next, aliquots of FcMeOH were injected sequentially into the test solution, and the intensity of the emitted light was recorded. The ECL intensity was observed to decrease monotonically as the concentration of FcMeOH increased. Representative image data acquired during a series of quenching experiments are shown in the inset to Figure 2.1. To prepare this image, individual digital captures were combined in Adobe Photoshop. Quantitative intensities were measured from the unprocessed JPEG image files using ImageJ. Relative, background (dark

current) corrected light intensity values are plotted as a function of elapsed time in Figure 2.1 (inset). The relative ECL intensity data (I_0/I) were then plotted as a function of [FcMeOH] (Figure 2.1), where I_0/I is seen to be a linear function of [FcMeOH] with a unit y-intercept, as expected for a diffusion-limited quenching process described by the Stern−Volmer equation (3).[20, 21]

$$I_0/I = 1 + k_q\tau_0[Q] = 1 + K_{sv}[Q] \quad (3)$$

In this equation, I_0/I is the observed ratio of ECL intensity in an unquenched sample to that in a quenched one, k_q is the quenching rate constant, K_{sv} is the Stern−Volmer constant, τ_0 is the photoluminescence lifetime of $Ru(bpy)_3^{2+}$ in the absence of quencher, and [Q] is the concentration of the quencher. Using the photoluminescence lifetime of $Ru(bpy)_3^{2+}$ in the absence of quencher (589 ns),[15] a value for K_{sv} of 921 M^{-1}, corresponding to a k_q of 2×10^9 M^{-1} s^{-1}, was calculated for FeMeOH. This value is reasonably close to the value of 3×10^9 M^{-1} s^{-1} measured by others using conventional electrochemical methods.[15, 22] These results clearly demonstrate the viability of using the attenuation of ECL signals in a bipolar cell for the detection of an analyte that can act as a quencher.

We investigated the use of ECL quenching in a bipolar cell to monitor the concentration of dissolved oxygen. The effect of oxygen is dependent on the coreactant system used to generate ECL. In the case of the $Ru(bpy)_3^{2+}$/TPA coreactant system, Zu et al. showed that the ECL intensity could be made sensitive or insensitive to [O_2] by adjusting the coreactant concentrations.[23] In an early paper, Rubinstein and Bard noted that ECL intensity generated by the $Ru(bpy)_3^{2+}$/oxalate system decreased significantly in the presence of dissolved oxygen.[17] This observation was studied

in greater detail by Vander Donckt, who demonstrated that the attenuation of ECL in the presence of O_2 was conventional luminescence quenching and displayed the expected Stern−Volmer dependence on [O_2] (eqs 11 and 12).[24]

To remove as much dissolved oxygen as possible prior to making measurements, a test solution containing 5 mM $Ru(bpy)_3^{2+}$ and 25 mM sodium oxalate was degassed with N_2 for 30 min, and the cell was blanketed with N_2 and isolated from air by closing the air inlet on the measuring cell (Scheme 2.1). An external voltage (15 V) was applied to the cell, and the steady-state ECL intensity was recorded. In order to validate the ECL quenching approach, readings were taken at the same time using a Clark O_2 sensor. Next, air was allowed to diffuse into the bipolar cell for a fixed increment of time (60 s), and the inlet was again sealed. The supporting electrolyte was mechanically stirred to ensure a well-mixed solution (this was required to ensure proper operation of the Clark sensor), and the O_2 concentration was measured using the Clark electrode. In parallel, the steady-state ECL intensity was recorded with the digital camera; this procedure was repeated to collect a complete set of data. The $(I_0 - I)/I$ and Clark sensor data are plotted together in Figure 2.2. The correlation is linear over the full range of O_2 concentrations studied (∼0 to ca. 6 ppm). This result demonstrates the robustness of the ECL quenching technique for the determination of dissolved oxygen levels using the bipolar sensor format. We estimated a detection limit of ca. 300 ppb under these conditions. Minimizing the detection limit was not the goal of these experiments. If necessary, higher sensitivity (lower detection limits) easily could be achieved by making longer exposures, increasing ISO, making measurements in a spectrometer, etc.

An important advantage of bipolar sensing platforms is their ability to report on analyte concentrations in proximity to the BPE.[3] Since the $Ru(bpy)_3^{2+*}$ excited state is electrogenerated at the anodic pole of the BPE, our expectation is that ECL quenching also will respond to analyte concentrations in close proximity to the anodic pole of the BPE. To demonstrate that this was the case, we repeated the O_2 dosing experiment described above without hydrodynamic mixing. In order to do this, we replaced the Clark sensor with a Pt disk located near the inlet of the cell (to measure O_2 chronoamperometrically) (Scheme 2.1). The configuration of the bipolar electrode in the cell was not altered. Thus, the Pt disk was expected to respond to dissolved oxygen levels near the cell inlet, while the BPE would respond to O_2 near the bottom of the cell (ca. 1 cm away). Our hypothesis was that initially the BPE response would report a lower concentration of O_2 than chronoamperometry (CA) due to the time it takes for O_2 to diffuse from the cell inlet to the anodic pole of the BPE. At longer times, as the level of dissolved oxygen approaches its limiting value throughout the cell, the results of the two measurements should converge. Typical results for time-dependent measurements are shown in Figure 2.3 and completely bear out this hypothesis. That is while the CA measurements were observed to increase smoothly as a function of time during the course of the experiment, the ECL quenching response is nonlinear. Initially, the response of the BPE sensor changes relatively slowly up to a time of about 6 mins, after which it rises rapidly, reaching a plateau value that shows the same time dependence as the CA measurement. This is consistent with a diffusion limited quenching of $Ru(bpy)_3^{2+*}$ electrogenerated near the anodic pole of the BPE by dissolved O_2.

2.5 CONCLUSIONS

We have demonstrated the use of ECL quenching in a bipolar electrochemical cell as a method to determine the concentration of FcMeOH and O_2. Our studies indicate that the sensor reports on the local concentration of the analyte near the anodic pole of the BPE. These results suggest that other small molecules that quench ECL can be detected in a similar fashion (indeed, the analyte itself need not be electrochemically active to be detected). Moving forward, the use of Stern−Volmer slopes to distinguish between multiple analytes will be investigated to address the issue of selectivity. It should be possible to enhance the performance of existing bipolar sensors by exploiting the concepts developed here.

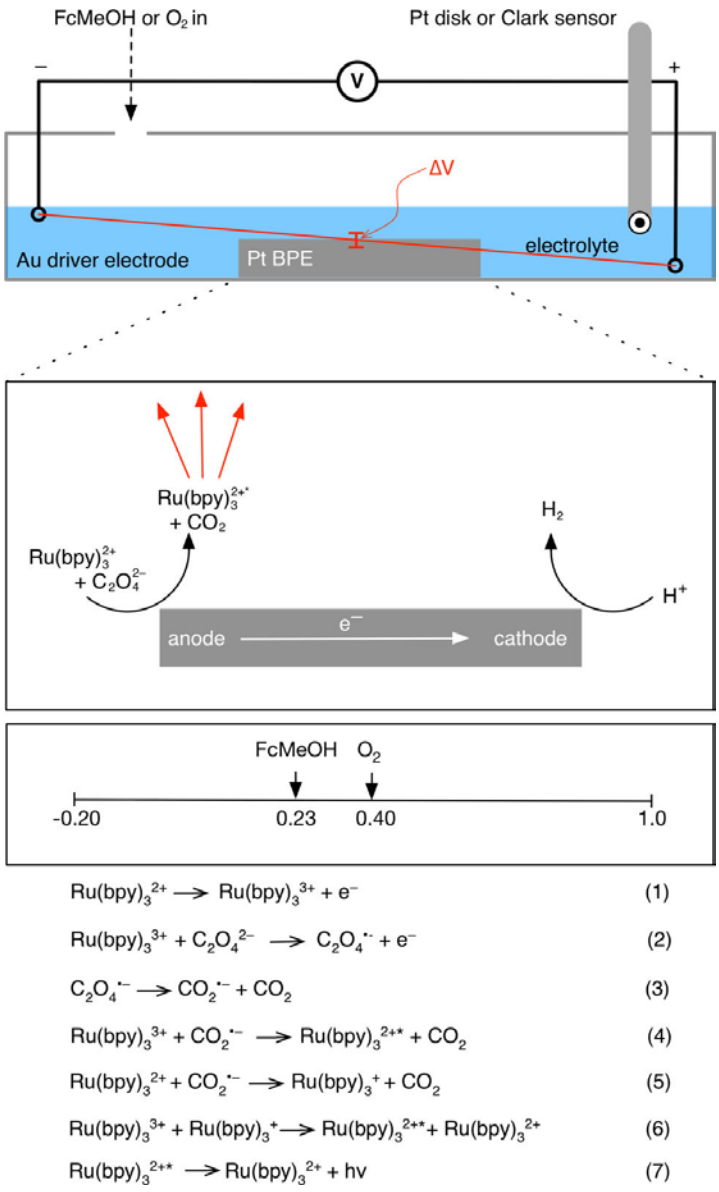

$$Ru(bpy)_3^{2+} \rightarrow Ru(bpy)_3^{3+} + e^- \quad (1)$$

$$Ru(bpy)_3^{3+} + C_2O_4^{2-} \rightarrow C_2O_4^{\bullet -} + e^- \quad (2)$$

$$C_2O_4^{\bullet -} \rightarrow CO_2^{\bullet -} + CO_2 \quad (3)$$

$$Ru(bpy)_3^{3+} + CO_2^{\bullet -} \rightarrow Ru(bpy)_3^{2+*} + CO_2 \quad (4)$$

$$Ru(bpy)_3^{2+} + CO_2^{\bullet -} \rightarrow Ru(bpy)_3^{+} + CO_2 \quad (5)$$

$$Ru(bpy)_3^{3+} + Ru(bpy)_3^{+} \rightarrow Ru(bpy)_3^{2+*} + Ru(bpy)_3^{2+} \quad (6)$$

$$Ru(bpy)_3^{2+*} \rightarrow Ru(bpy)_3^{2+} + hv \quad (7)$$

Scheme 2.1 Small Molecule Detection Using ECL Quenching.[25, 26]

Correction of equation (2): $Ru(bpy)_3^{3+} + C_2O_4^{2-} \rightarrow C_2O_4^{\bullet -} + Ru(bpy)_3^{2+}$

Upper diagram: bipolar measurement cell. Middle diagram: generation of ECL at a BPE. Lower diagram: potential scale showing $E_{1/2}$ values for FcMeOH oxidation, O_2 reduction, and the Pt BPE solvent window. Bottom: ECL mechanism. [Reprinted with permission from *Langmuir*, 2013, 29 (51), 16040–16044. Copyright (2013) American Chemical Society.]

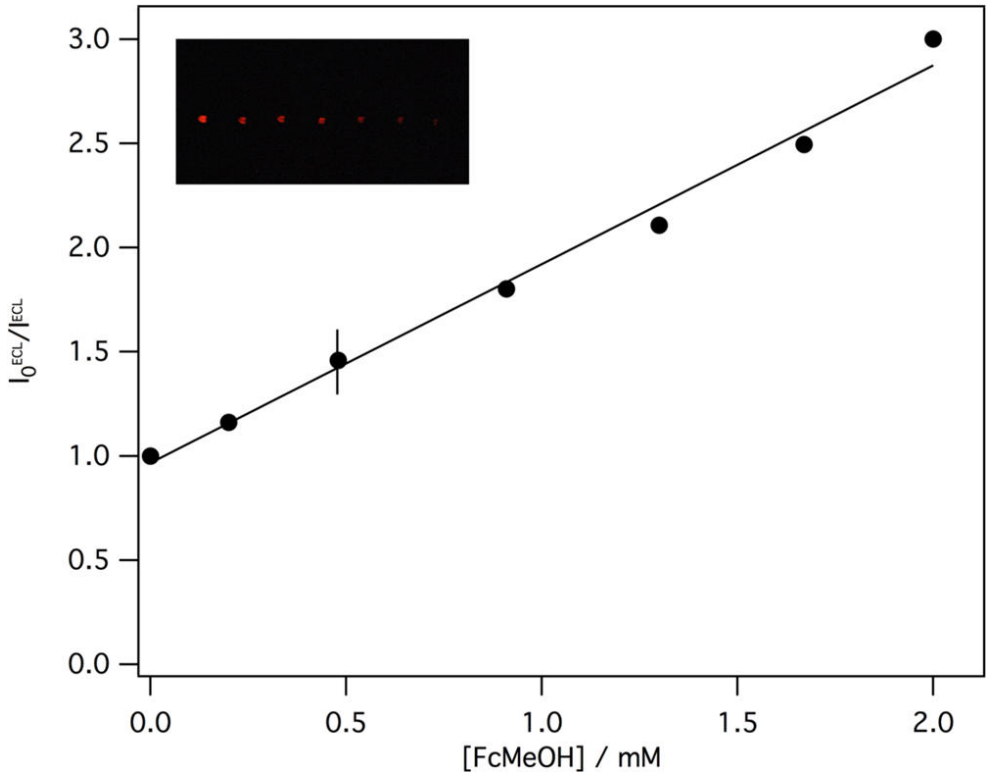

Figure 2.1 Stern−Volmer analysis of ECL quenching data for FcMeOH. Upper inset: composite image showing the dependence of steady-state ECL on [FcMeOH] (increases left to right). Lower inset: relative ECL intensity as a function of [FcMeOH]. An error bar representative of the entire data set is shown. [Reprinted with permission from *Langmuir*, 2013, 29 (51), 16040–16044. Copyright (2013) American Chemical Society.]

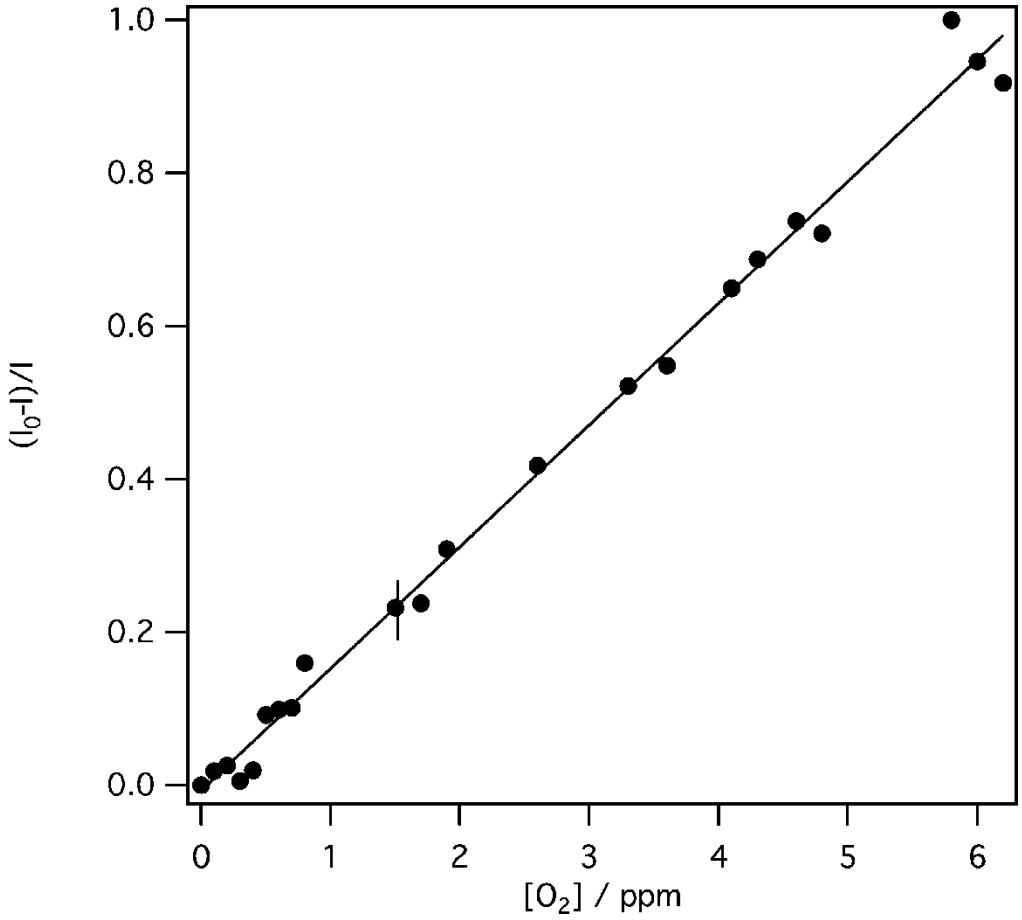

Figure 2.2 Calibration of relative ECL quenching intensities using a Clark O_2 sensor. Dissolved oxygen levels were measured every 60 s until steady state (~6 ppm) was reached. An error bar representative of the entire data set is shown. [Reprinted with permission from *Langmuir*, 2013, 29 (51), 16040–16044. Copyright (2013) American Chemical Society.]

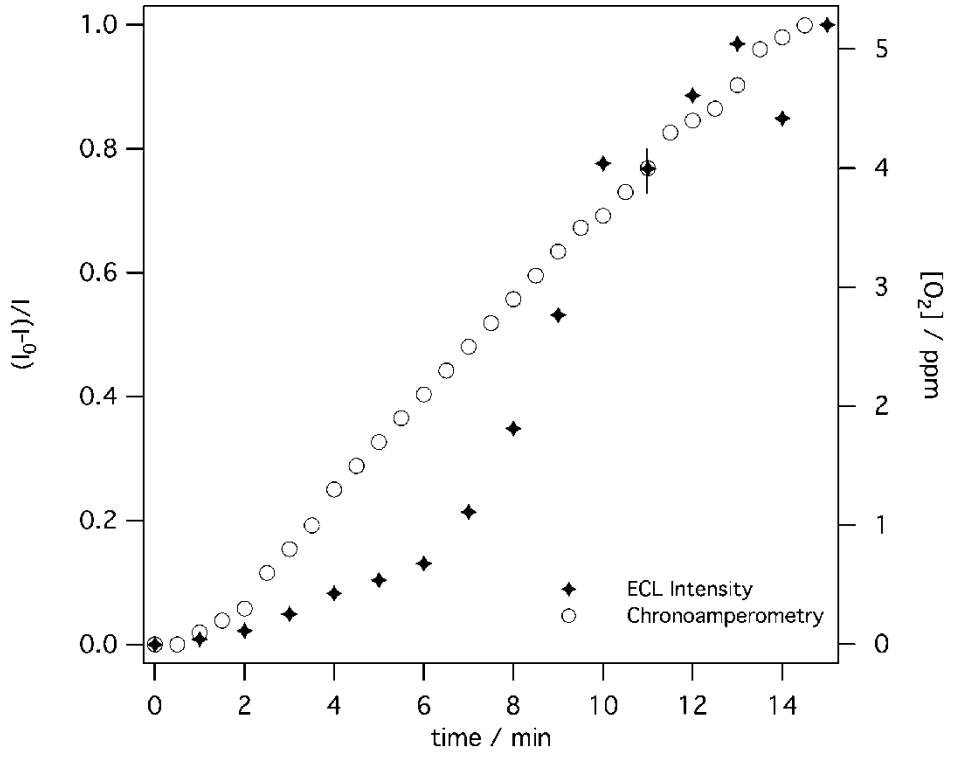

Figure 2.3 Time dependence of $[O_2]$ measured (1) near the gas inlet by chronoamperometry (open circles, right y-axis) and (2) near the bottom of the cell by ECL quenching (crosses, left y-axis). An error bar representative of the entire data set is shown. [Reprinted with permission from *Langmuir*, 2013, 29 (51), 16040–16044. Copyright (2013) American Chemical Society.]

Reference

1. Kimmel, D. W.; LeBlanc, G.; Meschievitz, M. E.; Cliffel, D. E. *Anal. Chem.* **2012**, 84, 685−707.

2. Wang, J. *J. Pharm. Biomed. Anal.* **1999**, 19, 47−53.

3. Fosdick, S. E.; Knust, K. N.; Scida, K.; Crooks, R. M. *Angew. Chem., Int. Ed.* **2013**, 52, 10438−10456.

4. Arora, A.; Eijkel, J. C. T.; Morf, W. E.; Manz, A. *Anal. Chem.* **2001**, 73, 3282−3288.

5. Chow, K.-F.; Mavre, F.; Crooks, R. M. *J. Am. Chem. Soc.* **2008**, 130, 7544−7545.

6. Zhan, W.; Alvarez, J.; Crooks, R. M. *J. Am. Chem. Soc.* **2002**, 124, 13265−13270.

7. Wei, H.; Wang, E. *Luminescence* **2011**, 26, 77−85.

8. Mavre, F.; Anand, R. K.; Laws, D. R.; Chow, K.-F.; Chang, B.-Y.; Crooks, J. A.; Crooks, R. M. *Anal. Chem.* **2010**, 82, 8766−8774.

9. Chow, K.-F.; Mavre, F.; Crooks, J. A.; Chang, B.-Y.; Crooks, R. M. *J. Am. Chem. Soc.* **2009**, 131, 8364−8365.

10. Mavre, F.; Chow, K.-F.; Sheridan, E.; Chang, B.-Y.; Crooks, J. A.; Crooks, R. M. *Anal. Chem.* **2009**, 81, 6218−6225.

11. Klett, O.; Nyholm, L. *Anal. Chem.* **2003**, 75, 1245−1250.

12. Chow, K.-F.; Chang, B.-Y.; Zaccheo, B.; Mavre, F.; Crooks, R. M. *J. Am. Chem. Soc.* **2010**, 132, 9228−9229.

13. Gaylord, B. S.; Heeger, A. J.; C. Bazan, G. C. *Proc. Natl. Acad. Sci. U. S. A.* **2002**, 99, 10954 −10957.

14. Roy, R.; Hohng, S.; Ha, T. A Practical Guide to Single-Molecule FRET. *Nat. Methods* **2008**, 5, 507−516.

15. Cao, W.; Ferrance, J. P.; Demas, J.; Landers, J. P. *J. Am. Chem. Soc.* **2006**, 128, 7572−7578.

16. Huaband, L.; Xu, G. Applications and Trends in Electrochemiluminescence. *Chem. Soc. Rev.* **2010**, 39, 3275−3304.

17. Rubinstein, I.; Bard, A. J. *J. Am. Chem. Soc.* **1981**, 103, 512−516.

18. Chang, M.-m.; Saji, T.; Bard, A. J. *J. Am. Chem. Soc.* **1977**, 99, 5399−5403.

19. Clark, C. D.; Debad, J. D.; Yonemoto, E. H.; Mallouk, T. E.; Bard, A. J. *J. Am. Chem. Soc.* **1997**, 119, 10525−10531.

20. Demas, J. N.; Adamson, A. W. *J. Am. Chem. Soc.* **1973**, 95, 5159−5168.

21. Keizer, J. *J. Am. Chem. Soc.* **1983**, 105, 1494−1498.

22. Ollino, M.; Cherry, W. R. *Inorg. Chem.* **1985**, 24, 1417−1418.

23. Zheng, H.; Zu, Y. *J. Phys. Chem. B* **2005**, 109, 12049−12053.

24. Malins, C.; Vandeloise, R.; Walton, D.; Vander Donckt, E. *J. Phys. Chem. A* 1997, 101, 5063−5068.

25. Israel, Rubinstein; Allen J. Bard. *J. Am. Chem. Soc.* **1981**, 103 (3), 512–516

26. Deniz, Ege; Becker, W. G.; Allen J. Bard. *Anal. Chem* **1984**, 56, 2413-2417

Chapter 3

Electrochemiluminescence Quenching by Halide Ions at Bipolar Electrodes

3.1 Abstract

Quenching of $Ru(bpy)_3^{2+}$ electrochemiluminescence (ECL) by Cl^-, Br^-, and I^- ions was studied as a function of halide concentration in a bipolar electrochemical cell. All of the halides investigated showed similar qualitative behavior: above a critical concentration, ECL intensity was found to decrease linearly as the halide ion concentration was increased, due to dynamic quenching of $Ru(bpy)_3^{2+}$ ECL. Stern-Volmer slopes (K_{SV}) of 0.111±0.003, 4.2±0.3, and 6.2±0.3 mM^{-1} were measured for Cl^-, Br^- and I^-, respectively. The magnitude of K_{SV} correlates with halide ion oxidation potential, consistent with an electron transfer quenching mechanism. Using the bipolar platform described herein, aqueous, halide-containing solutions could be quantified rapidly using the sequential standard addition method. The lower detection limit is determined by a complex mechanism involving the competitive electrooxidation of halide ions and the ECL co-reactants, as well as the passivation of the surface of the bipolar electrode, and was found to be 0.20±0.01, 0.08±0.01 and 10±1 mM, respectively, for I^-, Br^-, and Cl^-. The performance of the bipolar ECL quenching assay is comparable to previously published fluorescence quenching methods for the determination of halide ions, while being much simpler and less expensive to implement.

3.2 Introduction

There has been increased interest in the fundamental aspects of bipolar electrochemistry in recent years, leading to many new applications, including amperometric detection of analytes,[1-4] generation of particle motion,[5-7] analytical separations,[8] metal and polymer deposition,[9-14] formation of Janus particles,[15-17] the study of corrosion and the evaluation of electrocatalysts.[18,19] Since the original paper by Manz and coworkers,[20] the use of electrochemiluminescence (ECL) to monitor the state of bipolar electrodes optically has been successfully applied in the development of biosensors,[21-24] the study of particle dynamics,[25-27] fluorescence imaging and microscopy,[28-30] and the development of electrochemical integrated circuits.[31] Previously, our research group has demonstrated the feasibility of detecting small molecules such as ferrocene methanol (FcMeOH) and O_2 using ECL quenching in a bipolar electrochemical cell.[32]

The detection of halide ions is important in multiple areas of chemical analysis. For example, chloride contamination from salt water poses a significant threat to aquatic life and its determination is an important aspect of environmental analysis.[33] Detection of elevated chloride levels in saliva and sweat remains an important clinical method for the diagnosis of cystic fibrosis.[34] Determination of halide ions also is important in monitoring industrial waste streams and in the food industry.[35] Fluorescence quenching is a powerful method to detect halide ions (particularly Cl^-, Br^- and I^-) and this application was reviewed in detail by Geddes in 2001.[36]

In this work, we attempt to understand the dependence of $Ru(bpy)_3^{2+}$ ECL intensity on the concentration of halide ions in the context of bipolar electrochemistry, with the ultimate goal of using ECL quenching techniques to broaden the range of analytes that can be quantified using

bipolar sensing platforms. We first investigate quenching behavior under experimental conditions where quenching is well described using a simple Stern–Volmer model. We then explore the possibility of using this sensing platform to rapidly quantify aqueous halide-containing solutions using sequential standard addition. Finally, we show that the lower limit of detection of halide ions is determined by a competition between halide electrooxidation, the oxidation of the ECL co-reactant, and the formation of an oxide layer on the surface of the Pt sensing electrode.

3.3 Experimental section

Materials. Tris(2,2'-bipyridyl)dichlororuthenium(II) hexahydrate (99.95%), sodium oxalate (99.5+%), sodium perchlorate (90.0+%) sodium chloride (99.5+%), sodium bromide (99.5+%), sodium iodide (99.5+%), perchloric acid (70.0%), sulfuric acid (95.0-98.0%), ethanol (99.5+%) and hydrogen peroxide solution (30.0 wt.%) were purchased from Sigma-Aldrich (USA). All materials were used without further purification. Millipore-Q purified (DI) water (18.2 MΩ.cm) was used to prepare all solutions and to rinse electrodes.

Synthesis of $Ru(bpy)_3(ClO_4)_2$. $Ru(bpy)_3(ClO_4)_2$ was synthesized according to literature methods.[37] Specifically, 0.2 g $Ru(bpy)_3Cl_2$ dissolved in DI water was converted to $Ru(bpy)_3(ClO_4)_2$ by adding an excess of saturated $NaClO_4$ solution. The precipitate was collected and recrystallized twice in an ethanol-acetone solution (5:1, v/v). The product was dried in a vacuum oven at 130 °C and stored in a refrigerator at 4 °C.

Assembly of Bipolar Devices. A segment of platinum wire (l_{elec} = 1.4 cm, d = 0.7 mm) was used as bipolar electrode (BPE). The Pt electrode was polished using an aqueous slurry of 0.05 μm

alumina and was then washed with water and ethanol in an ultrasonic cleaner, finally it was immersed in a freshly prepared piranha solution (H_2SO_4/H_2O_2, 3:1, v/v) for about 5 min, rinsed with DI water, and dried under nitrogen gas. The two gold foil electrodes were cleaned using the same procedure. The Pt-BPE was then permanently affixed to the center of a glass cell (diameter = 5 cm) using epoxy. (*Caution: piranha solution is very corrosive and dangerous to human health and should be used with extreme caution and handled only in small quantities.*[32])

Apparatus and procedures. Test solutions consisted of 15.4 mg $Ru(bpy)_3(ClO_4)_2$, 50.2 mg $Na_2C_2O_4$ dissolved in 15 mL 1 mM $HClO_4$ solution purged with N_2 for about 30 mins to get rid of oxygen. A potential of 15 V was applied between the driver electrodes using a regulated dc power supply (Hewlett-Packardmodel 6010). ECL signals were recorded using a Nikon D3100 or an Olympus OMD-EM5 digital camera in a darkened room using an exposure of 1/10 s at f/2.0 and an ISO value of 1600. Images were processed and corrected for dark current using ImageJ software. We measured the average ECL intensity over the active (ECL emitting) part of the BPE anode. A background measurement was collected from a dark part of the image (using the same total area) and subtracted from the average ECL intensity. Cyclic voltammetry was performed with an Epsilon electrochemistry workstation (Bioanalytical System, Inc) using a traditional airtight three-electrode cell with a Pt disk (diameter = 1.6 mm, Bioanalytical System, Inc) as the working electrode, a Pt mesh as the counter electrode and a saturated Ag/AgCl reference electrode.

3.4 Results and discussion

The bipolar electrochemical circuit employed in this study is shown schematically in Figure 3.1. A Pt

bipolar electrode (BPE) is positioned at the center of the measuring cell and is submerged in the test solution. An external potential difference (E_{total}) applied between two Au driver electrodes generates a potential difference (ΔE_{elec}) across the Pt BPE, which drives simultaneous oxidation and reduction reactions at the two poles. In the experiments described here, hydrogen ions are reduced at their diffusion-limited rate at the cathodic pole, while $Ru(bpy)_3^{2+}$ electro- chemiluminescence (ECL) is generated at the anodic pole. Under these experimental conditions, a stable, steady-state ECL bright enough to be observed by the naked eye is recorded using a digital camera. Once halide ions (Cl^-, Br^- and I^-) are introduced into the system, the ECL intensity decreases in direct proportion to their concentration due to quenching.[32]

The mechanism of $Ru(bpy)_3^{2+}$/oxalate ECL has been discussed at length in the literature and will not be considered further here.[38-40] In the present context, the important fact is that, in the absence of any quenchers, the ECL intensity is a direct measure of the current flowing through the BPE.[41] Under conditions where protons are reduced at their diffusion limited rate at the cathodic pole, a stable ECL intensity, I_0, can be measured at the anodic pole of the BPE. When halide ions are admitted into the cell, this ECL is quenched, and an attenuated ECL intensity, I, is measured. Prior to making measurements, the cell is purged with N_2 for ca. 30 min to eliminate O_2, which, as noted earlier, is also able to quench ECL. We have previously reported that in the case of many small molecules, $Ru(bpy)_3^{2+}$ ECL quenching can be described adequately using the Stern-Volmer equation (Equation 1). By rearranging this equation, it can be seen that the quantity $(I_0 - I)/I$ should be a linear function of the quencher concentration (Equation 2).[42,43] Thus, calibration curves can

be constructed by plotting $(I_0 - I)/I$ as a function of halide concentration. The slope of the calibration curve is expected to be equal to the Stern-Volmer constant, K_{SV}.

$$I_0/I = 1 + K_{SV}[Q] \quad [1]$$

$$(I_0 - I)/I = K_{SV}[Q] \quad [2]$$

In these equations, I_0/I is the observed ratio of ECL intensity in an unquenched sample to that in a quenched one, and K_{sv} is the Stern-Volmer constant.

Representative concentration dependent quenching data are shown for each halide ion in Figure 3.2. All three of the halides studied exhibited similar quenching behavior. Above an ion-dependent critical concentration, $(I_0\text{-}I)/I$ was found to increase linearly with the increase of halide ion concentration due to dynamic quenching of $Ru(bpy)_3^{2+}$ ECL as predicted by Equation 2. Deviations from the linear behavior predicted by the Stern-Volmer equation at low concentration will be discussed in detail below. Linear least squares fits of the data are shown as dashed lines in Figure 3.2. Stern-Volmer slopes (K_{SV}) obtained from the linear portion of these curves are noted on the graphs in Figure 3.2 and are summarized in Table 3.1. K_{SV} values were found to correlate with the formal oxidation potential of the halides, as shown in Table 3.1. This phenomenon has been investigated previously by other groups, and supports a quenching mechanism that involves electron transfer between the halide ion and $Ru(bpy)_3^{2+}$.[43-45]

One of the advantages of a bipolar detection system is rapid, real time data acquisition. We therefore wished to explore the possibility of quantifying the concentration of halide ions using

sequential standard addition (SSA) techniques. Representative SSA quenching data acquired for a test solution initially containing 0.20 mM Br^- are shown in Figure 3.3 (open circles, dashed line). In this experiment, sequential additions of 15 µL of 50 mM Br^- standard solution were made to the test solution (V_0 = 15 mL). Starting from the Stern-Volmer relationship (Eqn. 2) it is straightforward to show that the ECL quenching response for SSA is given by Equation 3, which shows that the concentration of the test solution can be determined from the absolute value of the x-intercept of the SSA plot (Figure 3.3).

$$I_n(V/V_0)=K_{SV}^{Br-}[Br^-] + K_{SV}^{Br-}(nC'_{Br-}-V'_{Br-}/V_0) \quad [3]$$

In this equation, I_n is the ECL intensity after n standard additions, C'_{Br-} is the concentration of the Br^- standard solution, V'_{Br-} is the volume of standard added and V_0 is the initial volume of the test solution, and V/V_0 is the dilution factor. The slope of the SSA plot is 4.1±0.2 mM^{-1}, within 3% of the value measured for the Br^- calibration curve shown in Figure 3.2. From the x-intercept of the SSA plot, we calculate [Br^-] = 0.21±0.01 mM, in excellent agreement with the known value. The graphical determination of [Br^-] is also illustrated in Figure 3.3.

Next, we wished to test whether SSA could be used to determine [Br^-] in the presence of an interfering (ECL quenching) species such as I^-. Wolfbeis and Urbano[46] extended the Stern-Volmer equation to describe dynamic quenching in solutions containing a single fluorophore that interacts with multiple dynamic quenchers. In the case of two quenchers (such as Br^- and I^-), the modified

Stern-Volmer equation is given by Equation 4.

$$(I_0\text{-}I)/I = K_{SV}^{Br^-}[Br^-] + K_{SV}^{I^-}[I^-] \quad [4]$$

Here, the K_{SV} values are obtained from the single component calibration curves (i.e., the linear portion of Figure 3.2). Starting with Equation 4, it is straightforward to show that for a solution containing a mixture of I^- and Br^- that is analyzed by SSA of Br^-:

$$I_n(V/V_0) = K_{SV}^{I^-}[I^-] + K_{SV}^{Br^-}[Br^-] + K_{SV}^{Br^-}(nC'_{Br^-}V'_{Br^-}/V_0) \quad [5]$$

If $I_n(V/V_0)$ is plotted as a function of $(nC'_{Br^-}V'_{Br^-}/V_0)$, the x-intercept is given by $[I^-](K_{SV}^{I^-} / K_{SV}^{Br^-}) + [Br^-]$.

To validate this approach, we performed sequential standard addition (SSA) of Br^- on a test solution initially containing 0.20 mM Br^- and 0.30 mM I^-. Experimental data are plotted in Figure 3.3 (solid line). The slope of the line is 4.1±0.1 mM^{-1}, which is within experimental error of the previous SSA and calibration curve data. We modeled the ECL quenching response under these experimental conditions using Equation 5. Using $[I^-]$ = 0.30 mM, we found $[Br^-]$ 0.19±0.02 mM, in excellent agreement with the known value.

At lower concentrations of halide, the quenching behavior deviates from the Stern-Volmer behavior discussed above. Furthermore, there appears to be a critical halide concentration, $[X^-]_{crit}$,

where these effects onset, with an apparent ECL enhancement below $[X^-]_{crit}$. An expanded plot showing the quenching behavior of all three halide ions near $[X^-]_{crit}$ is shown in Figure 3.4. The critical halide concentration is ca. 2 mM for Cl^-, 0.02 mM for Br^- and 0.01 mM for I^-. This observation is consistent with the known adsorption strength of the halides on Pt, which increases in the order $Cl^- < Br^- < I^-$.[47-49] Halide chemisorption has been shown to inhibit the formation of Pt surface oxides, which would be expected to lead to an increase in the rate of oxidation of both $Ru(bpy)_3^{2+}$ and $C_2O_4^{2-}$, thus accounting for the apparent enhancement of ECL.[48,50] Cyclic voltammetry performed at low halide concentrations, confirms this effect, Figure 3.5. The data shown here clearly demonstrate that the potential required for Pt surface oxide formation shifts to more positive potentials in the presence of halide, consistent with inhibition of Pt oxide formation. Recently, Miao, et al.[50] reported enhanced ECL at Au electrodes in the presence of Cl^-, attributing this effect to the formation of gold-chloride complexes. In addition to the inhibition of the Pt oxidation reaction, it should be noted that $[X^-]_{crit}$ also correlates with the formal oxidation potential of the halide ions. Oxidation of halide ions at the anodic pole of the BPE reduces the effective concentration of quencher near the electrode surface, also contributing to the apparent increase in the ECL intensity. The combination of these three effects—the increased rate of co-reactant oxidation and the oxidation of halide ions near the electrode surface, which compete with the oxidation of the Pt surface—accounts for the complex concentration dependence observed at low halide concentrations, and ultimately sets the detection limit achievable using this technique.

3.5 Conclusions

In this paper, ECL quenching by halide ions was studied in a bipolar electrochemical cell. All halides exhibited a critical concentration above which the quenching was well described by the Stern-Volmer equation, yielding linear calibration curves. The lower detection limit was defined by several interacting factors including halide oxidation, Pt passivation and the efficiency of ECL co-reactant redox reaction. Within the Stern-Volmer region, the behavior of the halides is consistent with an electron transfer quenching mechanism. Using an extended Stern-Volmer model, we demonstrate the possibility of quantifying solutions of halides using sequential standard addition. The advantage of the bipolar platform is its experimental simplicity: quantitative measurements can be performed using a voltage source and a digital camera.

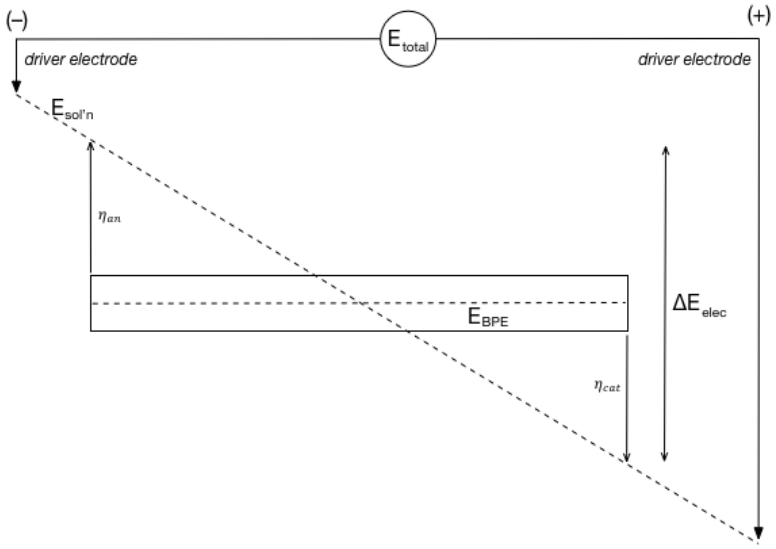

Figure 3.1 Schematic diagram of the bipolar electrochemical circuit used for ECL quenching measurements.

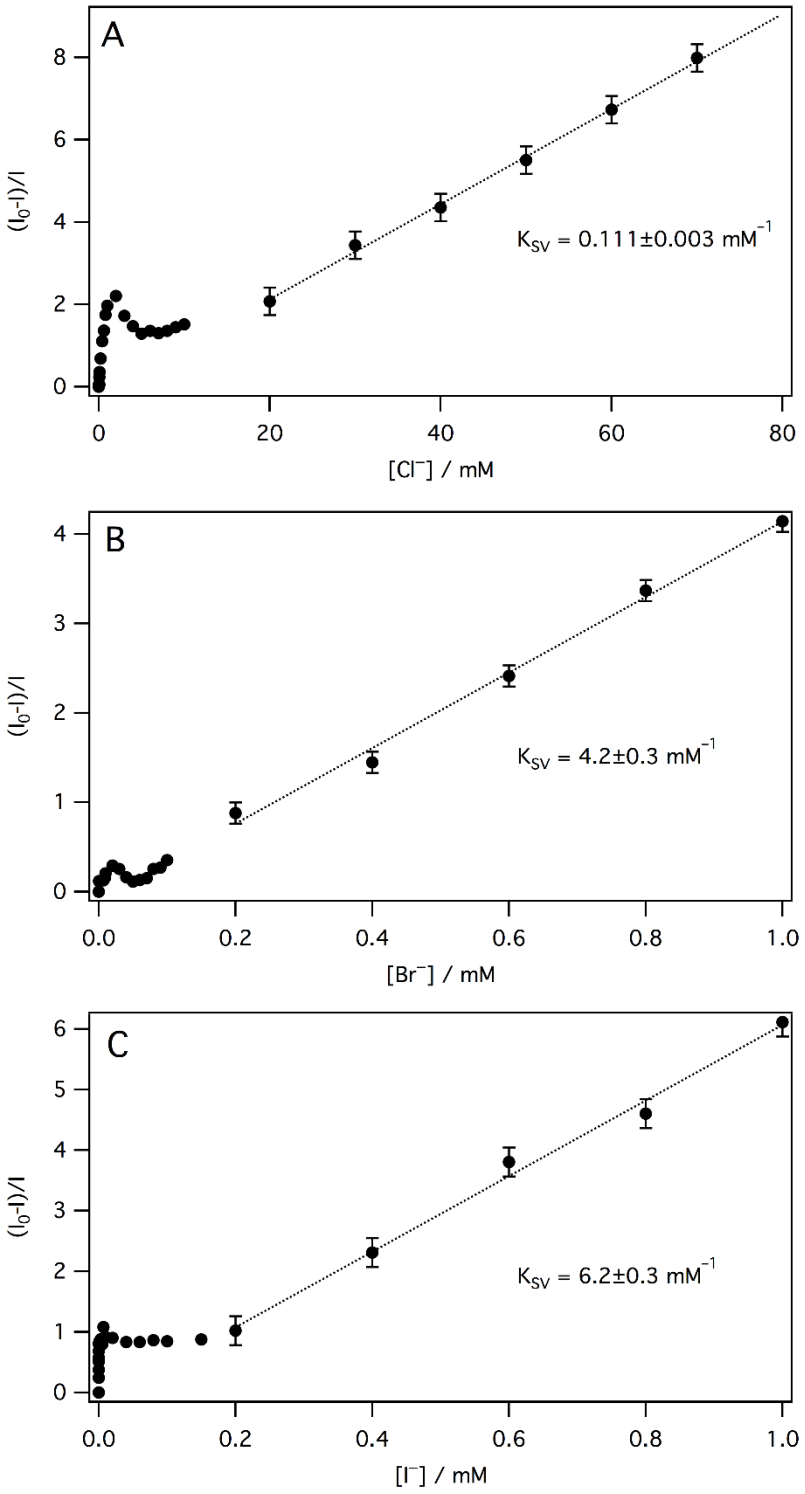

Figure 3.2 Concentration dependence of $Ru(bpy)_3^{2+}$ ECL quenching by I^-, Br^-, and Cl^-.

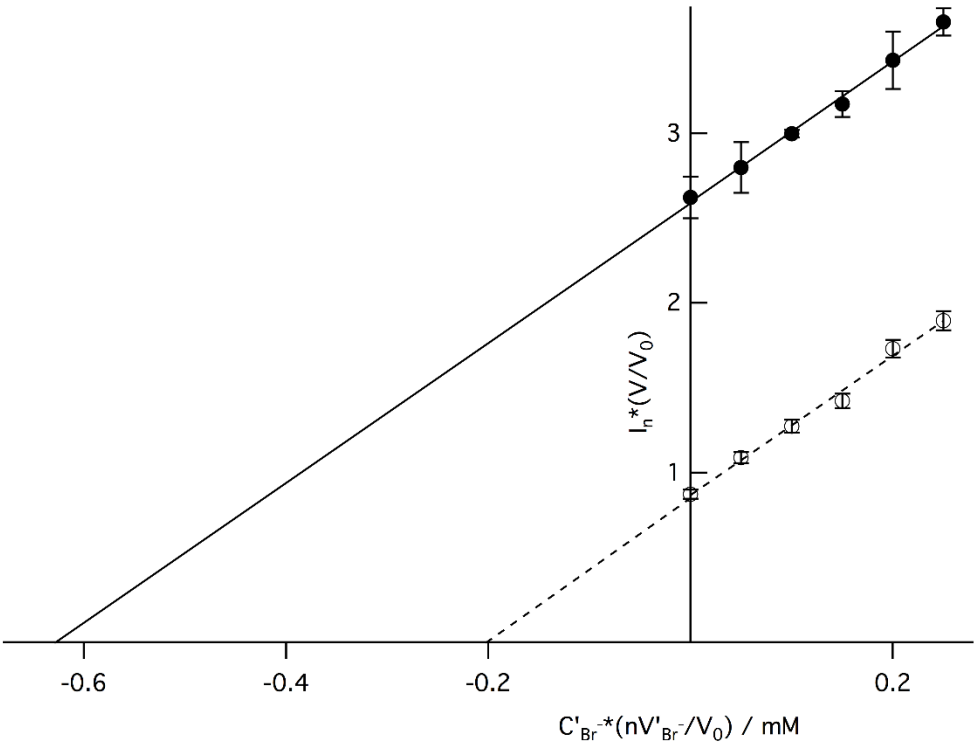

Figure 3.3 Quantitation of [Br^-] by sequential standard addition. Symbols are defined in the text.

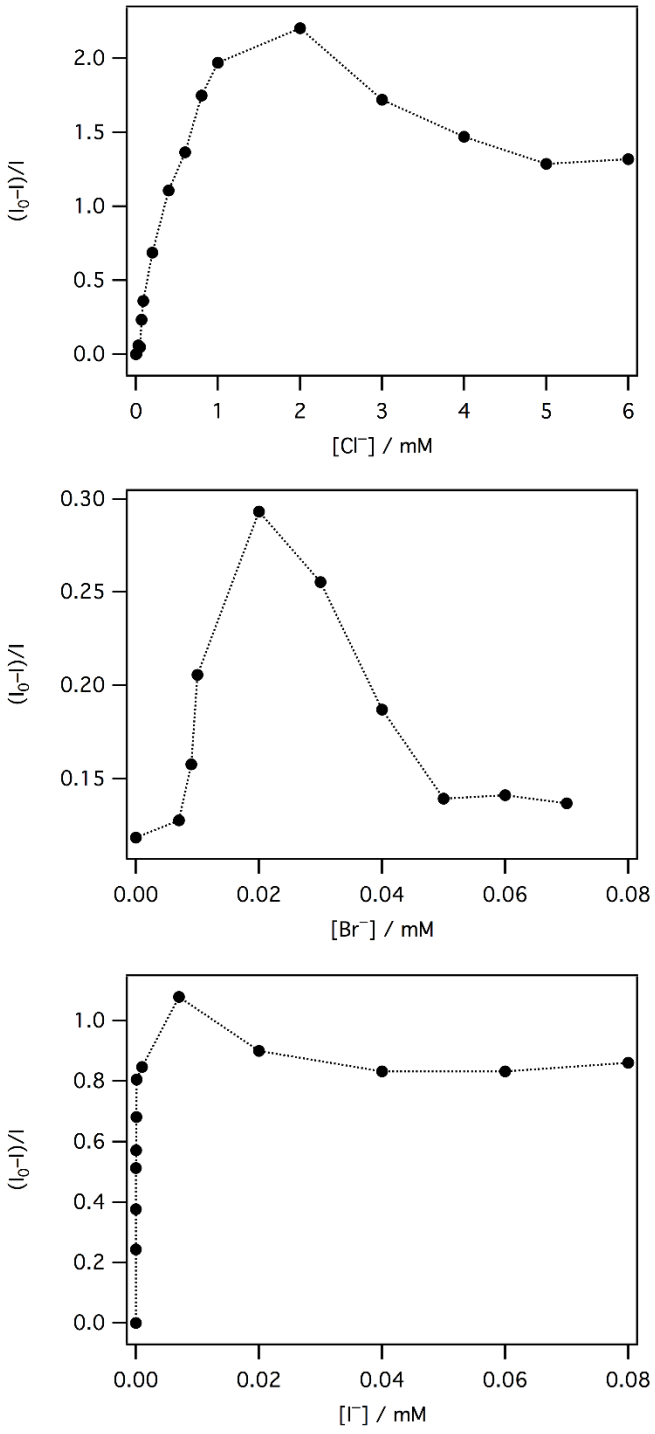

Figure 3.4 Concentration dependent quenching by halide ions near the lower detection limit. The dashed lines are guides to the eye.

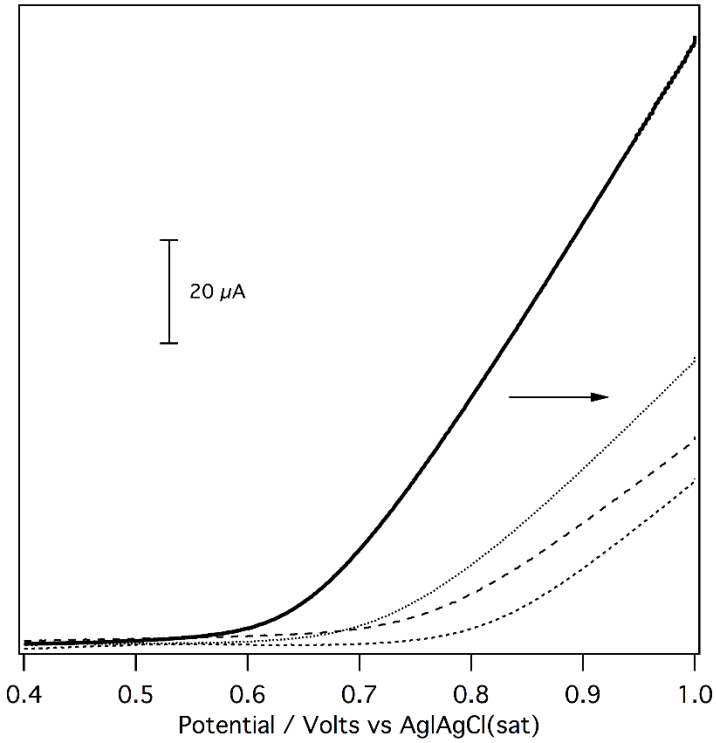

Figure 3.5 Cyclic voltammetry measured in a conventional three electrode cell showing the effect of halide on the kinetics of Pt oxide formation.

Table 3.1. Analysis of halide ion quenching of $Ru(bpy)_3^{2+}$ ECL.

Halide ion	Linear range (mM)	K_{sv} (mM^{-1})	Oxidation Potential (V)
I^-	0.2 to 1.0	6.2±0.3	0.535
Br^-	0.08 to 1.0	4.2±0.3	1.080
Cl^-	10.0 to 90.0	0.111±0.003	1.360

Reference

1. Zhan, W.; Alvarez, J.; Crooks, R. M. *J. Am. Chem. Soc* **2002,** *124* (44), 13265-13270.

2. Zhan, W.; Alvarez, J.; Crooks, R. M. *Anal. Chem* **2003,** *75* (2), 313-318.

3. Zhan, W.; Alvarez, J.; Sun, L.; Crooks, R. M. *Anal. Chem* **2003,** *75* (6), 1233-1238.

4. Chow, K. F.; Chang, B. Y.; Zaccheo, B. A.; Mavre, F.; Crooks, R. M. *J. Am. Chem. Soc* **2010,** *132* (27), 9228-9229.

5. Wang, Y.; Hernandez, R. M.; Bartlett, D. J.; Bingham, J. M.; Kline, T. R.; Sen, A.; Mallouk, T. E. *Langmuir* **2006,** *22* (25), 10451-10456.

6. Loget, G.; Kuhn, A. *J. Am. Chem. Soc* **2010,** *132* (45), 15918-15919.

7. Loget, G.; Kuhn, A. *Lab. Chip* **2012,** *12* (11), 1967-1971.

8. Laws, D. R.; Hlushkou, D.; Perdue, R. K.; Tallarek, U.; Crooks, R. M. *Anal. Chem* **2009,** *81* (21), 8923-8929.

9. Fattah, Z.; Garrigue, P.; Lapeyre, V.; Kuhn, A.; Bouffier, L. *J. Phys. Chem. C* **2012,** *116* (41), 22021-22027.

10. Inagi, S.; Nagai, H.; Tomita, I.; Fuchigami, T. *Angew. Chem. Int. Ed* **2013,** *52* (26), 6616-6619.

11. Ishiguro, Y.; Inagi, S.; Fuchigami, T. *Langmuir* **2011,** *27* (11), 7158-7162.

12. Inagi, S.; Ishiguro, Y.; Atobe, M.; Fuchigami, T. *Angew. Chem. Int. Ed* **2010,** *49* (52), 10136-

10139.

13. Ramakrishnan, S.; Shannon, C. *Langmuir* **2010,** *26* (7), 4602-4606.

14. Ramaswamy, R.; Shannon, C. *Langmuir* **2011,** *27* (3), 878-81.

15. Loget, G.; Roche, J.; Kuhn, A. *Adv. Mater* **2012,** *24* (37), 5111-5116.

16. Kumsapaya, C.; Bakai, M. F.; Loget, G.; Goudeau, B.; Warakulwit, C.; Limtrakul, J.; Kuhn, A.; Zigah, D. *Chem-Eur. J* **2013,** *19* (5), 1577-1580.

17. Loget, G.; Roche, J.; Gianessi, E.; Bouffier, L.; Kuhn, A. *J. Am. Chem. Soc* **2012,** *134* (49), 20033-20036.

18. Munktell, S.; Tyden, M.; Hogstrom, J.; Nyholm, L.; Bjorefors, F. *Electrochem. Commun* **2013,** *34*, 274-277.

19. Fosdick, S. E.; Berglund, S. P.; Mullins, C. B.; Crooks, R. M. *Acs. Catal* **2014,** *4* (5), 1332-1339.

20. Arora, A.; Eijkel, J. C. T.; Morf, W. E.; Manz, A. *Anal. Chem* **2001,** *73* (22), 5633-5633.

21. Zhang, X. W.; Chen, C. G.; Li, J.; Zhang, L. B.; Wang, E. K. *Anal. Chem* **2013,** *85* (11), 5335-5339.

22. Zhang, X. W.; Li, J.; Jia, X. F.; Li, D. Y.; Wang, E. K. *Anal. Chem* **2014,** *86* (11), 5595-5599.

23. Wu, M. S.; Yuan, D. J.; Xu, J. J.; Chen, H. Y. *Chem. Sci* **2013,** *4* (3), 1182-1188.

24. Feng, Q. M.; Pan, J. B.; Zhang, H. R.; Xu, J. J.; Chen, H. Y. *Chem. commun* **2014,** *50* (75),

10949-10951.

25. Sentic, M.; Loget, G.; Manojlovic, D.; Kuhn, A.; Sojic, N. *Angew. Chem. Int. Ed* **2012,** *51* (45), 11284-11288.

26. Bouffier, L.; Zigah, D.; Adam, C.; Sentic, M.; Fattah, Z.; Manojlovic, D.; Kuhn, A.; Sojic, N. *Chemelectrochem* **2014,** *1* (1), 95-98.

27. Sentic, M.; Arbault, S.; Goudeau, B.; Manojlovic, D.; Kuhn, A.; Bouffier, L.; Sojic, N. *Chem. commun* **2014,** *50* (71), 10202-10205.

28. Bouffier, L.; Doneux, T.; Goudeau, B.; Kuhn, A. *Anal. Chem* **2014,** *86* (8), 3708-3711.

29. Guerrette, J. P.; Percival, S. J.; Zhang, B. *J. Am. Chem. Soc* **2013,** *135* (2), 855-861.

30. Oja, S. M.; Guerrette, J. P.; David, M. R.; Zhang, B. *Anal. Chem* **2014,** *86* (12), 6040-6048.

31. Chang, B. Y.; Crooks, J. A.; Chow, K. F.; Mavre, F.; Crooks, R. M. *J. Am. Chem. Soc* **2010,** *132* (43), 15404-15409.

32. Wang, T.; Fan, S.; Erdmann, R.; Shannon, C. *Langmuir* **2013,** *29* (51), 16040-16044.

33. Cosentino, P.; Grossman, C.; Shieh, C.; Doi, S.; Xi, H.; Erbland, P. *J. Geotech. Eng.* **1995**, *121*, 610–17.

34. Quinton. P. M. *Physiology*, **2007**, *22*, 212-225.

35. Frassetto, L. A.; Morris, R. C., Jr.; Sellmeyer, D. E.; Sebastian, A. *J. Nutrition* **2008**, *138*, 419S-422S.

36. Geddes, C. D. *Meas. Sci. Technol.* **2001,** *12*, R53-R58.

37. Mccord, P.; Bard, A. J. *J. Electroanal. Chem* **1991,** *318* (1-2), 91-99.

38. Miao, W. J. *Chem. Rev* **2008,** *108* (7), 2506-2553.

39. Chang, M. M.; Saji, T.; Bard, A. J. *J. Am. Chem. Soc* **1977,** *99* (16), 5399-5403.

40. Rubinstein, I.; Bard, A. J. *J. Am. Chem. Soc* **1981,** *103* (3), 512-516.

41. Chow, K.-F.; Mavré, F.; Crooks, R. M. *J. Am. Chem. Soc.* **2008**, *130*, 7544-7545.

42. Lakowicz, J. R. *Plenum Press* **1983**.

43. Moriya, T. *B Chem. Soc. Jpn* **1984,** *57* (7), 1723-1730.

44. Giri, R. *Spectrochim. Acta. A* **2004,** *60* (4), 757-763.

45. Parker, D.; Senanayake, P. K.; Williams, J. A. G. *J. Chem. Soc. Perk T 2* **1998,** (10), 2129-2139.

46. Wolfbeis, O. S.; Urbano, E. *Anal. Chem* **1983**, *55*, 1904-1906.

47. Conway, B. E.; Phillips, Y.; Qian, S. Y. Y. *J. Chem. Soc. Faraday T* **1995,** *91* (2), 283-293.

48. Zu, Y. B.; Bard, A. J. *Anal. Chem* **2000,** *72* (14), 3223-3232.

49. Novak, D. M.; Conway, B. E. *J. Chem. Soc. Farad T 1* **1981,** *77*, 2341-2359.

50. Wang, S. J.; Neshkova, M. T.; Miao, W. J. *Electrochimica. Acta* **2008,** *53* (26), 7661-7667.

Chapter 4

Chemical Analysis Based on Surface Enhanced Raman Scattering at Bipolar Electrode

4.1 Abstract

Over the past few decades, bipolar electrochemistry has been an attractive and powerful technique for scientists because of its convenience and utility in various application ranging from analytical chemistry to material science. When enough voltage was applied, the redox reactions can be generated at the extremes of the bipolar electrode without direct connection with the driving electrode. More interestingly, there exists a potential gradient going across the surface of bipolar electrode. Many works have been done in the use of this gradient, however, they cannot identify the specific potential difference between the surface of bipolar electrode and the solution at certain points. Here, we develop a method for the detection of the potential gradient by using spectroelectrochemical characterization of bipolar electrode based on surface enhanced raman scattering (SERS). Specifically, the probe molecule 2-Anthraquinonyl sulfide (2-AQS) can be transformed electrochemically to 2-Hydroanthraquinonyl sulfide at the cathodic pole of the bipolar electrode because of the presence of potential difference along the bipolar electrode. Thus, the relative population of 2-AQS to 2-H_2AQS will vary accordingly resulting in a gradient in both species. SERS was used to monitor the intensity variation of them as a function of axial position

from the cathodic pole moving toward middle. The result is that the dependence of SERS response on the applied potential was found to follow the Nernst equation such that the specific potential difference existing at the interface between the solution and the bipolar electrode can be calculated.

4.2 Introduction

Over the past few decades, bipolar electrochemistry has received considerable attention because as a powerful electrochemical technique it offers a useful tool to detect analytes of interest,[1-3] observe motions,[4-7] separate materials,[8-10] deposit metals and polymer,[11-14] synthetize janus particles,[15-17] study corrosion[18] and evaluate electrocatalyst[19, 20] without a direct connection to the working electrode. Upon sufficient voltage was applied on the driving electrode, two coupled redox reactions were generated at the extremes of the bipolar electrode simultaneously, that is, reduction reaction in the cathodic pole of bipolar electrode and oxidation reaction in the anodic pole of bipolar electrode. The key point is that there exists a interfacial potential gradient that is the driving force for electron transfer between the electrode and the solution.[21] It should be note that the interfacial potential difference between a point on the bipolar electrode and the solution varies laterally along the surface, which will go down from the poles toward middle. The rates of redox reactions are highest at the extremes of the bipolar electrode and then dropped down towards middle, because of the interfacial potential difference serving as the driving force for electrochemical reactions. Surface gradients of various chemical and physical properties can be generated by this variation in interfacial potential difference. The development of sophisticated patterning techniques such as lithography led to changes and advances in patterning surface with

chemical or physical properties[22, 23]. It should be noted that the patterns made in this way have very sharp boundaries between the distinct chemical or physical regions on the substrate. However, they can be applied in different domains, for example, they can be used to move liquids across a given surface,[24] they can also be used in property screening with a lower cost.[25, 26] New catalysts and drugs can be designed[27] and protein adsorption can also be monitored.[28, 29] Most of the techniques for creating material gradients rely on processes such as deposition,[30] diffusion,[31, 32] and immersion,[33, 34] electric fields,[35] electrochemical method[36, 37] and microfluidics.[38, 39] Larsen and coworkers recently used "electro click chemistry" to create a concentration gradient of alkyne-terminated molecules on an azide-funtionalized polymer substrate.[40] In the comparison with these previous work in generating gradients, bipolar electrochemistry seems more convenient to set up and easier to control the gradient by the adjustment of eternal voltage. For this reason, it has garnered considerable research attention to date. Most recently, Shinsuke Inagi and co-workers investigated electro-click reaction of azide-function-alized poly (3,4-ethylenedioxythiophene) (PEDOT-N_3) and a terminal alkyne catalyzed by a gradient distribution Cu(I) generated on the surface of bipolar electrode and this trend was also proved by UV-Vis spectrophotometer.[41] Fredrik and co-workers developed imaging surface plasmon resonance to display the variation on the surface of bipolar electrode, which will vary in accordance to the electrochemical reactions generating the refractive index change close to the surface.[42] Although lots of work was made to measure the potential, the exact potential difference was not obtained or indirect values were calculated approximately.[42-44] In this work, we report a non-destructive patterning of a SAM of a

thiol-funtionalized moiety. 2-Anthraquinonyl sulfide (2-AQS) can be transformed electrochemically to 2-Hydroanthraquinonyl sulfide (2-H_2AQS) on the cathodic part of bipolar electrode when external potential is sufficient. Because of the presence of potential difference along the bipolar electrode, thus, the relative population of 2-AQS to 2-H_2AQS will vary accordingly, and it results in a gradient in both species. SERS was used to monitor the intensity variation of them as a function of axial position from the cathodic pole moving toward middle. The result demonstrated the dependence of SERS response on the potential difference between bipolar electrode and solution was found to follow the Nernst equation such that the specific potential difference and x_0 at which the potential difference is zero exiting at the interface between the solution and the bipolar electrode can be calculated. Additionally, the position on bipolar electrode at which 2-AQS initially reduced will shift to middle when applying more voltage on the bipolar cell.

4.3 Experimental section

Materials. Butanethiol, 2-chloroanthraquinone, ethanol, hydrogen tetrachloroaurate(III) and N,N-dimethylacetamide were of analytical grade from Aldrich and were used as received. Stainless steel and gold plate (99.99%) were purchased from Aldrich. Alumina slurry and microfiber polishing cloth were purchased from Buehler. A 0.1M Britton – Robinson buffer (pH = 7) as the electrolyte was used in all electrochemical measurements. Millipore-Q purified (DI) water (18.2 MΩ.cm) was used to prepare all solutions and to rinse electrodes. 2-anthraquinonylbutylsulfide (2-AQS) was synthesized according to the methods in literature.[45]

Assembly of Bipolar Devices. 2 cm stainless steel was polished by using 0.05 μm size Alumina paste and then sonicated in distilled water and ethanol mixed solution for 5 mins. It was then rinsed with distilled water. Au plates as driving electrodes were polished using an aqueous slurry of 0.05 μm alumina and were then washed with water and ethanol in an ultrasonic cleaner. Au was deposited on one side (ca. 1 cm) of stainless steel in hydrogen tetrachloroaurate(III) solution under 2 V direct voltage using a regulated dc power supply (Hewlett-Packardmodel 6010). The stainless steel with gold was immersed in a 1 mM 2-AQS solution for 12 hrs.

Electrochemical Measurements. Cyclic voltammetry was performed in 0.1M Britton – Robinson buffer using traditional setup with an Epsilon electrochemistry workstation (Bioanalytical Systems, Inc.), in which the working electrode was as prepared gold substrate on which 2-AQS assembled, counter electrode was a Pt gauze, and reference electrode was Ag/AgCl/KCl (1 M) (Bioanalytical Systems, Inc.) Note: the buffer solution was purged with N_2 for 30 mins to drive away the dissolved O_2.

Raman Spectroscopy Measurement. After immersing stainless steel with gold in 1 mM 2-AQS for 12 hrs, it was fixed in the middle of a glass cell (diameter = 5 cm) with a 0.1M Britton – Robinson buffer. Note: the buffer solution was purged with N_2 for 30 mins to drive away the dissolved O_2. Two golden plates were used as driving electrodes, which also connected to a power supply (Hewlett-Packardmodel 6010). Raman scattering was excited with a 514 nm laser (ca. 34 mW) and signals were collected and analyzed using a Renishaw InVia confocal Raman microscope.

4.4 Result and discussion

The cyclic voltammetry experiment indicated that 2-AQS is an electrochemically active material that can be used as a probe in the following bipolar electrochemical experiments. Specifically, the oxidation and reduction peaks were at -0.508 V and -0.562 V, (Reference electrode: Ag/AgCl/KCl 1.0 M) respectively. Additionally, the oxidation current is linearly related to the scan rate in Figure 4.2, indicating that 2-AQS was absorbed on the surface of gold.

In order to find a proper voltage to run the experiment, different voltages were tested with the aid to find Raman signal change. In Figure 4.3 illustrated in situ SERS spectra of 2-AQS SAM on an Au/stainless steel bipolar electrode (at cathodic end) recorded in B&R buffer (pH 7.00) at different potentials in a bipolar electrochemical setup. Note: the buffer solution was purged with N_2 for 30 mins to drive away the dissolved O_2. No change of the Raman spectra can be observed until the voltage reached 8 V, specifically, the signal of C=O stretch at 1656 cm^{-1} resulting from 2-AQS disappeared while a new signal of O-H bend at 1421 cm^{-1} due to 2-H_2AQS appeared, due to the reduction reaction of 2-AQS to 2-H_2AQS at the cathodic end of bipolar electrode. Investigating the interfacial potential distribution along the Au/stainless steel bipolar electrode in a bipolar cell was one of the purposes in this project. Raman spectra were recorded at different positions along the Au/stainless steel bipolar electrode, moving from the cathodic extreme towards the point at which no 2-AQS can transfer to 2-H_2AQS. Figure 4.4 demonstrated the in situ SERS spectra of 2-AQS SAM on an Au/stainless steel bipolar electrode in B&R buffer (pH 7.00). The spectra were obtained at different positions at 8 V, going from the edge towards the middle. As we mentioned before, a potential drop goes through the solution along the bipolar electrode when the

external potential is sufficient to trigger the redox reactions at two ends of BPE, as a result, the amount of reduced 2-AQS varies along the bipolar electrode from cathodic edge toward middle in terms of a changeable potential at various positions. Specifically, the intensity of C=O stretch close to the cathodic end at 1656 cm^{-1} resulting from 2-AQS disappeared, and then begun to appear and grow away from the cathodic end, while the intensity of O-H bend at 1421 cm^{-1} generated from 2-H_2AQS was the strongest at the cathodic extreme and gradually decreased to zero at position close to middle, where no reduction reaction of 2-AQS occurred. The change of the intensity of 1656 cm^{-1} and 1421 cm^{-1} in the SERS spectra was corresponding to the amount of 2-AQS and 2-H_2AQS at various positions on the Au/stainless steel. That is, the amount of H_2AQS at the cathodic extreme was highest and decreased gradually away from the cathodic extreme, however, the amount of AQS at cathodic extreme was lowest and increased gradually toward the middle of BPE.

4.5 Conclusion

In this work, we demonstrate the potential distribution along the bipolar electrode using 2-AQS as a probe in B&R buffer (pH 7.00) at different potentials in a bipolar electrochemical setup. 2-AQS was reduced to 2-H_2AQS at the cathodic extreme and the amount of them was monitored using surface enhanced Raman scattering by observing characteristic peaks. 1656 cm^{-1} was assigned to C=O stretch in 2-AQS and 1421 cm^{-1} was assigned to O-H bend in 2-H_2AQS. The intensity of C=O stretch was the lowest at the cathodic extreme and increased away from it, on the contrary, the intensity of O-H bend was the highest at the cathodic extreme and decreased toward middle of BPE, indicating the amount of H_2AQS at the cathodic extreme was highest and decreased

gradually away from the cathodic extreme, however, the amount of AQS at cathodic extreme was lowest and increased gradually toward the middle of BPE, because of the potential drop linearly going through the solution along the bipolar electrode.

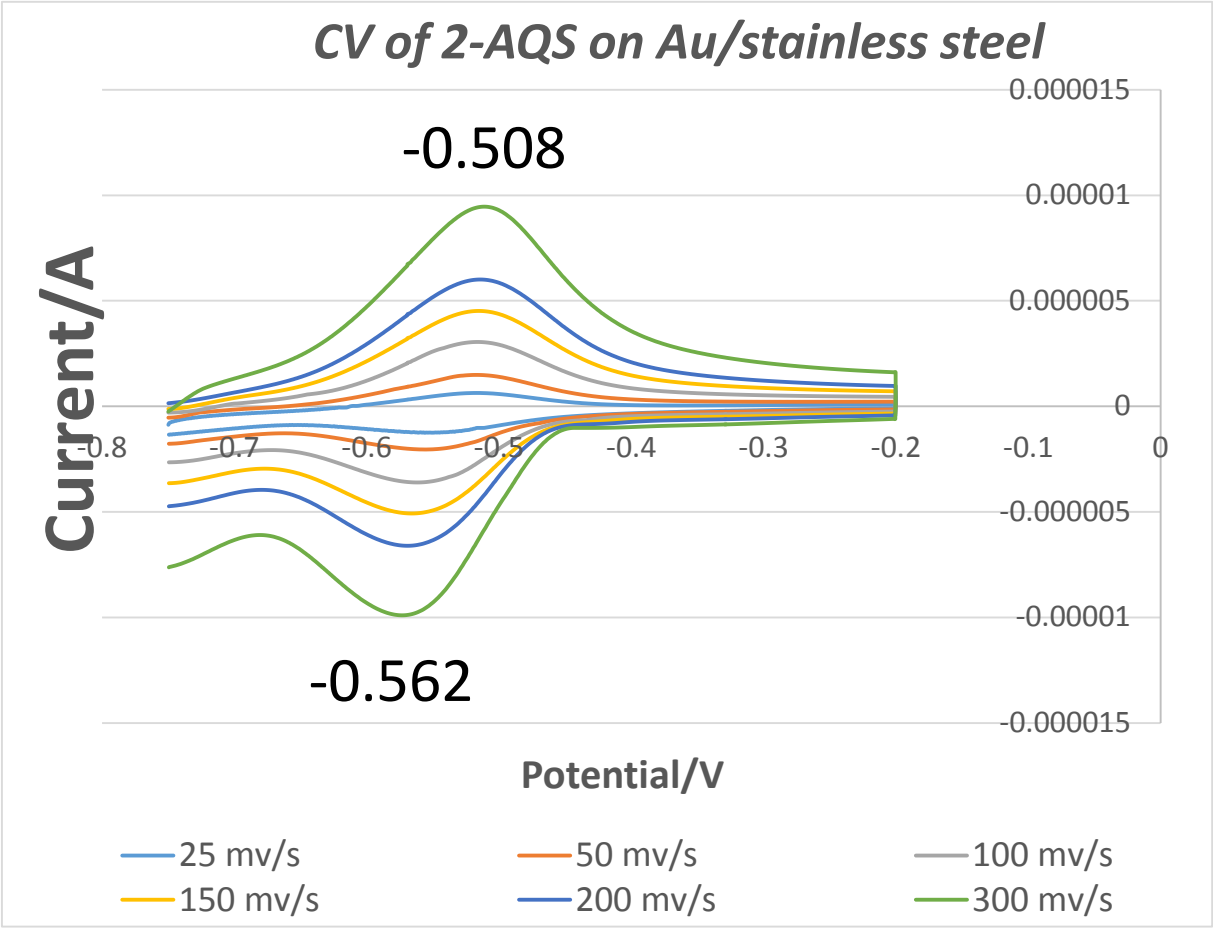

Figure 4.1 Cyclic voltammetry behavior of 2-AQS on Au/stainless steel was performed in in 0.1M Britton – Robinson buffer, which was purged by N_2 for 30 mins before use.

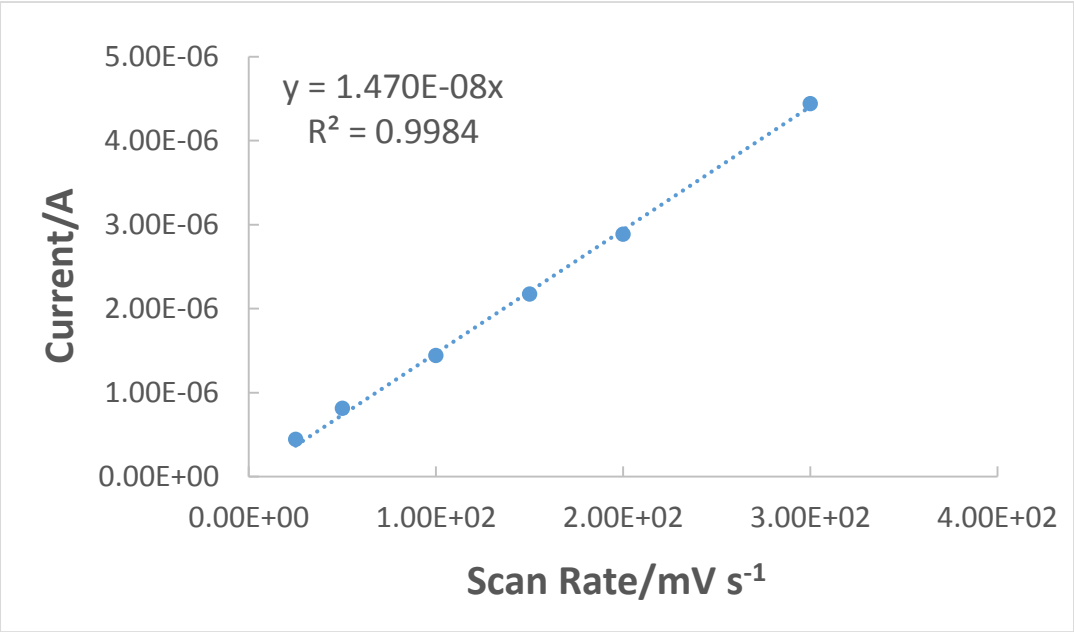

Figure 4.2 The plot of the dependence of current on the scan rate.

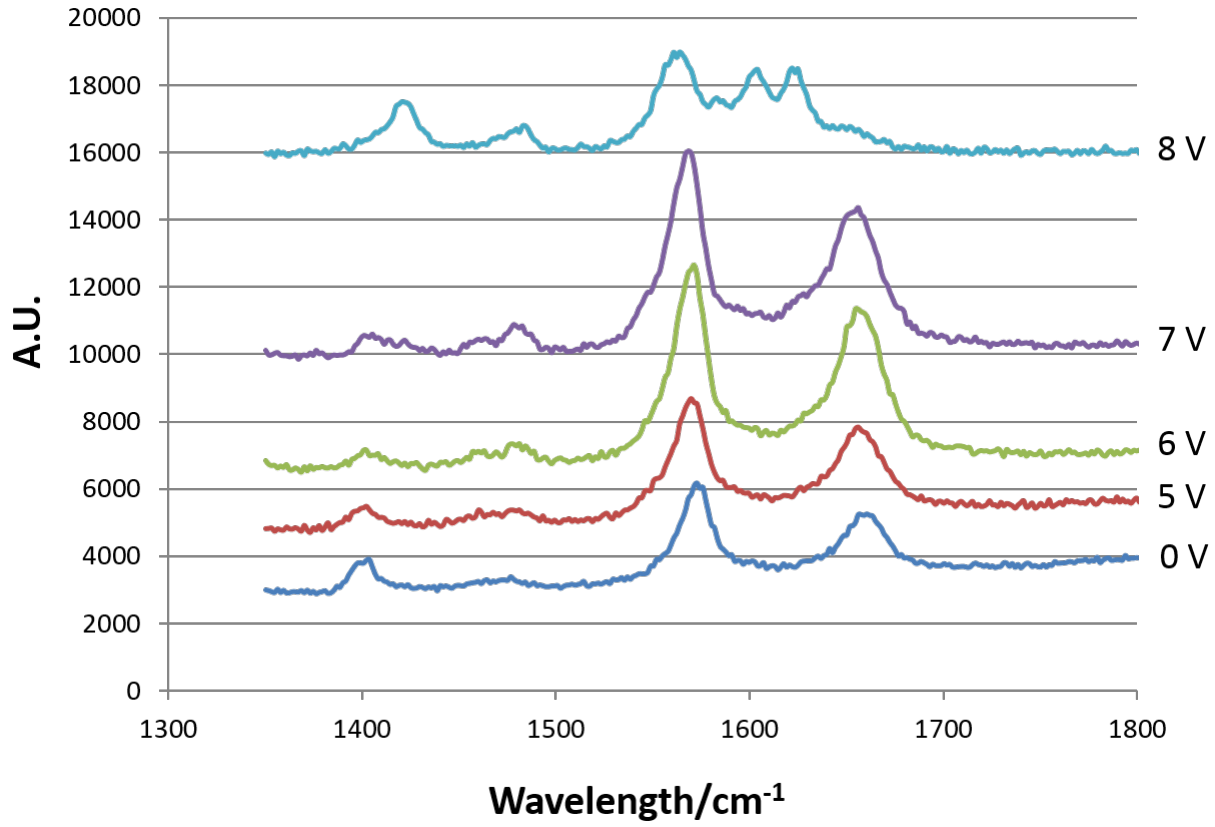

Figure 4.3 In situ SERS spectra of 2-AQS SAM on an Au/stainless steel bipolar electrode (cathodic end) recorded in B&R buffer (pH 7.00) at different potentials in a bipolar electrochemical setup.

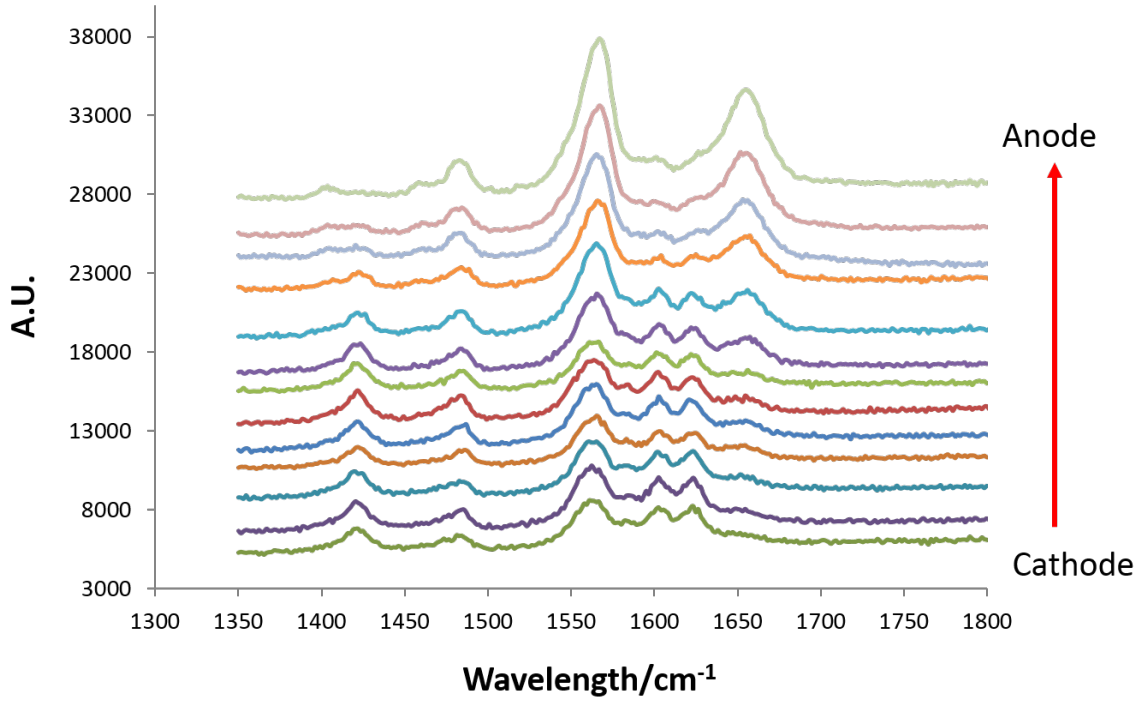

Figure 4.4 In situ SERS spectra of 2-AQS SAM on an Au/stainless steel bipolar electrode in B&R buffer (pH 7.00). The spectra were obtained at different positions at 8 V, going from the edge towards the middle. Each Raman line was obtained every 0.055 cm away from the cathodic end.

Reference

1. Zhan, W.; Alvarez, J.; Crooks, R. M. *J. Am. Chem. Soc* **2002**, 124 (44), 13265-13270.

2. Feng, Q. M.; Pan, J. B.; Zhang, H. R.; Xu, J. J.; Chen, H. Y. *Chem. commun* **2014**, 50 (75), 10949-10951.

3. Zhang, X.; Li, X.; Zhang, Q.; Peng, Q.; Zhang, W.; Gao, F. New insight into the biological treatment by activated sludge: the role of adsorption process. *Bioresour. Technol* **2014**, 153, 160-164.

4. Wang, Y.; Hernandez, R. M.; Bartlett, D. J., Jr.; Bingham, J. M.; Kline, T. R.; Sen, A.; Mallouk, T. E. *Langmuir* **2006**, 22 (25), 10451-10456.

5. Loget, G.; Kuhn, A. *J. Am. Chem. Soc* **2010**, 132 (45), 15918-15919.

6. Loget, G.; Kuhn, A. Bipolar electrochemistry for cargo-lifting in fluid channels. *Lab. Chip* **2012**, 12 (11), 1967-1971.

7. Roche, J.; Carrara, S.; Sanchez, J.; Lannelongue, J.; Loget, G.; Bouffier, L.; Fischer, P.; Kuhn, A. *Sci. Rep* **2014**, 4, 6705.

8. Laws, D. R.; Hlushkou, D.; Perdue, R. K.; Tallarek, U.; Crooks, R. M. *Anal. Chem* **2009**, 81 (21), 8923-8929.

9. Sheridan, E.; Knust, K. N.; Crooks, R. M. *Analyst* **2011**, 136 (20), 4134-4137.

10. Knust, K. N.; Hlushkou, D.; Tallarek, U.; Crooks, R. M. *Chemelectrochem* **2014**, 1 (5), 850-857.

11. Ramaswamy, R.; Shannon, C. *Langmuir* **2011**, 27 (3), 878-881.

12. Fattah, Z.; Garrigue, P.; Lapeyre, V.; Kuhn, A.; Bouffier, L. *J. Phys. Chem. C* **2012**, 116 (41), 22021-22027.

13. Inagi, S.; Ishiguro, Y.; Atobe, M.; Fuchigami, T. *Angew. Chem. Int. Ed* **2010**, 49 (52), 10136-10139.

14. Kong, S. W.; Fontaine, O.; Roche, J.; Bouffier, L.; Kuhn, A.; Zigah, D. *Langmuir* **2014**, 30 (11), 2973-2976.

15. Loget, G.; Roche, J.; Gianessi, E.; Bouffier, L.; Kuhn, A. Indirect Bipolar Electrodeposition. *J. Am. Chem. Soc* **2012**, 134 (49), 20033-20036.

16. Loget, G.; Roche, J.; Kuhn, A. *Adv. Mater* **2012**, 24 (37), 5111-5116.

17. Sopha, H.; Roche, J.; Svancara, I.; Kuhn, A. *Anal. Chem* **2014**, 86 (21), 10515-10519.

18. Munktell, S.; Tyden, M.; Hogstrom, J.; Nyholm, L.; Bjorefors, F. *Electrochem. Commun* **2013**, 34, 274-277.

19. Fosdick, S. E.; Berglund, S. P.; Mullins, C. B.; Crooks, R. M. *Anal. Chem* **2013**, 85 (4), 2493-2499.

20. Fosdick, S. E.; Berglund, S. P.; Mullins, C. B.; Crooks, R. M. *Acs. Catal* **2014**, 4 (5), 1332-1339.

21. Mavre, F.; Anand, R. K.; Laws, D. R.; Chow, K. F.; Chang, B. Y.; Crooks, J. A.; Crooks, R. M. *Anal. Chem* **2010**, 82 (21), 8766-8774.

22. Xia, Y. N.; Whitesides, G. M. Soft lithography. *Angew. Chem. Int. Ed* **1998**, 37 (5), 551-575.

23. Piner, R. D.; Zhu, J.; Xu, F.; Hong, S. H.; Mirkin, C. A. *Science* **1999**, 283 (5402), 661-663.

24. Dorri, N.; Shahbazi, P.; Kiani, A. *Langmuir* **2014**, 30 (5), 1376-1382.

25. Van Dover, R. B.; Schneemeyer, L. D.; Fleming, R. M. *Nature* **1998**, 392 (6672), 162-164.

26. Jandeleit, B.; Schaefer, D. J.; Powers, T. S.; Turner, H. W.; Weinberg, W. H. *Angew. Chem. Int. Ed* **1999**, 38 (17), 2494-2532.

27. Miller, O. J.; El Harrak, A.; Mangeat, T.; Baret, J. C.; Frenz, L.; El Debs, B.; Mayot, E.; Samuels, M. L.; Rooney, E. K.; Dieu, P.; Galvan, M.; Link, D. R.; Griffiths, A. D. *Proc. Natl. Acad. Sci.* U S A **2012**, 109 (2), 378-383.

28. Mrksich, M.; Grunwell, J. R.; Whitesides, G. M. Biospecific. *J. Am. Chem. Soc* **1995**, 117 (48), 12009-12010.

29. Tidwell, C. D.; Ertel, S. I.; Ratner, B. D.; Tarasevich, B. J.; Atre, S.; Allara, D. L. *Langmuir* **1997**, 13 (13), 3404-3413.

30. Carter, S. B. *Nature* **1965**, 208 (5016), 1183-1187.

31. Chaudhury, M. K.; Whitesides, G. M. *Science* **1992**, 256 (5063), 1539-1541.

32. Riepl, M.; Ostblom, M.; Lundstrom, I.; Svensson, S. C. T.; van der Gon, A. W. D.; Schaferling, M.; Liedberg, B. *Langmuir* **2005**, 21 (3), 1042-1050.

33. Morgenthaler, S.; Lee, S. W.; Zurcher, S.; Spencer, N. D. *Langmuir* **2003**, 19 (25), 10459-10462.

34. Tomlinson, M. R.; Efimenko, K.; Genzer, J. *Macromolecules* **2006**, 39 (26), 9049-9056.

35. Lee, K. Y. C.; Klingler, J. F.; Mcconnell, H. M. *Science* **1994**, 263 (5147), 655-658.

36. Terrill, R. H.; Balss, K. M.; Zhang, Y. M.; Bohn, P. W. *J. Am. Chem. Soc* **2000**, 122 (5), 988-989.

37. Plummer, S. T.; Wang, Q.; Bohn, P. W.; Stockton, R.; Schwartz, M. A. *Langmuir* **2003**, 19 (18), 7528-7536.

38. Jeon, N. L.; Dertinger, S. K. W.; Chiu, D. T.; Choi, I. S.; Stroock, A. D.; Whitesides, G. M. *Langmuir* **2000**, 16 (22), 8311-8316.

39. Park, S. H.; Krull, U. *Analytica. Chimica. Acta* **2006**, 564 (2), 133-140.

40. Hansen, T. S.; Lind, J. U.; Daugaard, A. E.; Hvilsted, S.; Andresen, T. L.; Larsen, N. B. *Langmuir* **2010**, 26 (20), 16171-16177.

41. Shida, N.; Ishiguro, Y.; Atobe, M.; Fuchigami, T.; Inagi, S. *Acs Macro. Lett* **2012**, 1 (6), 656-659.

42. Ulrich, C.; Andersson, O.; Nyholm, L.; Bjorefors, F. *Angew. Chem. Int. Ed* **2008**, 47 (16), 3034-3036.

43. Mavre, F.; Chow, K. F.; Sheridan, E.; Chang, B. Y.; Crooks, J. A.; Crooks, R. M. *Anal. Chem* **2009**, 81 (15), 6218-6225.

44. Inagi, S.; Ishiguro, Y.; Shida, N.; Fuchigami, T. *J. Electrochem. Soc* **2012**, 159 (11), G146-G150.

45. Nishiyama, K.; Tahara, S.; Uchida, Y.; Tanoue, S.; Taniguchi, I. *J. Electroanal. Chem* 1999, 478 (1-2), 83-91.

Chapter 5

Summary and Future Outlook

5.1 Summary

This dissertation demonstrated the application of bipolar electrochemistry in chemical electroanalysis due to its low price, simpleness, viability, and easy preparation. It is the fact that bipolar electrochemistry is controlled without direct connection and redox reactions occur at two end point simultaneously when external potential is sufficient to trigger them. Because it is impossible to measure the current flowing through bipolar electrode, electrochemiluminescence proportional to the current is introduced in chemical electroanalysis. Ferrocenemethanol (FcMeOH) and O_2, that are capable of quenching ECL, can be detected on bipolar electrochemistry by measuring the intensity of ECL as the function of the concentration of them. The data of ECL we got was analyzed by Stern−Volmer equation, exhibiting a liner dependence of [O_2] and [FcMeOH]. The work opened up a new application of bipolar electrochemistry in utilizing quenching ECL to detect small molecules. Afterwards, we analyzed the quenching behavior of Cl^-, Br^-, and I^- ions based on the same principle of bipolar electrochemistry. These three halide ions exhibited different quenching effect following the order $I^- > Br^- > Cl^-$, corresponding to their formal oxidation potential. In addition, at low concentration, the enhancement of ECL emerged due to the inhibition of oxidized film and a delay of the passivation of metals absorbed by halide ions, resulting in a strong increase of oxidation of coreactant. A linear potential gradient across the bipolar electrode was created when a bipolar cell was applied an external potential. It is an issue

that we do not `know the exact potential distribution on bipolar cell. We herein proposed to measure it by observing intensity of Raman spectra of 2-AQS and 2-H_2AQS. The ratio of the intensity of Raman spectra of them corresponded to the amount of them on the surface of bipolar electrode, which also correlated with the potential gradient across the bipolar electrode.

5.2 Future outlook

ECL quenching analysis on bipolar electrochemistry can be extended to detect similar compounds with different functional group that are capable of quenching ECL. And they can be discriminated with different quenching rate constant. Some factors may also affect the intensity of ECL, such as temperature. The quenching effect depending on the temperature will be another topic in this field. Similarly, temperature depending SERS on bipolar electrode is also of great interest to study. The SERS behaviors of molecules on bipolar electrode depend on not only external potential but also the pH values. Changing the condition on pH value and interrogating electrochemical behaviors by SERS is our future work in bipolar electrochemistry.